NTIA Report 91-277

Wideband HF Noise/Interference Modeling Part I: First-Order Statistics

John J. Lemmon
Christopher J. Behm

U.S. DEPARTMENT OF COMMERCE
Robert A. Mosbacher, Secretary

Janice Obuchowski, Assistant Secretary
for Communications and Information

May 1991

CONTENTS

Page

LIST OF FIGURES

Page

List of Figures (cont.)

Page

List of Figures (cont.)

Page

List of Figures (cont.)

Page

List of Figures (cont.)

Page

WIDEBAND HF NOISE/INTERFERENCE MODELING
PART I: FIRST-ORDER STATISTICS

John J. Lemmon and Christopher J. Behm*

This report discusses the development of a wideband HF noise/interference model. The model is based on measured data and is suitable for implementation in a wideband HF channel simulator. The measured data are described and analyses performed on the data are discussed. Then the proposed noise/interference model is presented. Example results from the model are compared with measured data, and aspects of the model development which require further investigation are discussed.

Key words: channel simulator; noise/interference; wideband HF

1. INTRODUCTION

1.1 Background

There is currently widespread interest in HF communications over large bandwidths (on the order of 1 MHz or more), motivated by the application of spread spectrum technology to HF systems. The advantages of spread spectrum technology for communication systems are well known (Dixon, 1984), and include low-probability-of-intercept (LPI) communications, noise/interference rejection, and simultaneous operation of several transmitters in the same frequency band (code division multiple access). These advantages, which depend on the process gain inherent in spread spectrum systems, require use of the widest possible rf bandwidth.

On the other hand, there exist many uncertainties concerning the performance of HF systems over wide bandwidths. Channel simulation enables one to evaluate the performance of communication equipments without the cost of building hardware and running extensive field tests. Other advantages of channel simulation include accuracy, repeatability, stationarity, availability, and parameter variation (Hoffmeyer and Vogler, 1987). However,

* The authors are with the Institute for Telecommunication Sciences, National Telecommunications and Information Administration, U.S. Department of Commerce, Boulder, CO 80303-3328.

the design and implementation of a channel simulator requires a channel model which accurately describes the real-world conditions encountered on communication links.

Motivated by the possibility of constructing a wideband HF channel simulator, an investigation of channel models that represent the HF channel was conducted (Hoffmeyer and Nesenbergs, 1987). One conclusion of the study was that no validated channel model which accurately describes the wideband HF channel had been developed.

As a result, the Institute for Telecommunication Sciences has undertaken the development of a wideband HF channel model. The objective of the modeling effort is to develop a mathematical model of the HF channel which is accurate over wide bandwidths (on the order of 1 MHz or more), which can be validated with measured data, and which is suitable for implementation (in software and hardware) in a wideband HF channel simulator. The model is to include wideband HF noise and interference, as well as a model of the channel transfer function, describing the characteristics of ionospheric sky-wave propagation.

The wideband propagation model which has been developed has been discussed in detail elsewhere (Vogler et al., 1988; Vogler and Hoffmeyer, 1988 and 1990). The purpose of this report is to discuss the development of a wideband HF noise/interference model.

1.2 Objectives

The noise/interference model presented in this report differs in one important respect from previously developed models. In past developments noise/interference models have consisted of descriptions of the statistical characteristics of the received noise/interference at the output of a narrowband receiver. From this point of view noise/interference processes can be classified as Class A or Class B, depending on whether the bandwidth of the process is less than (Class A) or greater than (Class B) the bandwidth of the receiver front end. Numerous models have been developed for Class A and Class B processes, and can be grouped into two general categories: empirical models, which are designed to fit certain measured statistics of the noise/interference, and physical models, which attempt to take into account the physics of the noise/interference processes themselves. Summaries of existing noise/interference models have been provided by

Spaulding (1977 and 1982), Hall (1966), Giordano (1970), Ibukun (1966), and Spaulding and Middleton (1975). Such models are useful for the theoretical determination of communication system performance and for the design of systems with optimum performance in the real world noise/interference environment.

This is not the objective of the present work, however. Instead, what is required is a model which can be used to simulate the noise/interference over wide bandwidths in the propagation channel, rather than describing statistical characteristics of the noise/interference. Thus, the objective of the present work is to obtain a model of the noise/interference processes themselves.

It is necessary that such a model have the attributes of simplicity and flexibility, and that the model incorporate as many physical ideas as possible. The need for simplicity and flexibility seems obvious, because it is intended to implement the model in a noise/interference simulator with the capability to simulate any environment which could conceivably be encountered on HF communications links. However, the development and verification of any such model must be based on measured data, which is necessarily of limited scope. For example, the model discussed in this report is based on data obtained in Bedford, MA during March, 1989, whereas the model should have the capability to describe other environments as well. If the parameters of the model relate to the physical circumstances causing the noise/interference, it is possible to ascertain how to vary those parameters in order to describe environments other than those upon which the model development is based. To have this kind of predictive capability, the model must therefore be a physical model, as opposed to an empirical model which simply attempts to fit certain measured statistics of the noise/interference, and whose parameters do not relate to the physics of the noise/interference processes.

1.3 Scope

The model development discussed in this report has primarily involved generating probability distribution functions that describe various statistical characteristics of measured noise/interference and developing a model which exhibits those same characteristics. Clearly, many such characteristics could be examined. For example, noise models often

specify distributions of the received instantaneous voltage, amplitude, phase, and the average level crossing rate of the noise envelope. Other quantities of interest include power spectra and distributions of power in the frequency domain (spectral occupancy).

These quantities are useful for characterizing the time-averaged behavior of the noise/interference. However, a complete description of the noise/interference process requires higher-order statistics as well. These statistics are necessary to specify the relationships between the noise/interference process at different instants in time. For example, given the average number of level crossings of the noise envelope per unit time, higher-order statistics are required to describe how the envelope crossings are distributed in time (pulse width and pulse spacing distributions). In addition, measured noise/interference is decidedly nonstationary, and knowledge of the time scales over which the characteristics of the noise/interference vary is necessary for a complete specification of the noise/interference process.

In this report, attention is restricted to the first-order statistics of the noise/interference. Investigation of higher-order statistics, including pulse width and pulse spacing distributions, as well as nonstationarity time scales, has been reserved for future work.

2. ANALYSIS OF NOISE/INTERFERENCE DATA

2.1 Description of Data

As part of its experimental wideband HF communications program, the Mitre Corporation has made recordings of wideband HF noise/interference. These data were obtained using a wideband HF communications test facility, which includes a simplex link from Homestead, FL to Bedford, MA.

The equipment used in the experiments is described by Perry and Rifkin (1989). Briefly, the communications system uses a direct sequence spread spectrum signal with a chipping rate of 512 kb/s. At the receive terminal a horizontally polarized log-periodic antenna (H/LPA) was used when the data in this report were obtained. The H/LPA has a directivity of about 10 dBi.

The wideband receiver converts the signal from rf to baseband where the complex (in-phase and quadrature) components are low-pass filtered (bandwidth = 400 kHz) and digitized at a sampling rate of 1.024 MHz. These filters truncate the received signal spectrum to an equivalent rf bandwidth of 800 kHz. Eight-bit analog to digital converters were used. In addition, a variable attenuator (0-31 dB) was used at the receiver front-end to avoid saturating the receiver.

An important part of Mitre's wideband HF test facility is a frequency-domain interference suppressor which excises narrowband interference above a chosen threshold. However, the data discussed in this report are raw data that were obtained prior to interference excision.

The data consist of 42 one-second records of the digitized, baseband in-phase (I) and quadrature (Q) components of the received noise/interference. The data were collected during experiments performed in March, 1989 in Bedford, MA at various times of day and at various frequencies in the HF band (3-30 MHz). The times, dates, and center frequencies of the data, and the values of the variable attenuation that were used are listed in Table 1 of the Appendix. Also shown in the Appendix are example plots of the raw data (both I and Q). Each plot shows the first 4 ms (4096 samples) of a one-second noise/interference record.

The fact that the noise/interference is characterized by baseband I and Q components, whose bandwidth is less than the carrier frequency, implies that the noise/interference can be viewed as a narrowband process with a well-defined envelope and phase. However, the noise/interference is referred to as "wideband" in the sense that one is dealing with bandwidths on the order of 1 MHz as opposed to bandwidths on the order of several kHz.

2.2 Analysis Tools

To analyze the noise/interference data, software has been developed to generate the following quantities:

- plots of raw data (I and Q)
- probability density function (pdf) of raw data
- pdf of voltage envelope $\sqrt{(I^2 + Q^2)}$
- pdf of power envelope $(I^2 + Q^2)$
- pdf of phase $(\tan^{-1} Q/I)$
- cumulative distribution function (cdf) of power envelope
- distribution of average level crossing rate of the voltage envelope
- autocorrelation function of raw data
- power spectrum
- cdf of power in the frequency domain (sum of the squares of the real and imaginary parts of the complex Fourier transform of the raw data)
- pdf of phase in the frequency domain (phase of the complex Fourier transform of the raw data)

In addition, software has been developed to perform the following functions:

- frequency domain excision of narrowband interference
- simulations of noise/interference

The purpose of generating the rather large number of quantities listed above is to examine the noise/interference from many points of view simultaneously. This is necessary,

because, as discussed above, the objective of the present effort is not simply to model certain statistical characteristics of the noise/interference, but to obtain a model of the noise/interference process itself. Nevertheless, it may be noted that taken together, these quantities contain some redundancy. For example, the cdf of the power envelope is the integral of the pdf of the power envelope, and the latter quantity is related to the pdf of the voltage envelope through a simple transformation of variables. However, as will be seen in the examples below, certain characteristics of the noise/interference are sometimes more readily apparent in one quantity than in another which, in principle, contains the same information.

On the other hand, these quantities do not provide a complete characterization of the noise/interference. As was pointed out above, the higher-order statistics have not been examined in the present effort, although we intend to do so in future work.

2.3 Case Studies

The general strategy which has been used to analyze the noise/interference data is as follows. First, plots of the raw data, examples of which appear in the Appendix, were examined qualitatively to identify data which seemed typical of the total data set. Next, the data so identified was analyzed in detail with the intent of developing a simple physical model of the noise/interference capable of describing the data. Then the raw data was reexamined for examples which seemed qualitatively different from the typical case. Finally, these examples were analyzed to determine whether the tentative model could also describe these cases, and, if not, to determine how the model could be modified and/or extended to include these cases. Thus, a variety of case studies were conducted.

2.3.1 Case Study 1.

The data analyzed in this case study are typical of the wideband noise/interference records which have been examined. These data were obtained on 10 March 1989 at 9:58:10 UT at a center frequency of 5.936 MHz.

A plot of the first 4 ms of the I-channel data is shown in Figure 1. The pdf of these data is shown in Figure 2 in the form of a histogram, which resembles a Gaussian

distribution. This is not surprising, because over an 800 kHz bandwidth one expects contributions to the noise/interference from many independent sources, which, by the central limit theorem, may be expected to approximate a Gaussian process. If the noise/interference is a complex, zero-mean Gaussian process, the voltage envelope is Rayleigh distributed. Figure 3 shows the pdf of the voltage envelope, which does indeed resemble a Rayleigh distribution. The pdf of the phase is shown in Figure 4, and is approximately a uniform distribution, which again is expected if the I and Q data correspond to independent, identically distributed zero-mean Gaussian processes.

However, Figure 5, which shows the pdf of the power envelope, indicates that the noise/interference cannot adequately be described by a Gaussian process alone. Whereas the power envelope for a Gaussian process is exponentially distributed, the pdf in Figure 5 shows a pronounced dip for small values of power. In fact, the distribution resembles a Rician power distribution, which arises from one or more sine waves in the presence of Gaussian noise. Thus, it appears that the noise/interference can be described by a combination of Gaussian noise and narrowband interference (sine waves).

The cdf of the power envelope, plotted as the logarithm of the probability that the power exceeds some threshold as a function of the logarithm of that threshold, is shown in Figure 6. Although this function in principle contains the same information as the power pdf in Figure 5, log-log plots reveal the tails of probability distributions more clearly than linear plots. Examples of this effect can be seen in some of the case studies discussed below.

The level crossing distribution of the voltage envelope is shown in Figure 7. Plotted is the number of upgoing crossings (in a time interval of 4 ms) of the voltage envelope across a given threshold as a function of that threshold. Thus, the number of crossings divided by 4 ms gives the average level crossing rate in crossings per second. It can be shown that the average level crossing rate of the voltage envelope is proportional to the pdf of the voltage envelope for a Gaussian process (Rice, 1944 and 1945), but not for random processes in general (see, for example, Hall, 1966). However, comparing Figure 7 with

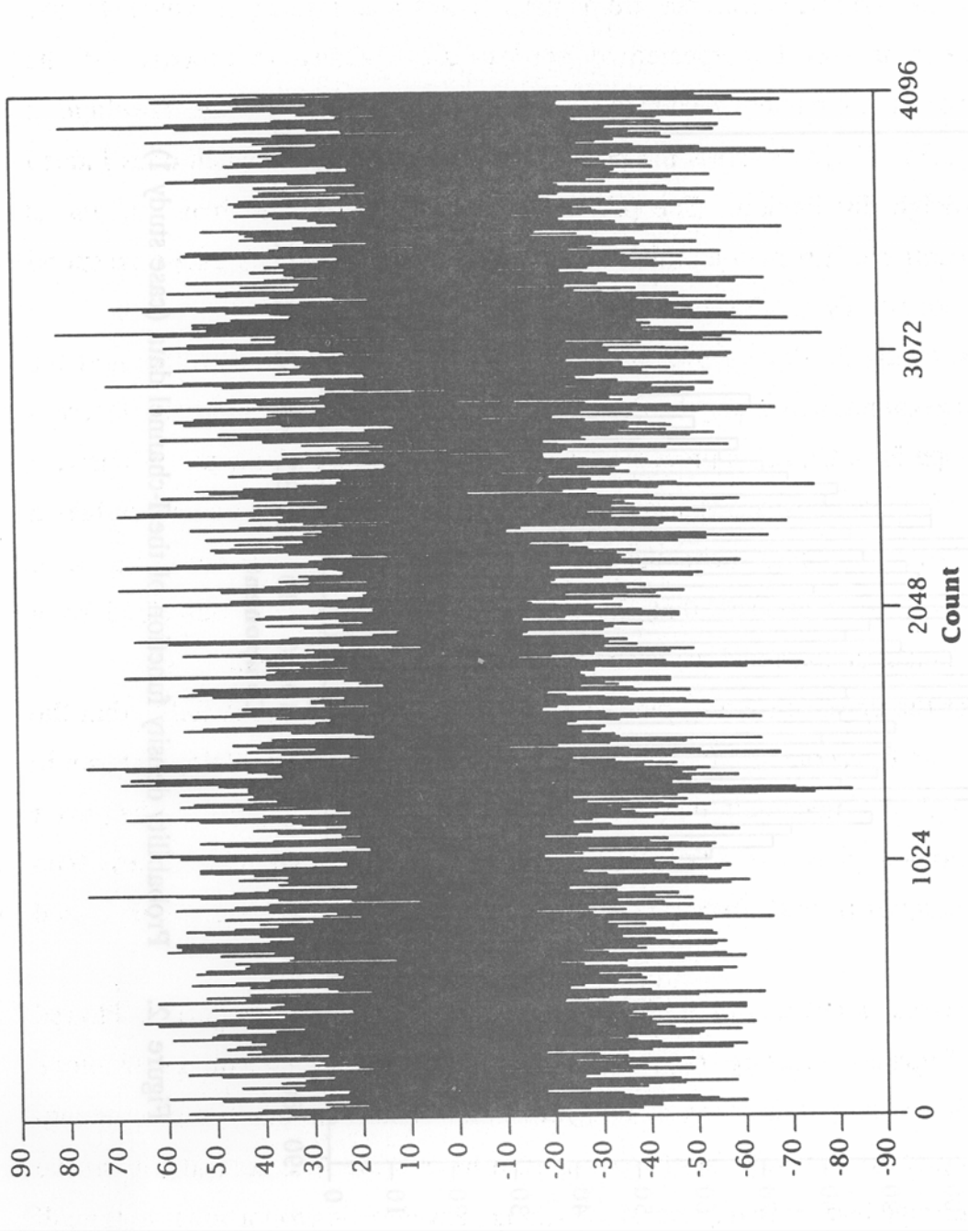

Figure 1. Measured noise/interference in the I-channel at 5.936 MHz (case study 1).

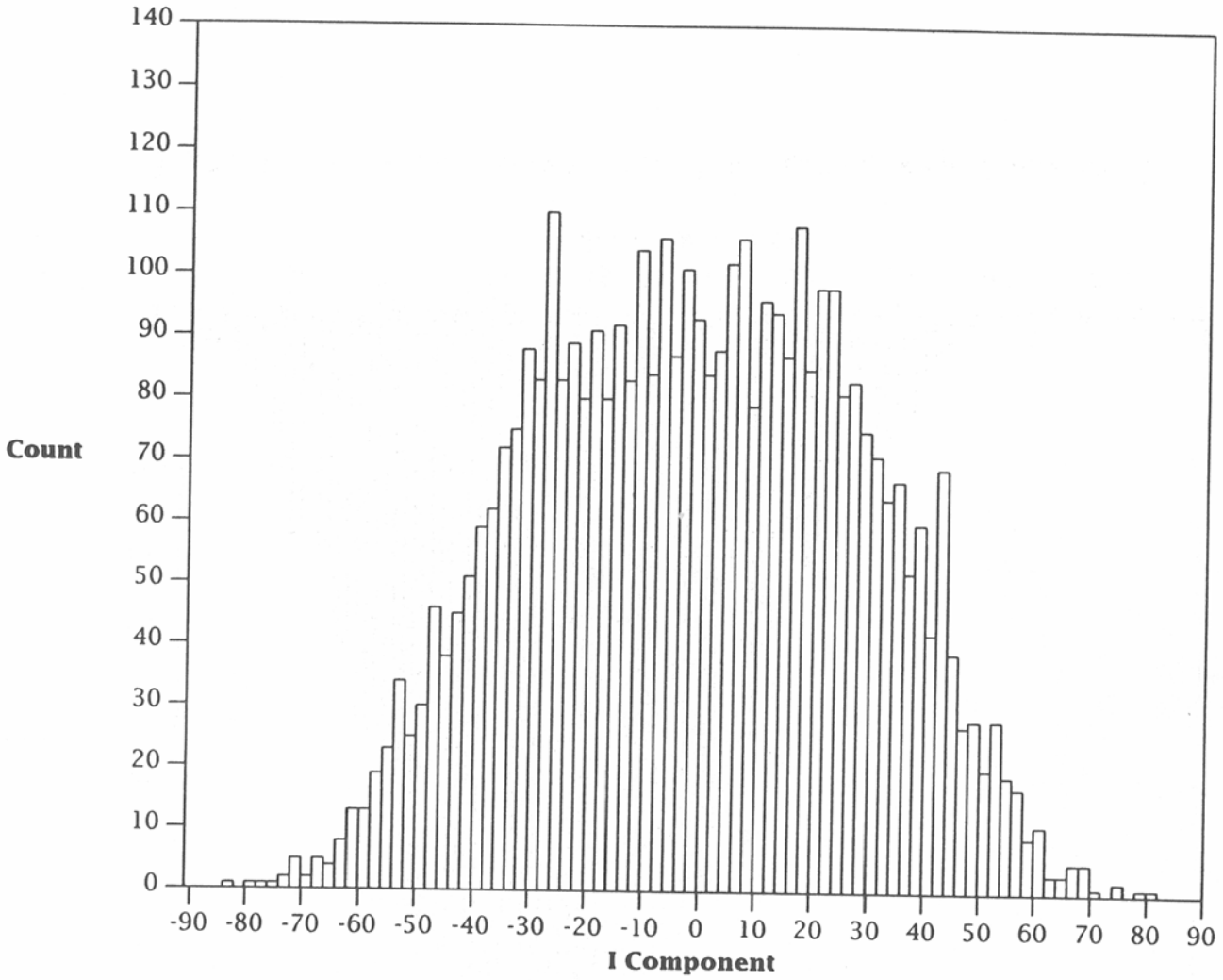

Figure 2. Probability density function of the I-channel data (case study 1).

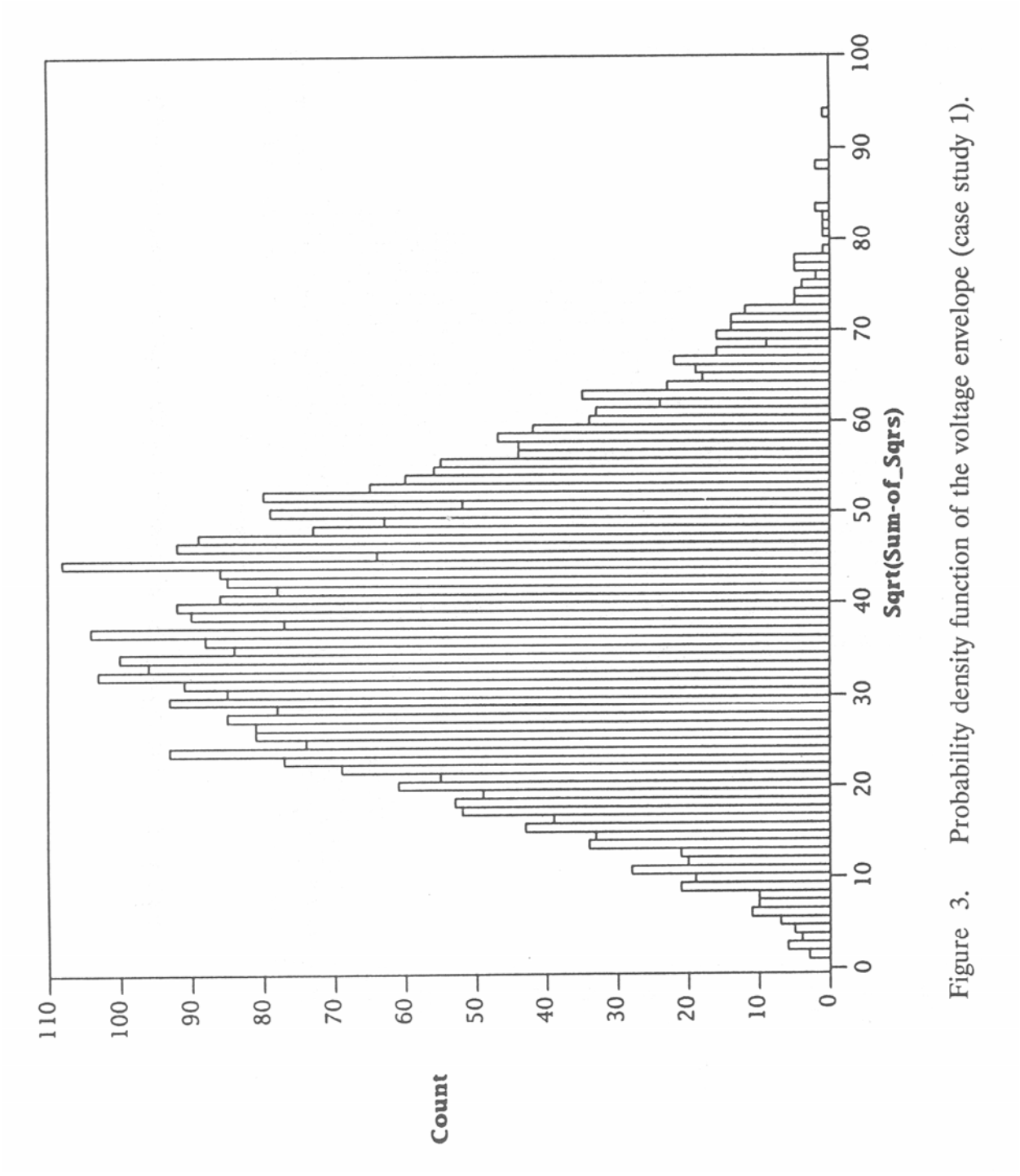

Figure 3. Probability density function of the voltage envelope (case study 1).

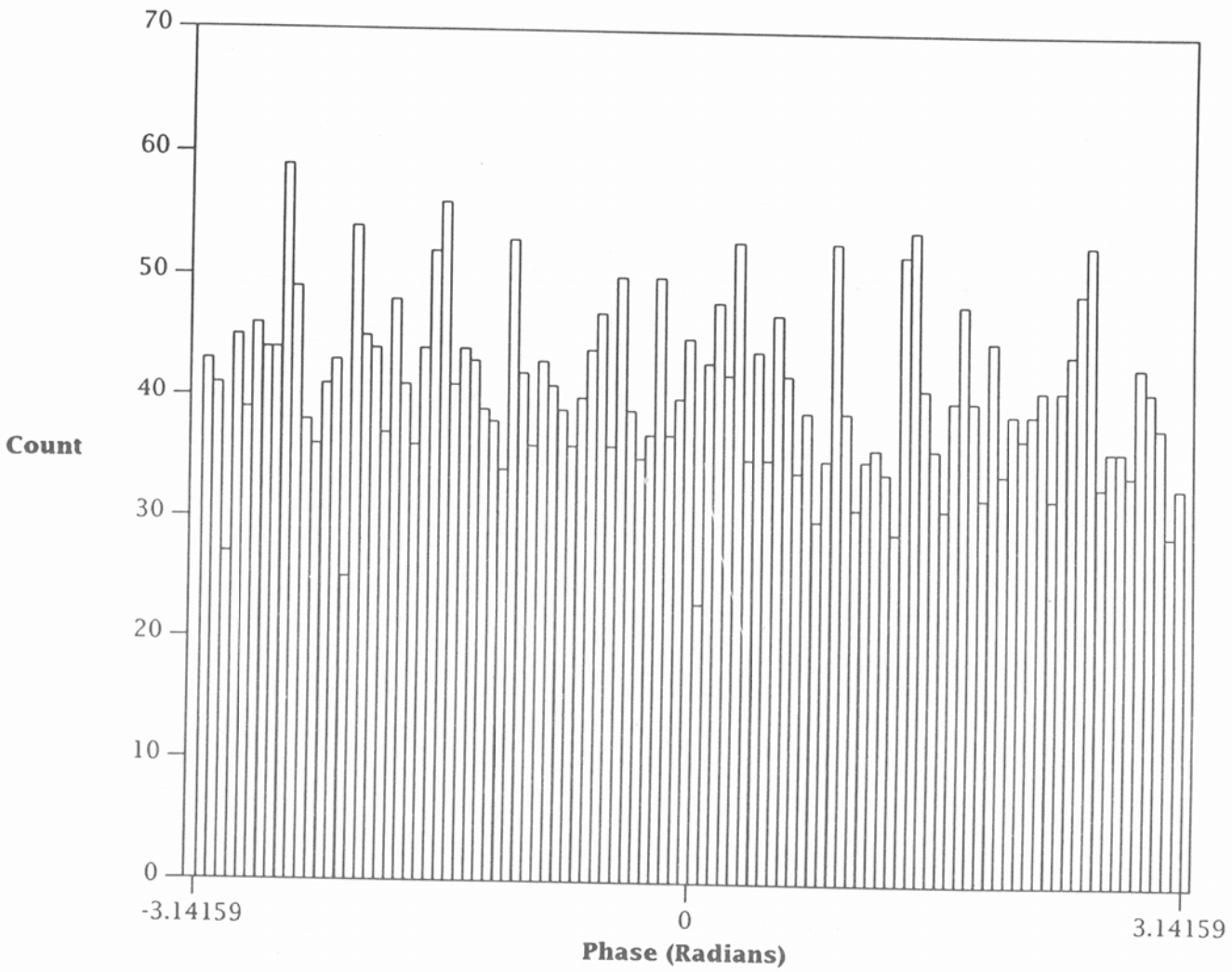

Figure 4. Probability density function of the phase (case study 1).

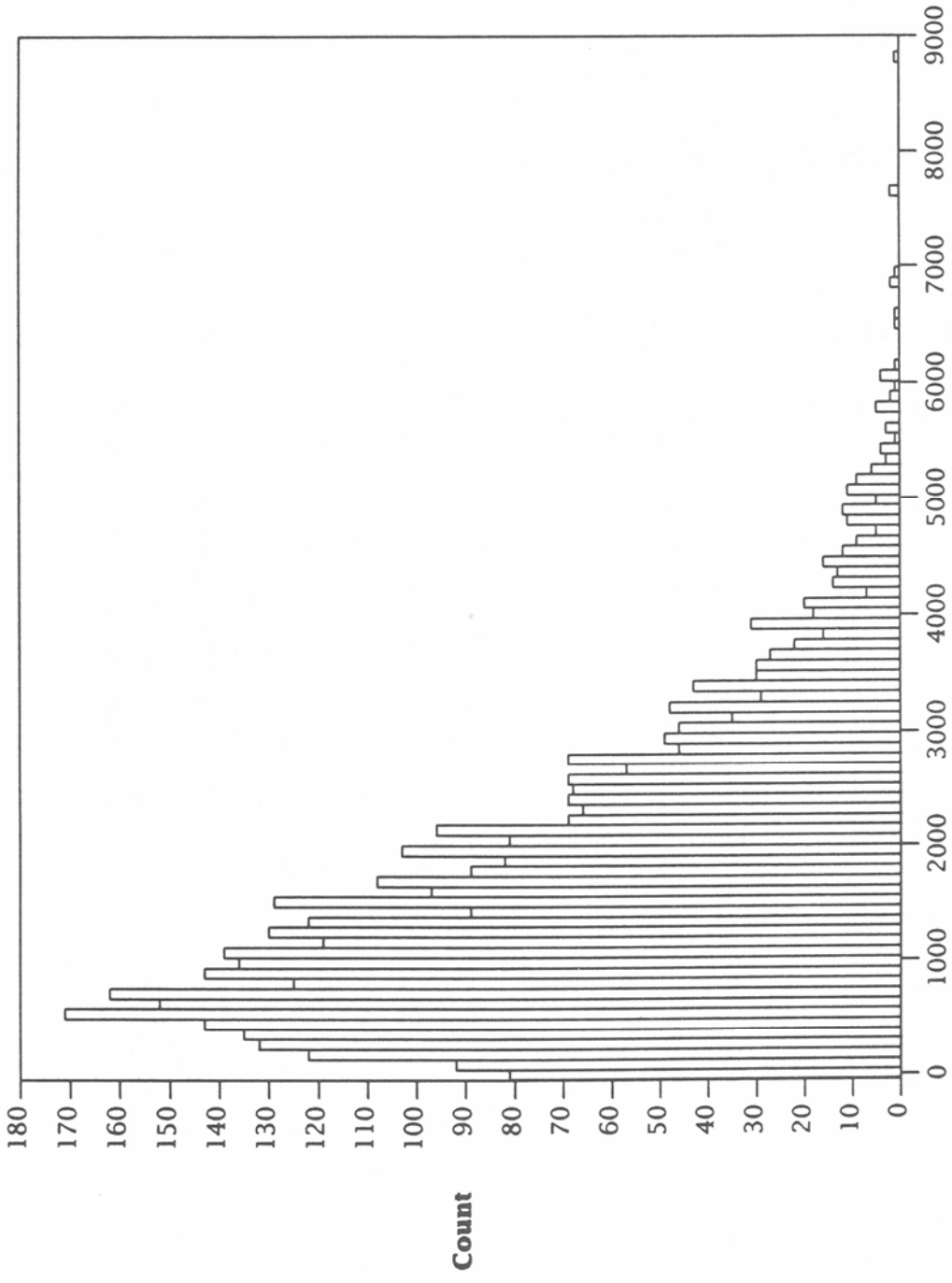

Figure 5. Probability density function of the power envelope (case study 1).

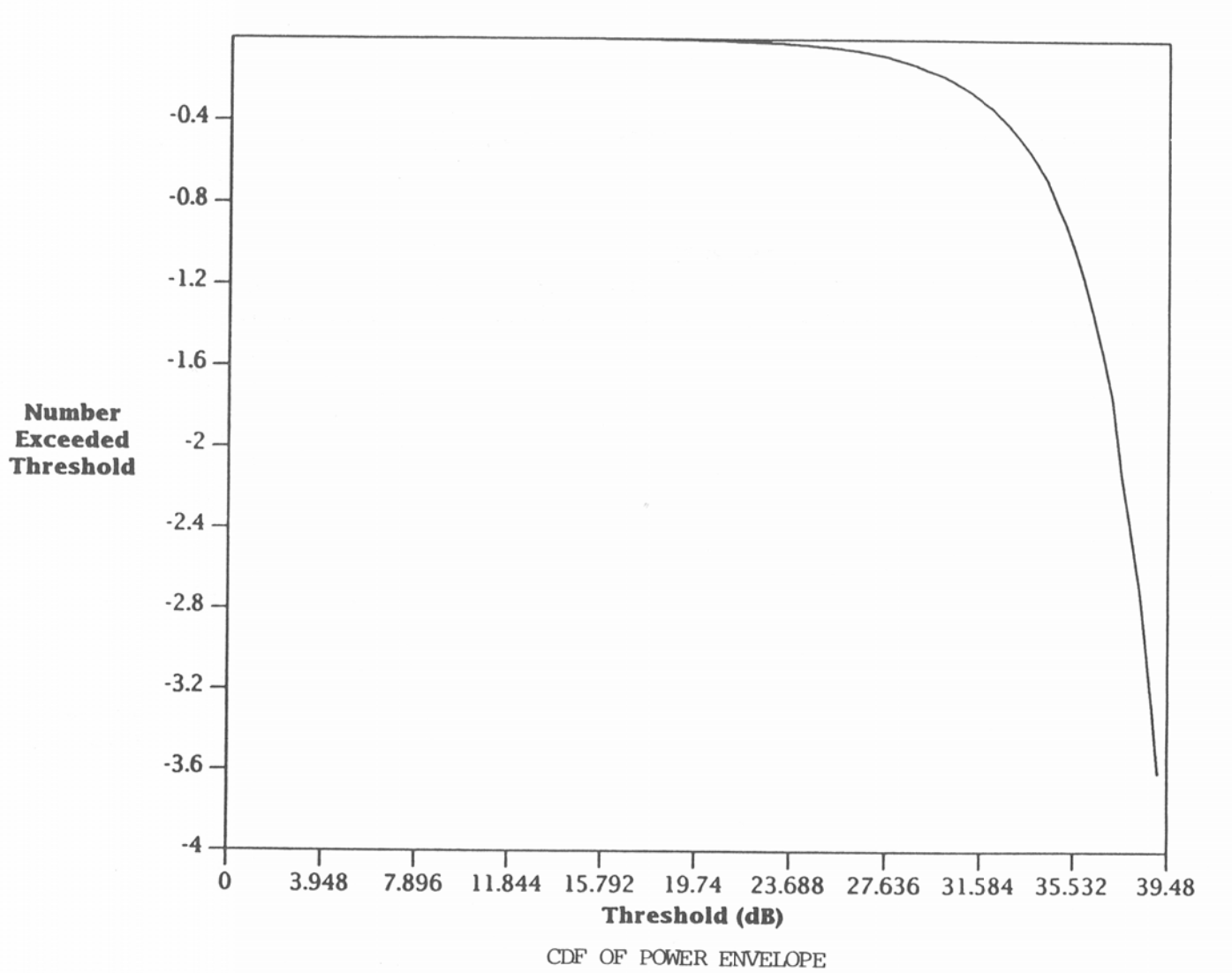

Figure 6. Cumulative distribution function of the power envelope (case study 1).

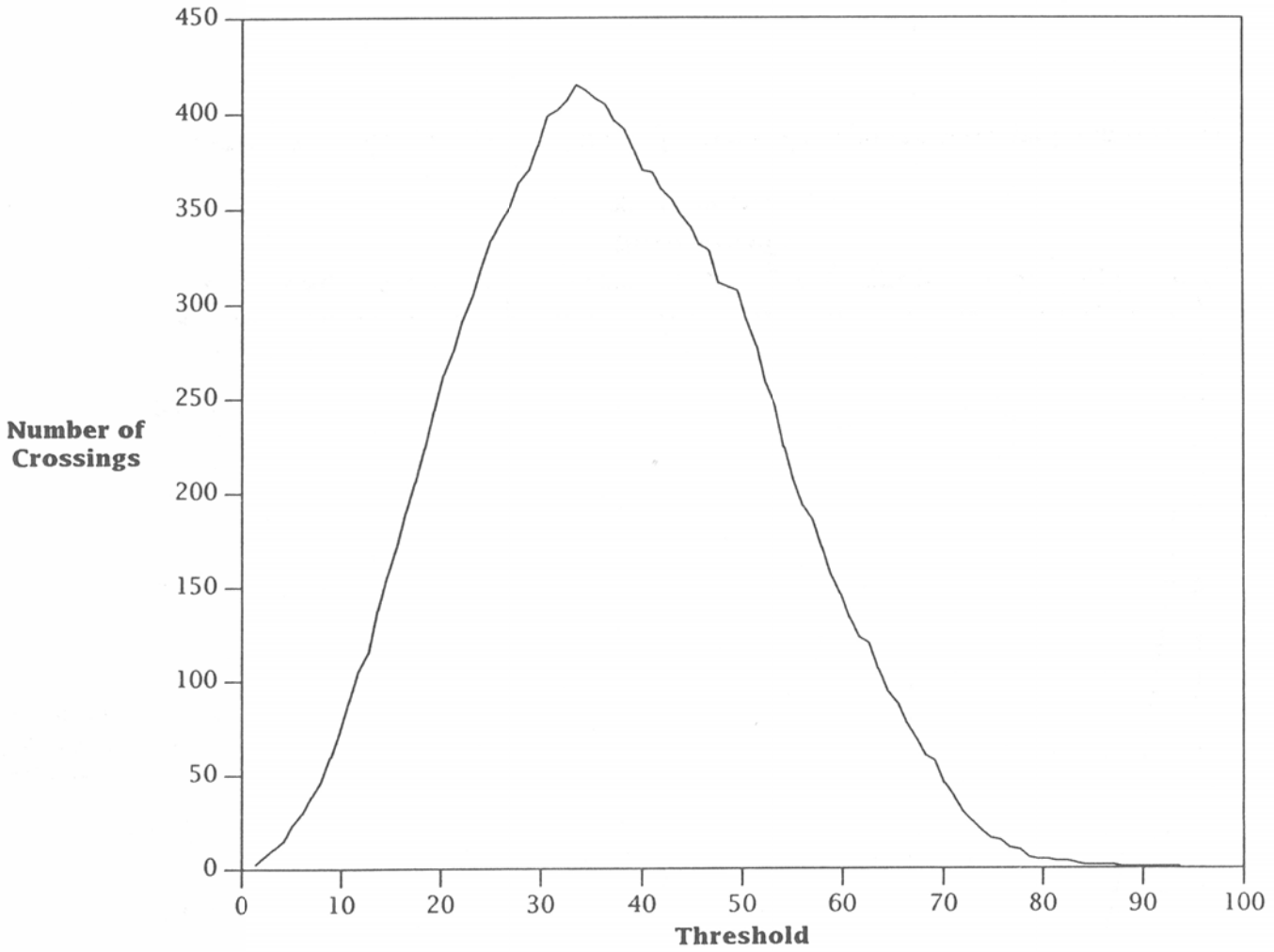

Figure 7. Level crossing distribution of the voltage envelope (case study 1).

Figure 3 (voltage envelope pdf) shows that the crossing rate is approximately proportional to the envelope pdf in this case.

The analyses discussed so far provide a description of the first-order statistics (average behavior of the envelope and phase) of the noise/interference in time. However, it remains to investigate the spectral properties of the process.

Figure 8 shows the power spectrum, obtained by computing the sum of the squares of the real and imaginary parts of the complex Fourier transform of the raw data. Because the transform is a discrete transform of a 4 ms record sampled at 1.024 MHz, the power spectrum spans a bandwidth of 1.024 MHz with a spectral resolution of 250 Hz. The spectrum has been folded so that the zero frequency at baseband (center frequency at rf) appears at the far left and right ends of the frequency scale. Also note that the power spectral density is plotted on a logarithmic (dB) scale.

The power spectrum clearly reveals the presence of many narrowband interferers. The absence of these interferers from the center of the plot is due to the fact that this part of the spectrum is outside the bandpass of the lowpass filter in the wideband receiver.

To characterize the amplitude distribution of the narrowband interferers, the cdf of the power envelope (sum of the squares of the real and imaginary parts) of the Fourier transform has been computed and is shown in Figure 9. As was done for the power cdf in the time domain (Figure 6), the logarithm of the probability that the power exceeds a threshold is plotted as a function of that threshold in dB. The form of the cdf in Figure 9 closely resembles analogous results obtained independently by Perry and Abraham (1988) and shown by Lemmon (1989) to be well described by a combination of a Gaussian process and an impulsive process defined by a model developed by Hall (1966). This observation has proved to be of considerable practical value in developing a noise/interference model because the Hall model involves simple analytical expressions.

Finally, the pdf of the phase of the Fourier transform is shown in Figure 10. Unlike the phase distribution in the time domain, the distribution in Figure 10 is clearly nonuniform.

To summarize, the results obtained thus far suggest that the noise/interference can be viewed as a combination of a Gaussian process and many narrowband interferers.

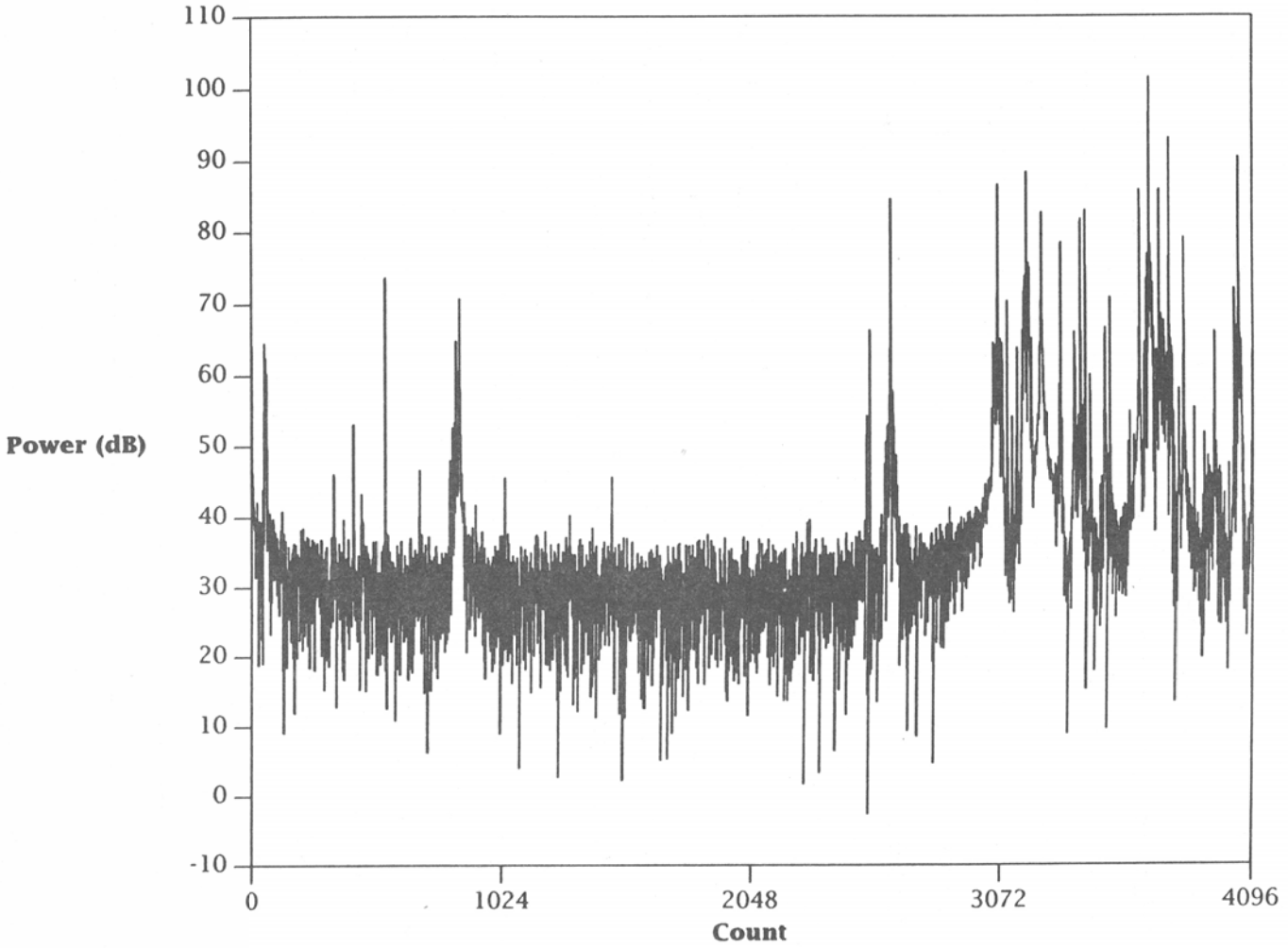

Figure 8. Power spectrum over a bandwidth of 1.024 MHz (case study 1).

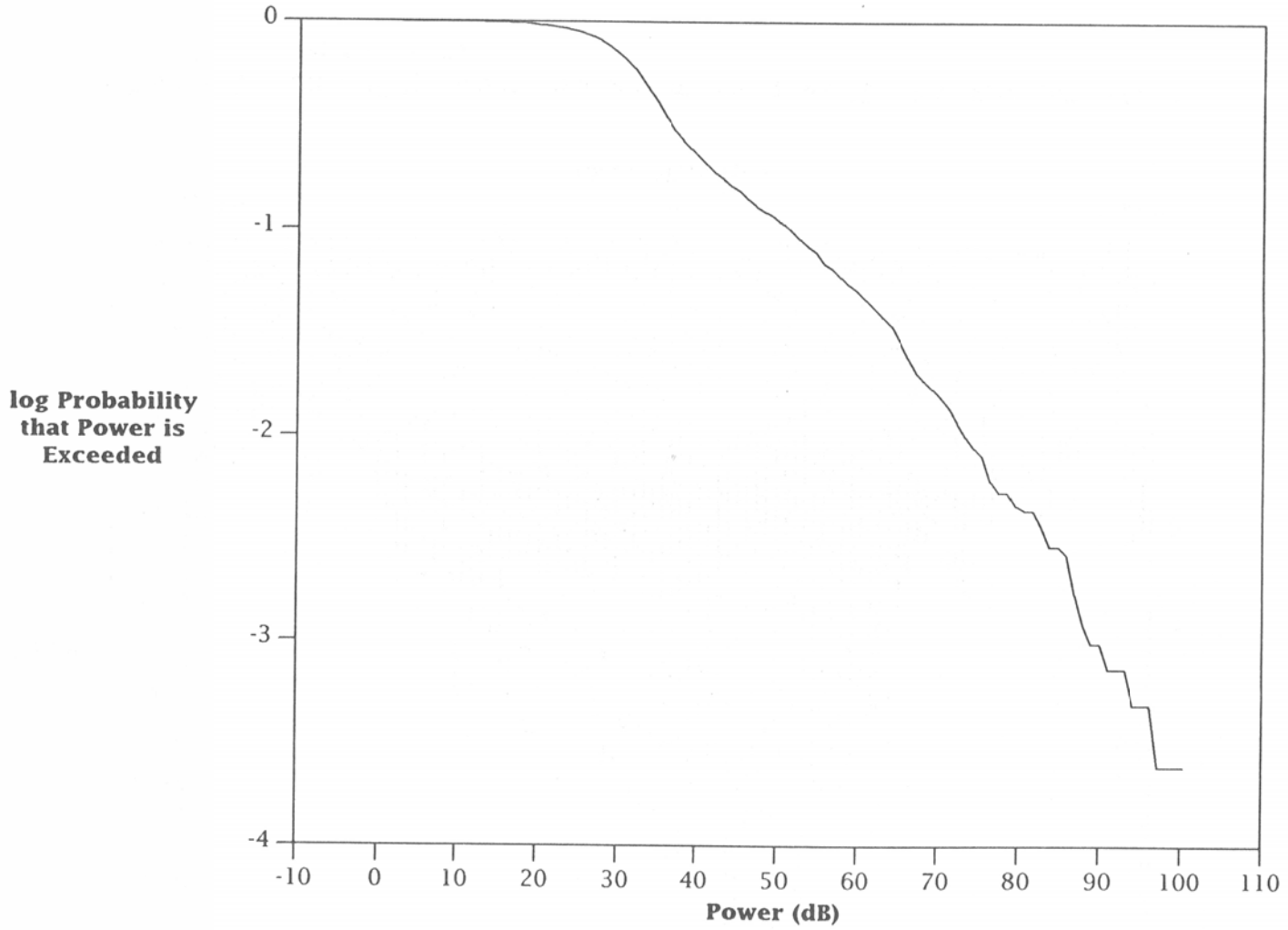

Figure 9. Cumulative distribution function of the power envelope in the frequency domain (case study 1).

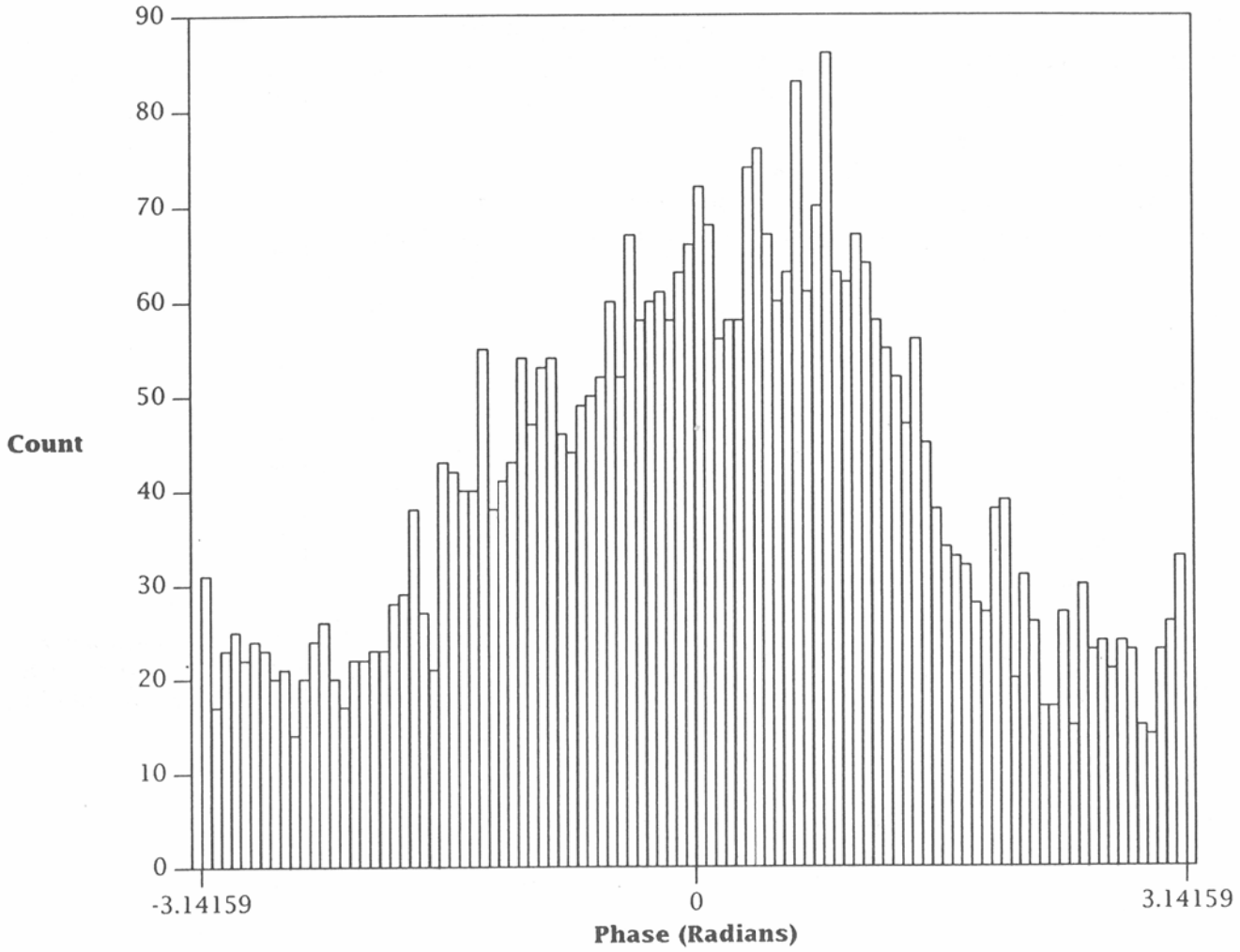

Figure 10. Probability density function of the phase in the frequency domain (case study 1).

2.3.2 Case Study 2.

This case study involves data that were obtained at 22:10:39 UT on 28 March 1989 at a center frequency of 19.29 MHz. A plot of the first 4 ms of the I-channel data is shown in Figure 11. This case was selected because the raw data shows a characteristic envelope modulation that is not present in most of the raw data records.

The pdf and the cdf of the power envelope in the time domain are shown in Figures 12 and 13, respectively. These distributions are qualitatively similar to the corresponding distributions in the previous case study, except that the pdf in the present case shows a more pronounced dip at small power levels. In terms of a Rician model (Gaussian noise combined with cw interferers), this simply means that the ratio of cw power to Gaussian power is greater in the present case.

It remains to explain the envelope modulation in the raw data. At first glance the modulation appears similar to the beating pattern resulting from the sum of two sine waves closely spaced in frequency, that is, a carrier at the average frequency, amplitude modulated by a sine wave of half the difference frequency. Note that modulation by a sine wave of half the difference frequency results in a beat frequency (number maxima of the envelope per unit time) equal to the frequency difference.

The power spectrum, shown in Figure 14, clearly reveals the presence of two strong narrowband interferers closely spaced in frequency, as well as a third, stronger interferer. However, the frequency difference between the two closely spaced interferers is approximately 8 kHz, whereas the beat frequency in the raw data is approximately 4 kHz. Moreover, a careful examination of the raw data shows that the positive voltage envelope does not coincide (in time) with the negative voltage envelope (as it does for the sum of two sine waves), but is displaced by one half cycle.

It can be shown, however, that the presence of a third sine wave, at the appropriate frequency, can indeed result in this type of pattern. To show that this is the case, one component of the spectral doublet was excised from the Fourier transform of the raw data, and the result was inverse Fourier transformed. The I-component of the resulting noise/interference is shown in Figure 15; the envelope modulation is clearly absent.

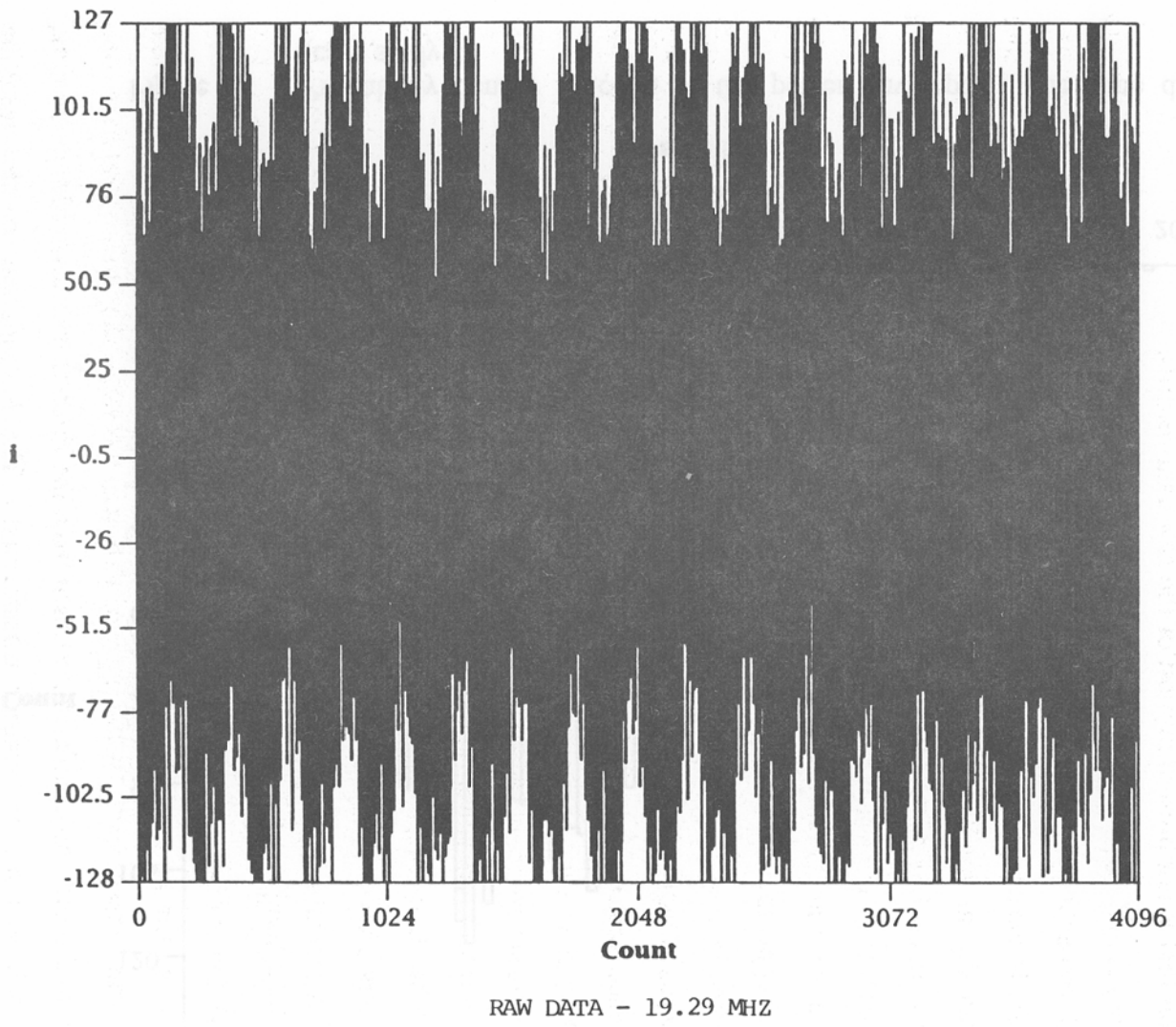

Figure 11. I-channel data at 19.29 MHz (case study 2).

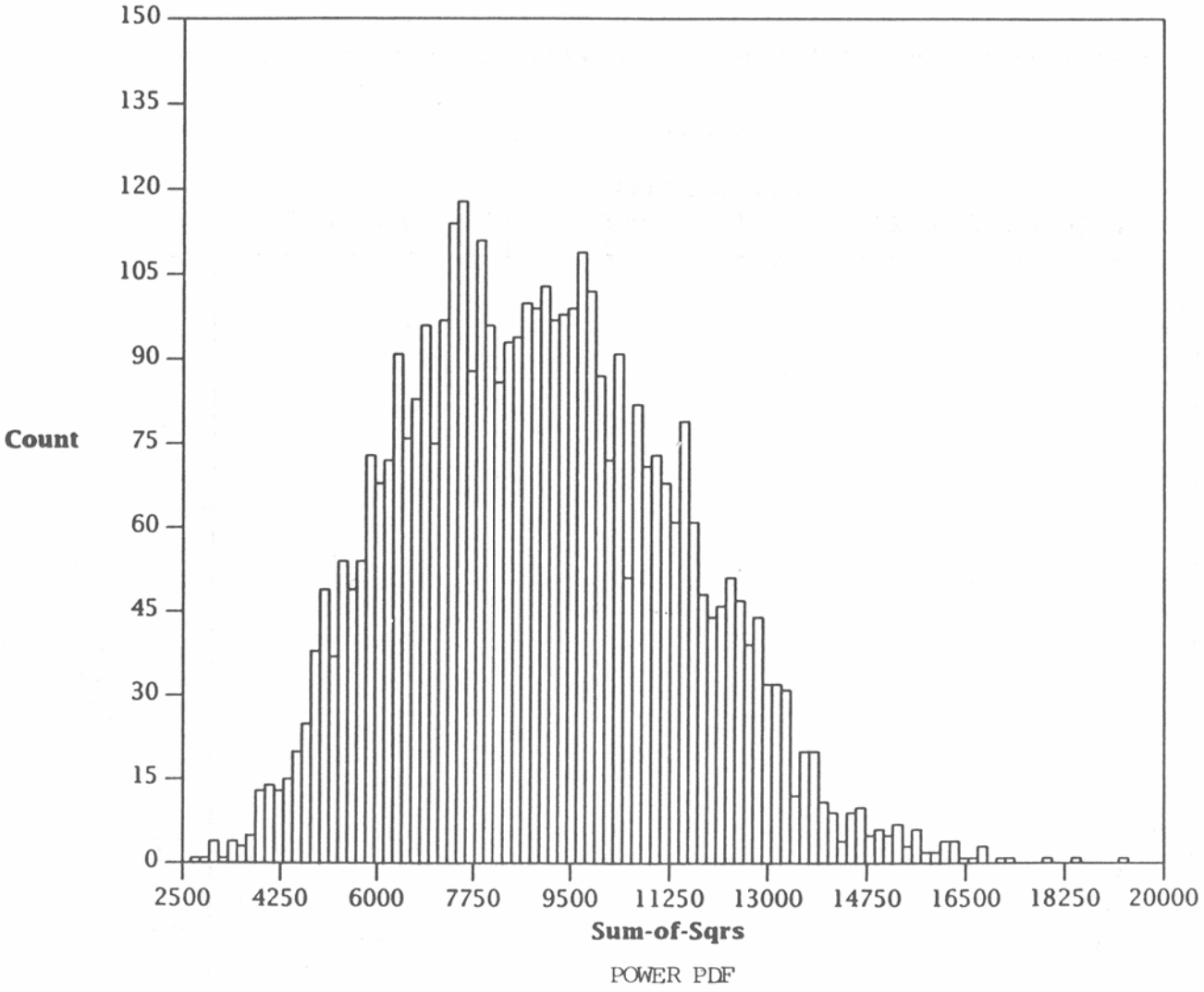

Figure 12. Probability density function of the power envelope in the time domain (case study 2).

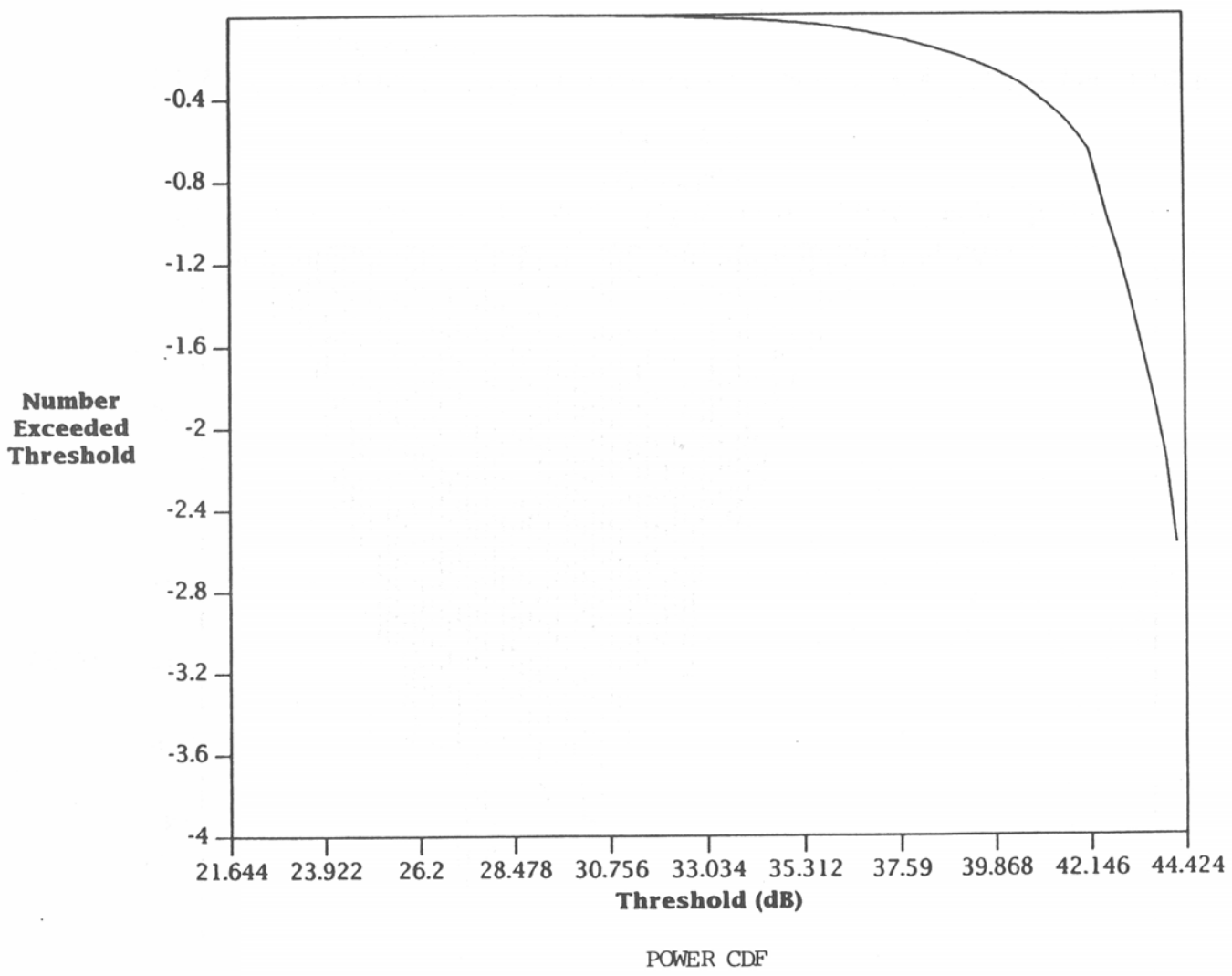

Figure 13. Cumulative distribution function of the power envelope in the time domain (case study 2).

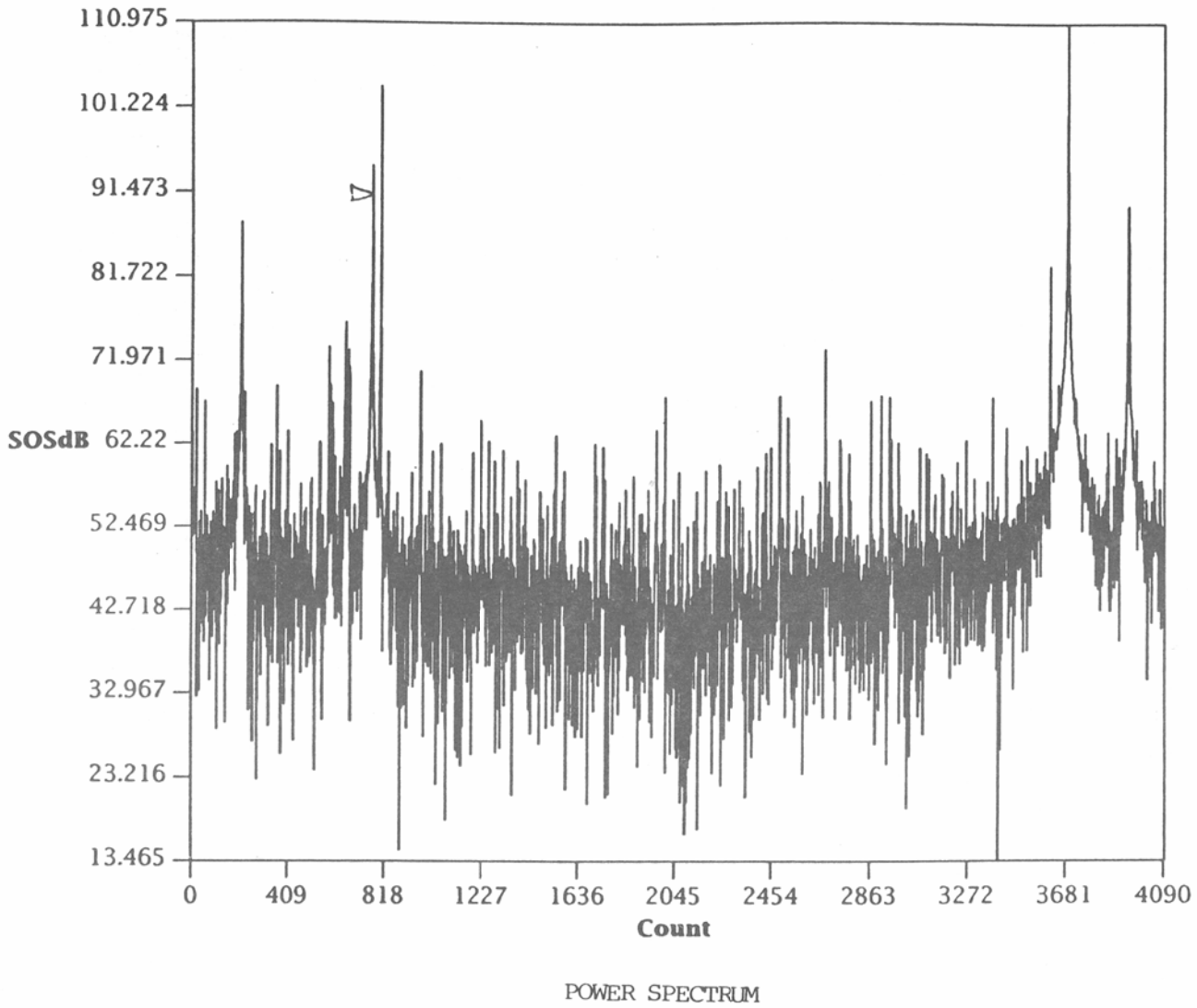

Figure 14. Power spectrum over a bandwidth of 1.024 MHz (case study 2).

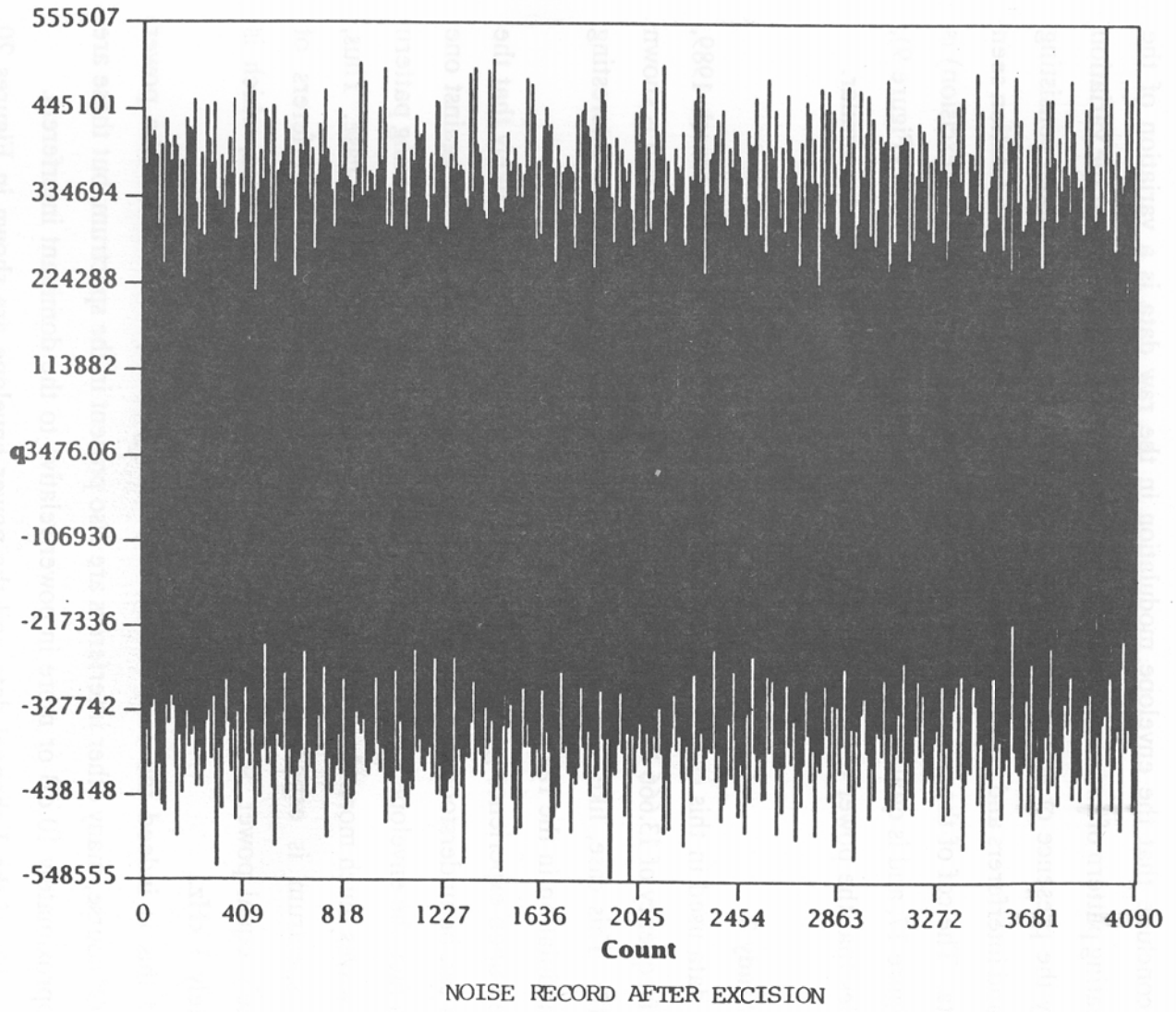

Figure 15. I-channel data after excision of a single narrowband interferer (case study 2).

It is also of interest to compare the pdf of the power envelope in the time domain after excision, shown in Figure 16, with the corresponding pdf before excision (Figure 12). The change in the shape of the pdf due to excision can be understood in terms of a Rician power distribution with a smaller ratio of cw power to Gaussian power.

We conclude that the envelope modulation in the raw data is a variation of the standard beating pattern of two closely spaced narrowband interferers, and that the variation is caused by the presence of additional narrowband interferers. Thus, a model consisting of narrowband interferers and Gaussian noise can account for the envelope modulation seen in these data. The cdf of the power envelope in the frequency domain (before excision) is shown in Figure 17, and is qualitatively similar to that in the previous case study (Figure 9), which implies that the power distribution of the narrowband interferers is also similar.

2.3.3 Case Study 3.

The data used in this case study were obtained at 10:26:47 UT on 28 March 1989, at a center frequency of 13.666 MHz. A plot of the first 4 ms of the I-channel data is shown in Figure 18. This case, like the previous case, was selected because of the interesting envelope modulation in the raw data.

Based upon experience gained from the previous case study, it seems likely that the modulation can be understood in terms of two narrowband interferers beating against one another. In fact, the envelope modulation in the present case resembles the beating pattern of two sine waves much more closely than does the modulation in the previous case. Thus, the power spectrum is expected to show two dominant narrowband interferers of approximately equal power, separated by the beat frequency in the raw data, which is approximately 3 kHz.

That this is indeed the case can be seen in Figure 19, which shows the power spectrum. Of course, many other interferers are also present in the spectrum, but these are down by approximately 10 dB or more in power relative to the dominant interferers.

The pdfs of the I-channel data and the power envelope are shown in Figures 20 and 21, respectively. These distributions resemble inverse power laws more closely than the corresponding pdfs in the previous case studies (the tails of Gaussian and Rician

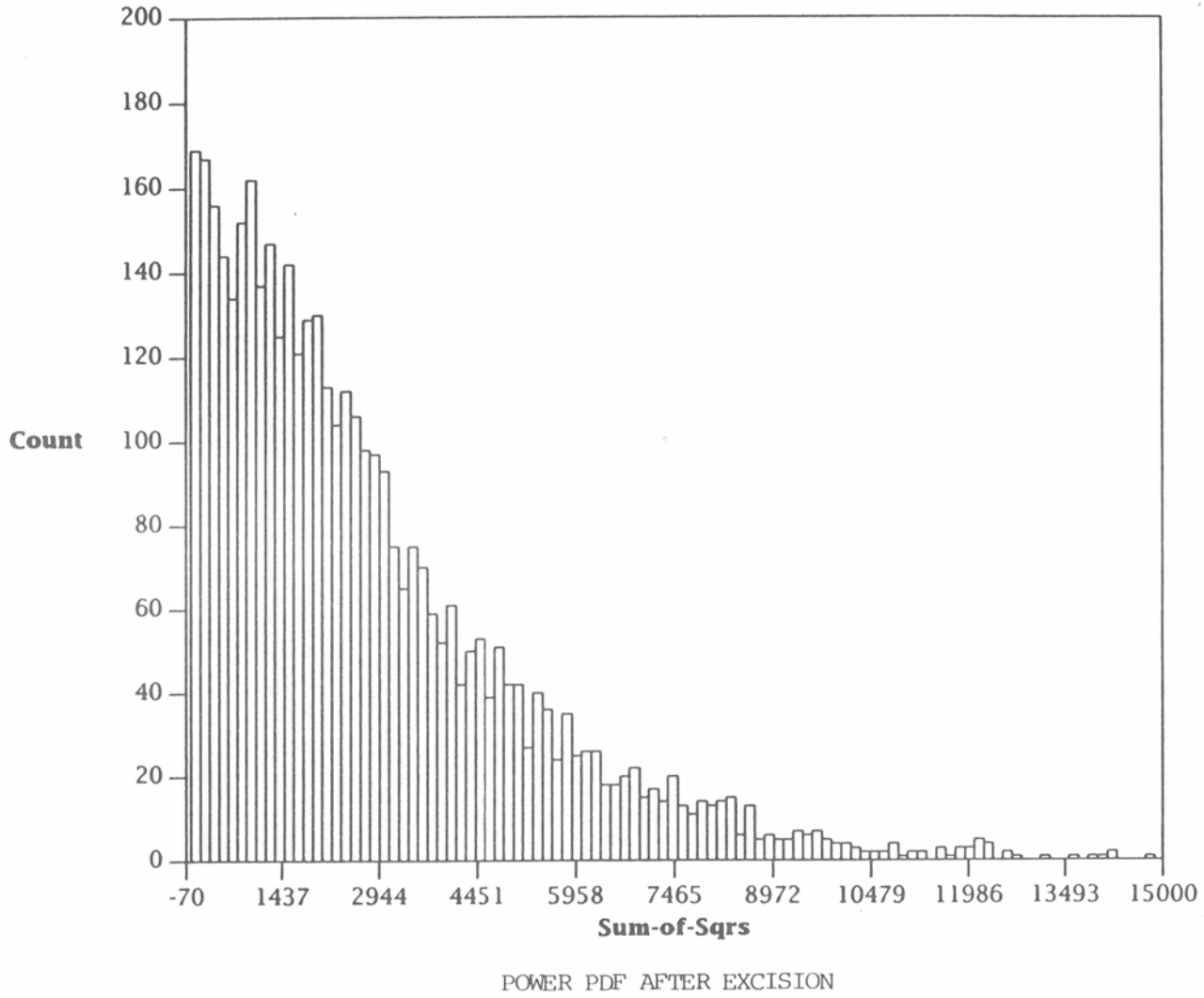

Figure 16. Probability density function of the power envelope in the time domain after excision of a single narrowband interferer (case study 2).

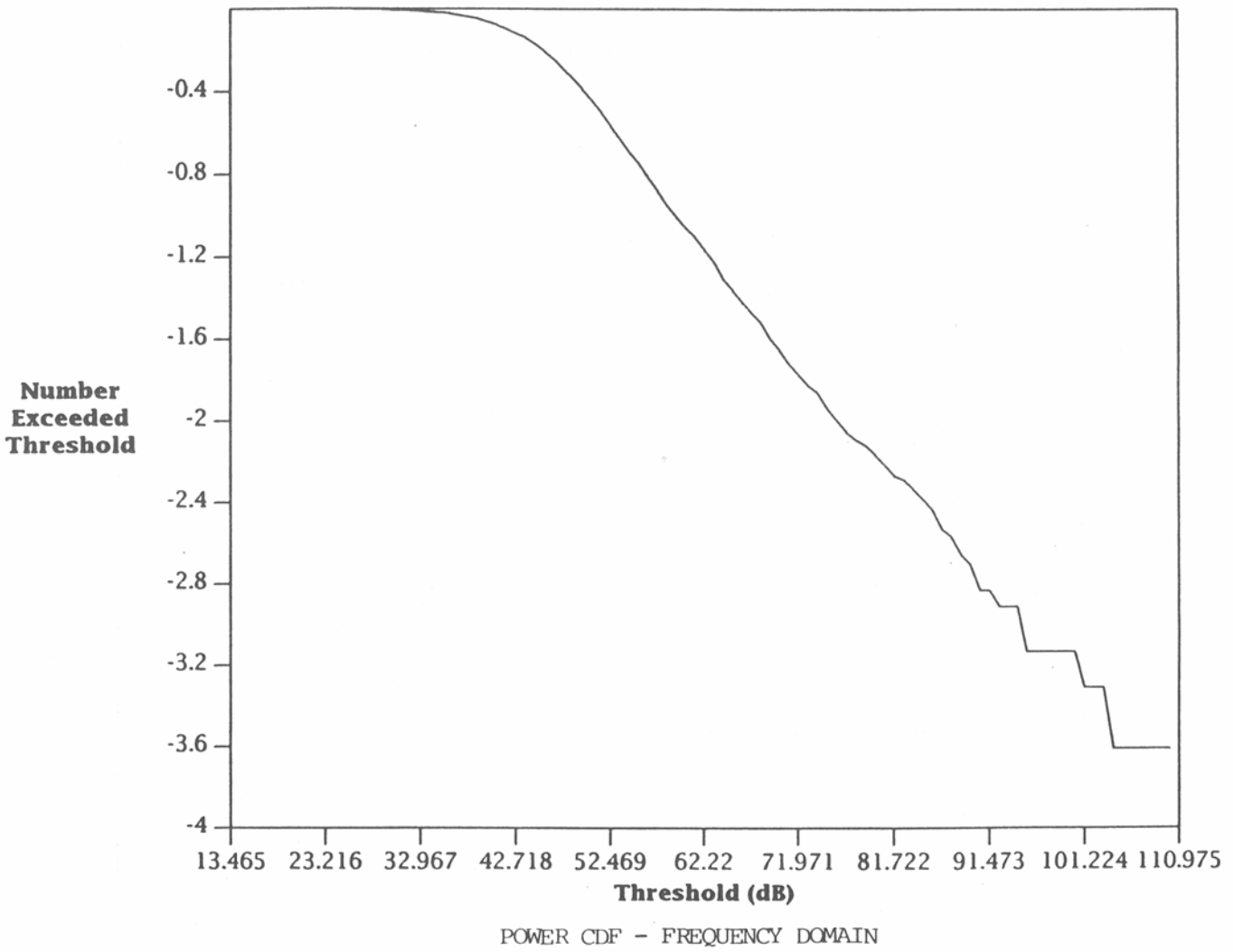

Figure 17. Cumulative distribution function of the power envelope in the frequency domain before excision (case study 2).

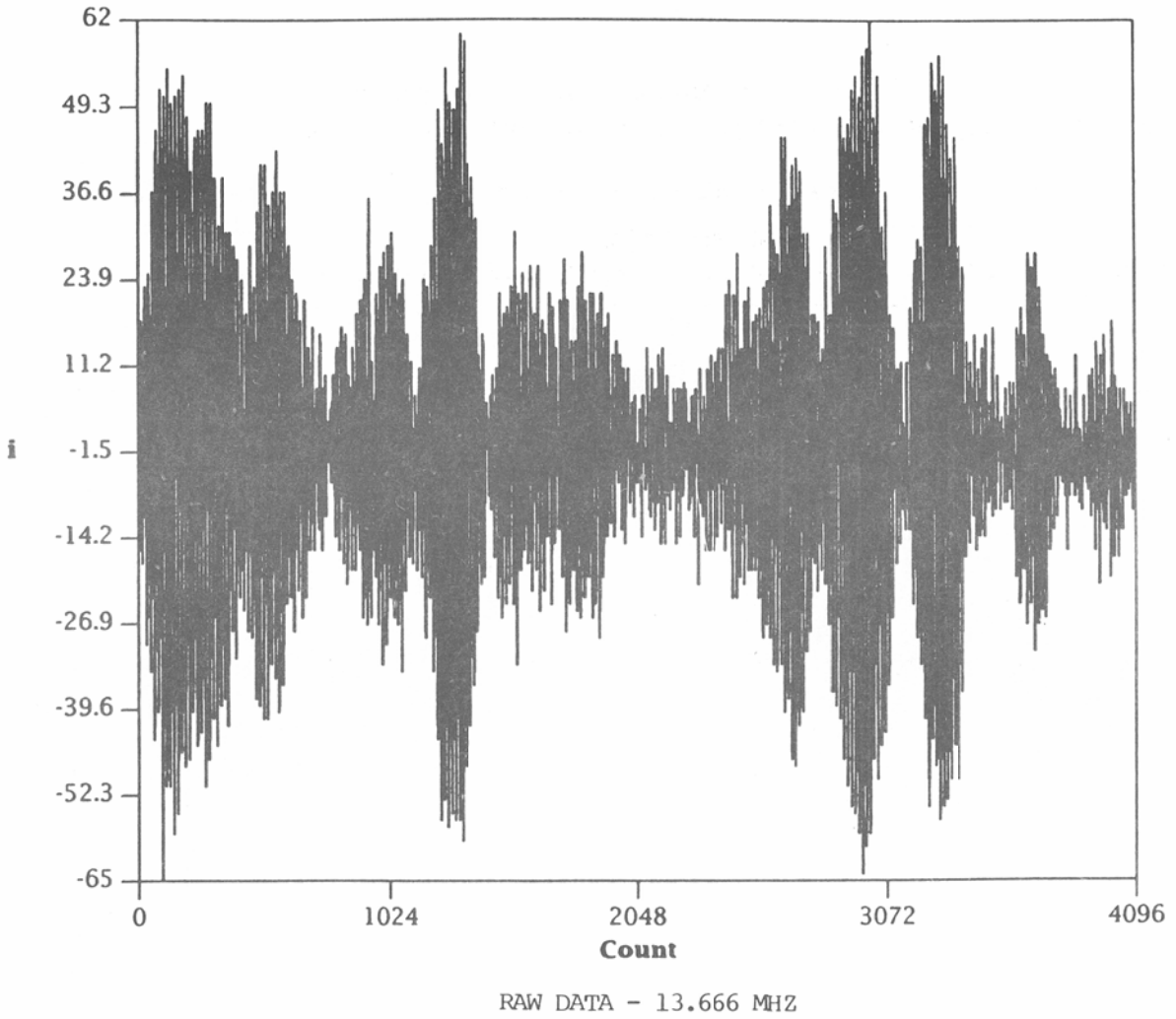

Figure 18. I-channel data at 13.666 MHz (case study 3).

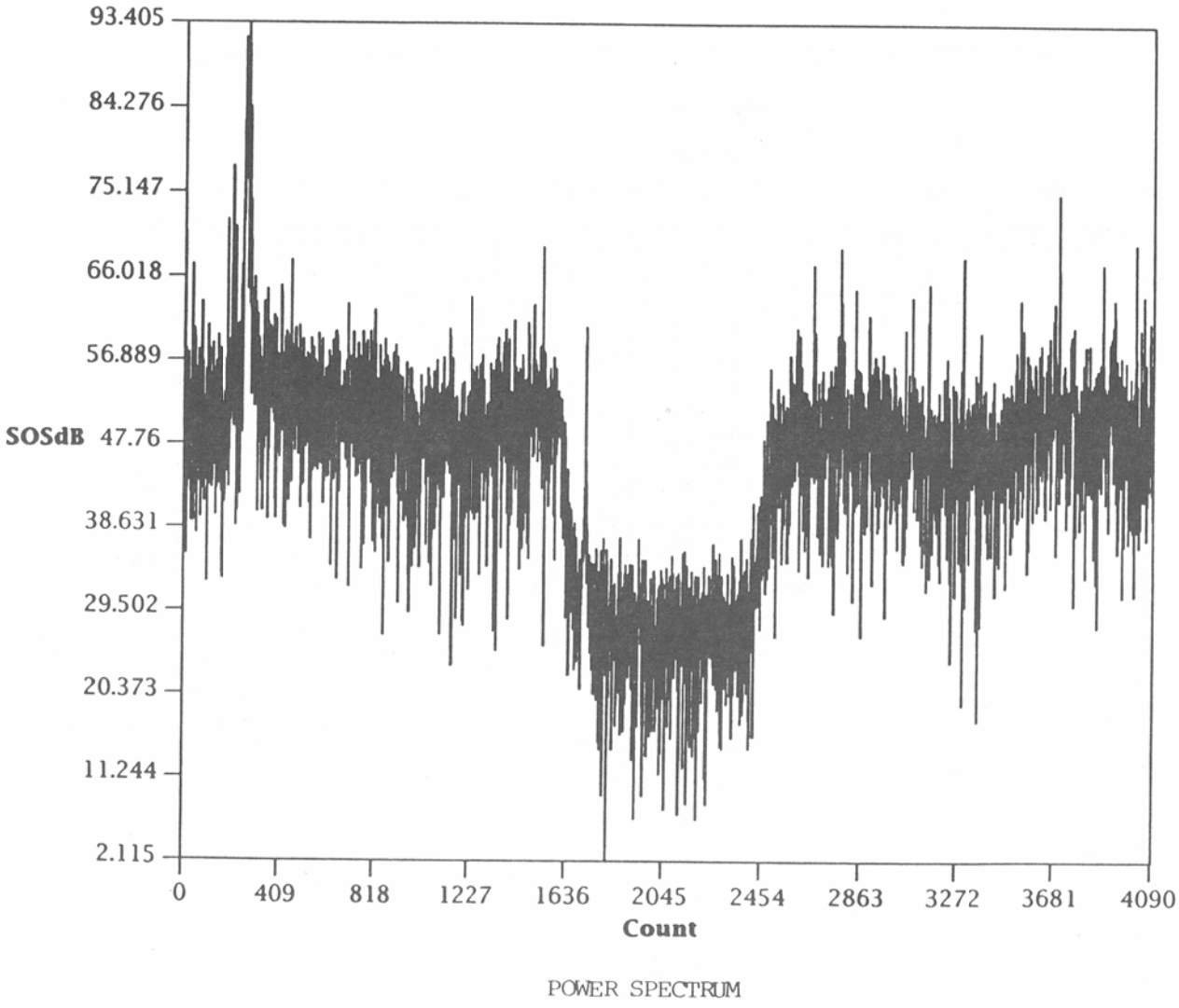

Figure 19. Power spectrum over a bandwidth of 1.024 MHz (case study 3).

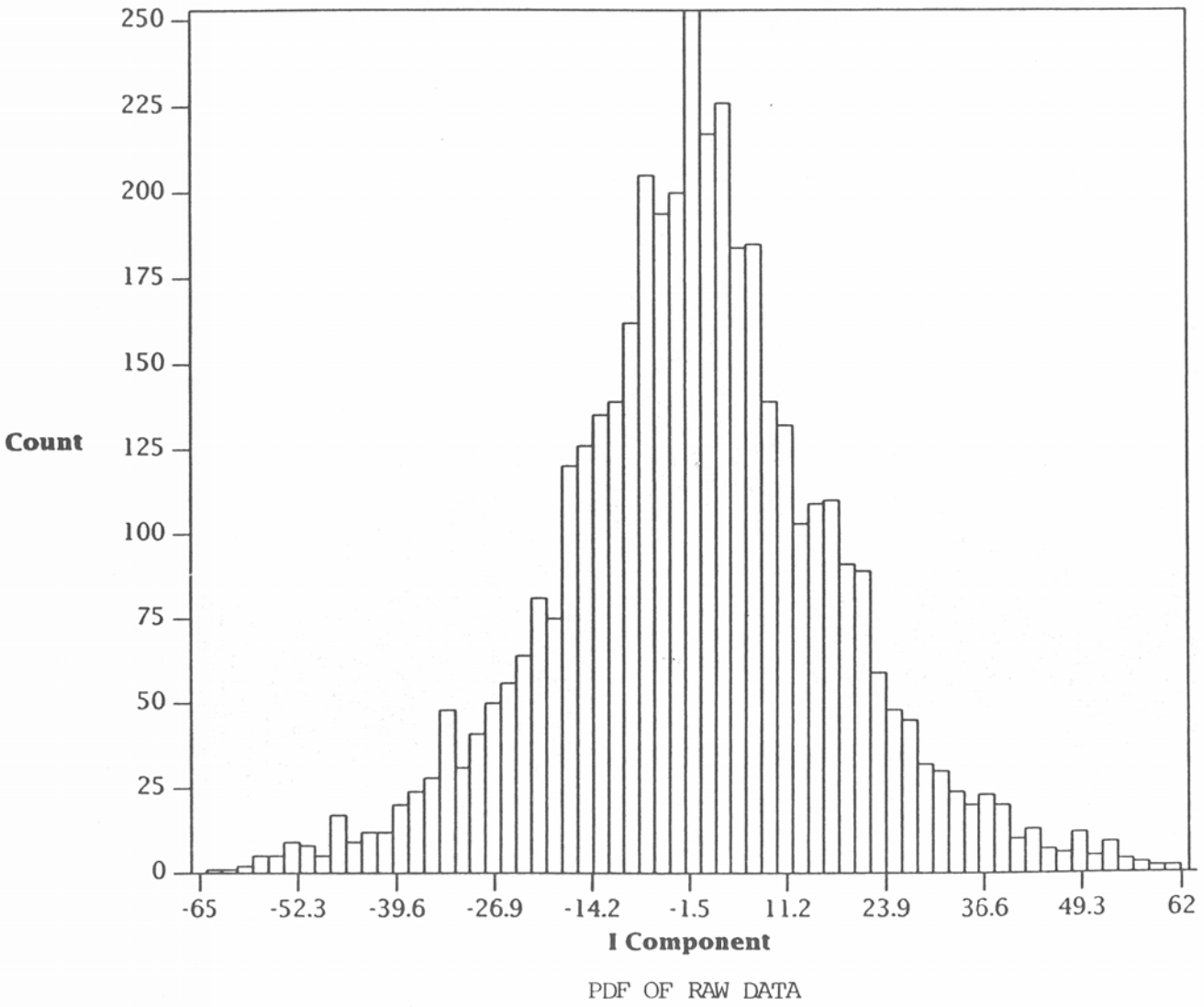

Figure 20. Probability density function of the I-channel data (case study 3).

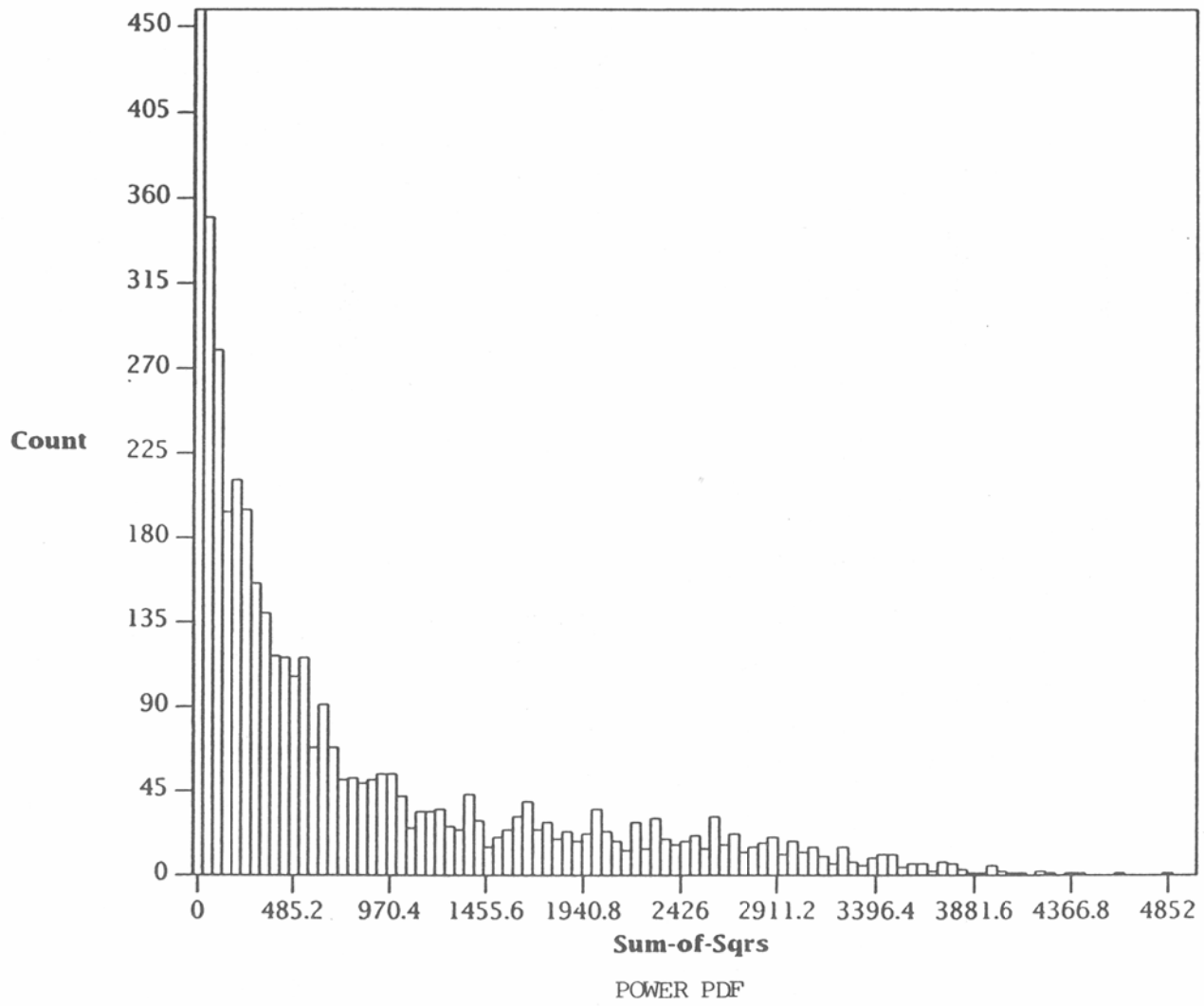

Figure 21. Probability density function of the power envelope in the time domain (case study 3).

distributions fall off exponentially). The existence of long tails is suggestive of an impulsive phenomenon; examples of this are discussed below. However, the cdf of the power envelope in the present case, shown in Figure 22, appears qualitatively similar to those of the previous cases. Thus, the appearance of the distributions in Figures 20 and 21 is presumably due to the strong envelope modulation in the raw data, and is not due to a truly impulsive process.

The cdf of the power envelope in the frequency domain is shown in Figure 23, and is also similar to those of previous cases, although the tail of the distribution is somewhat more pronounced. However, it will be shown in Section 3 that a combination of Gaussian noise and cw interferers whose amplitudes are distributed according to the Hall model can generate frequency domain cdfs which are quite similar to that in Figure 23, as well as those in the previous cases, depending on the values of the model parameters.

We conclude that once again the noise/interference can be viewed as a combination of a Gaussian process and many narrowband interferers.

2.3.4 Case Study 4.

The data in this case study were obtained at 02:31:33 UT on 29 March 1989, at a center frequency of 13.666 MHz. A plot of the first 4 ms of the I-channel data is shown in Figure 24. This case was selected because of the periodic oscillations in the data, which suggest that the noise/interference is dominated by a single strong narrowband interferer.

The pdf of the I-channel data is shown in Figure 25, and does indeed resemble the pdf for a single sine wave (recall that the pdf for the process $x=A \sin(\omega t)$ is $p(x) = 1/\pi\sqrt{(A^2-X^2)}$). The power spectrum is shown in Figure 26, and does reveal the presence of a single strong narrowband interferer whose power is more than 10 dB greater than that of any of the other interferers.

Nevertheless, it would be incorrect to conclude that the statistics of the noise/interference can be described by those of a single narrowband interferer. The power pdf's in both time and frequency for a single sine wave consist of delta functions, and the cdf's therefore consist of step functions. On the other hand, the cdf's of the power envelope

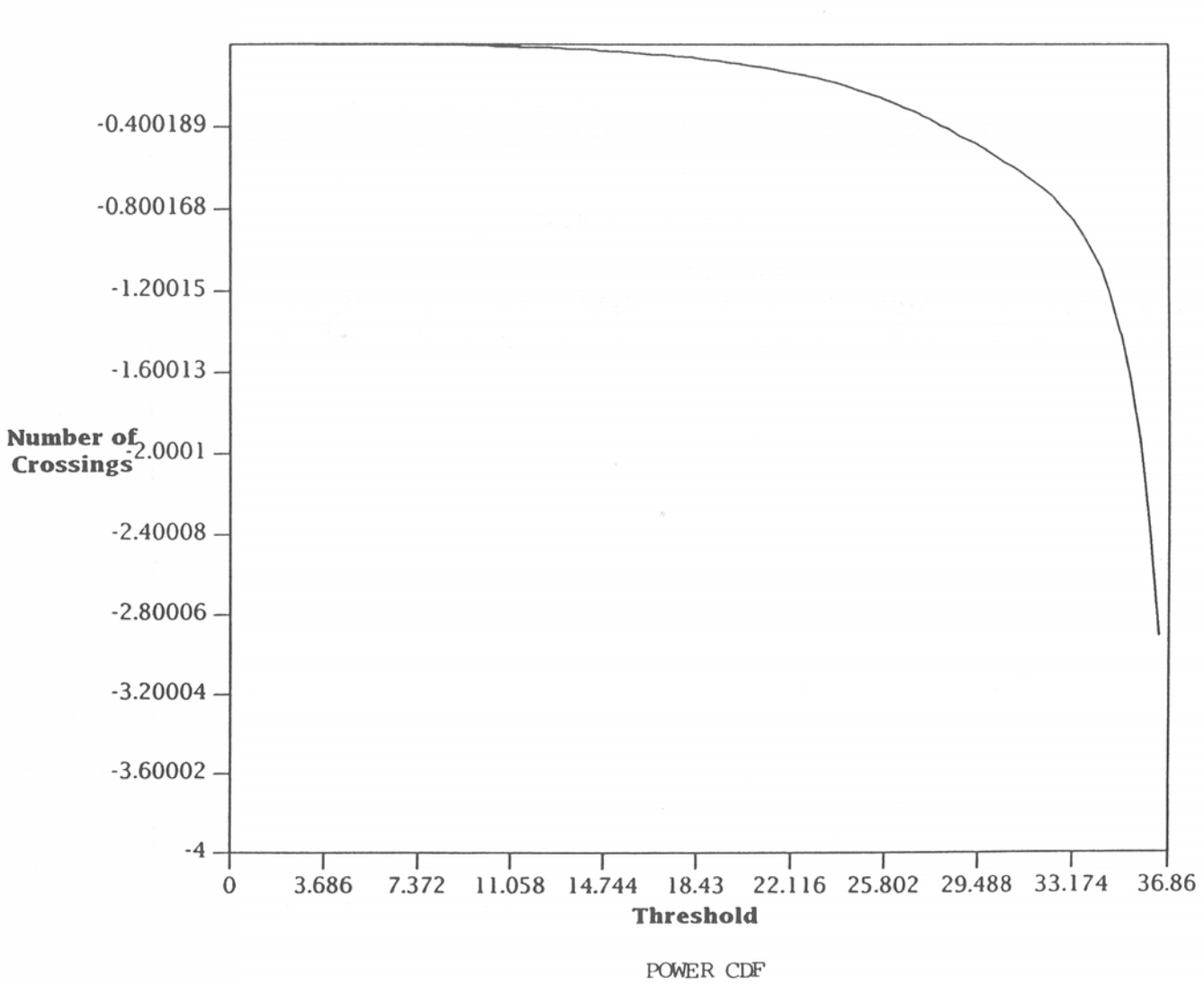

Figure 22. Cumulative distribution function of the power envelope in the time domain (case study 3).

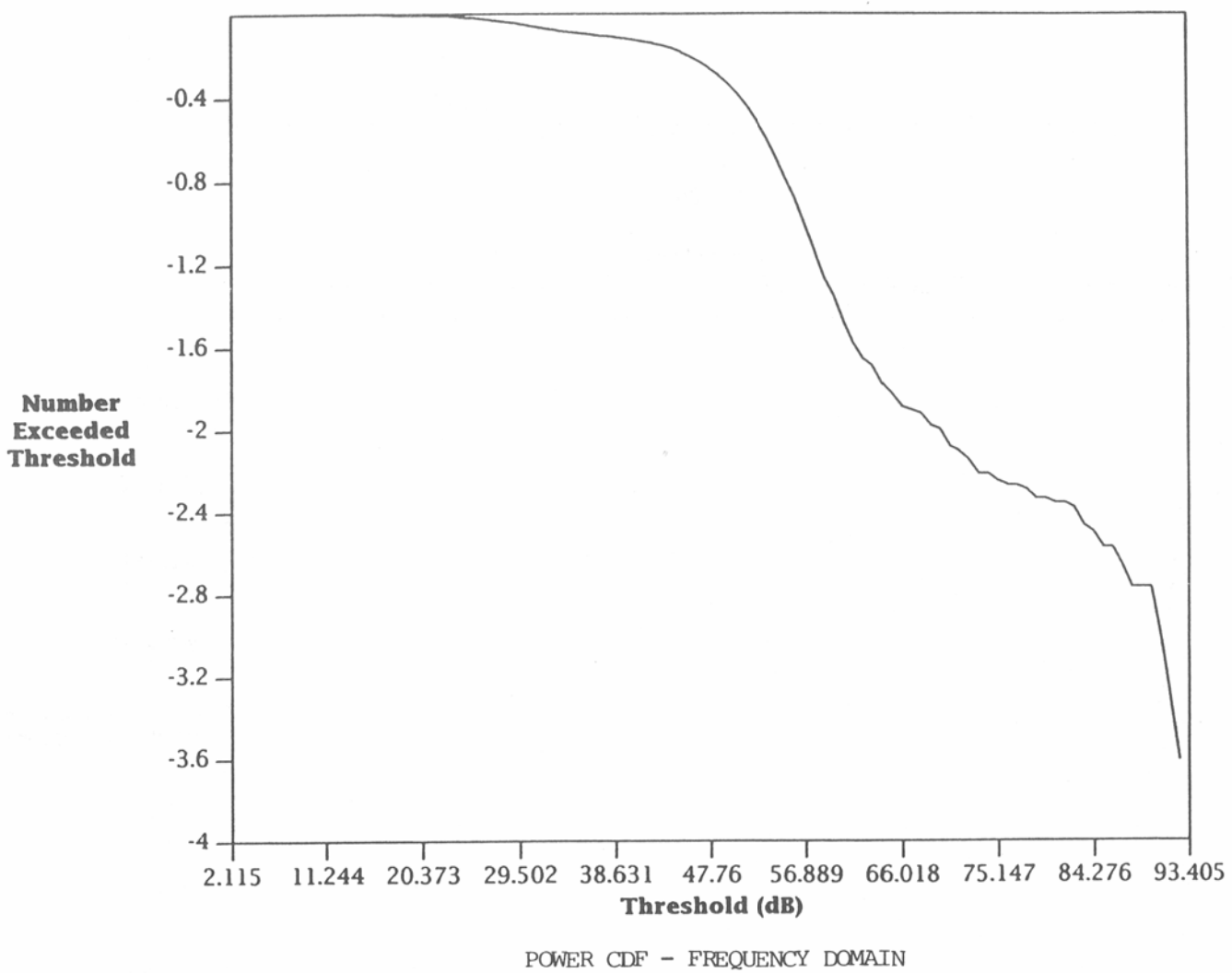

Figure 23. Cumulative distribution function of the power envelope in the frequency domain (case study 3).

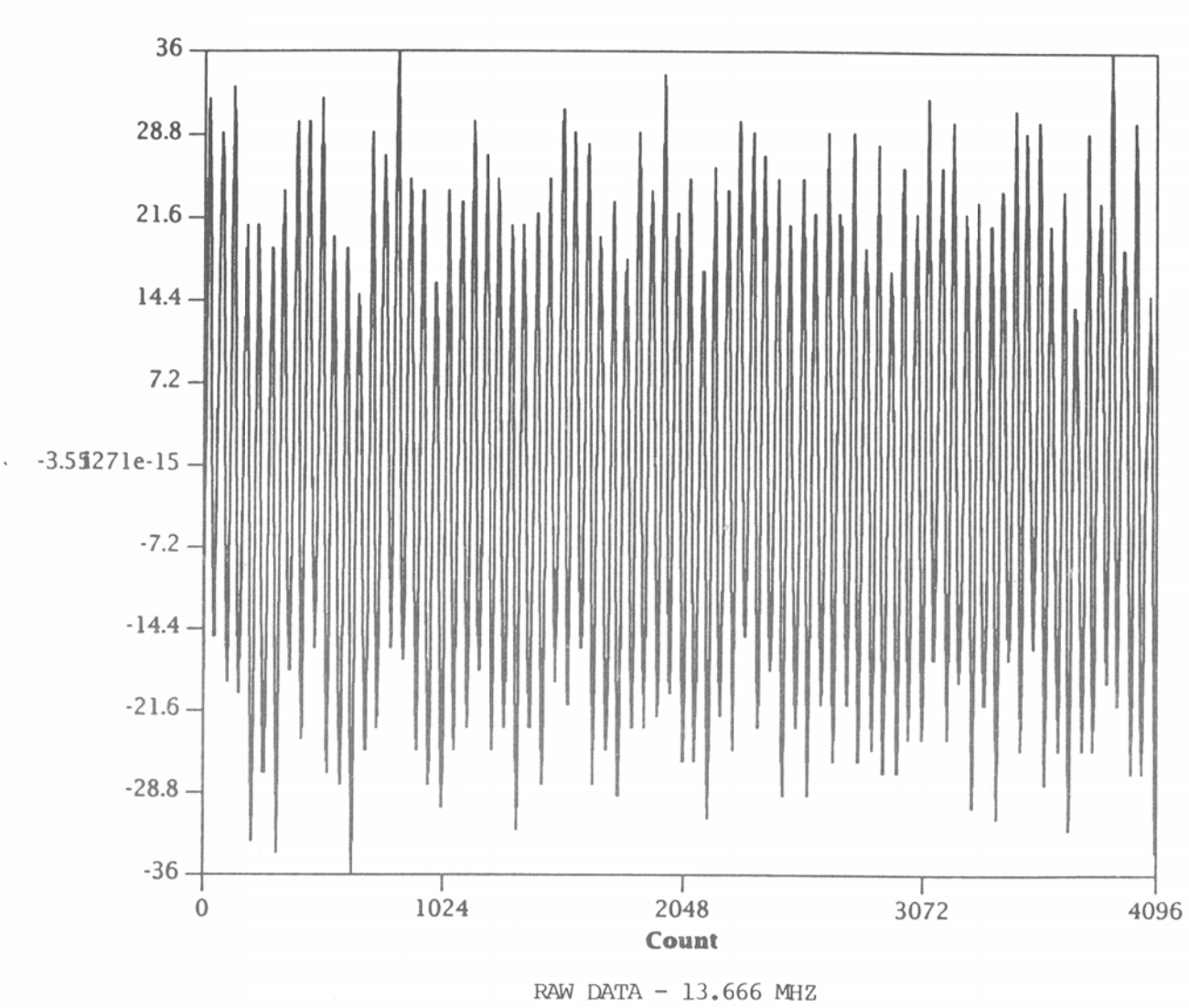

Figure 24. I-channel data at 13.666 MHz (case study 4).

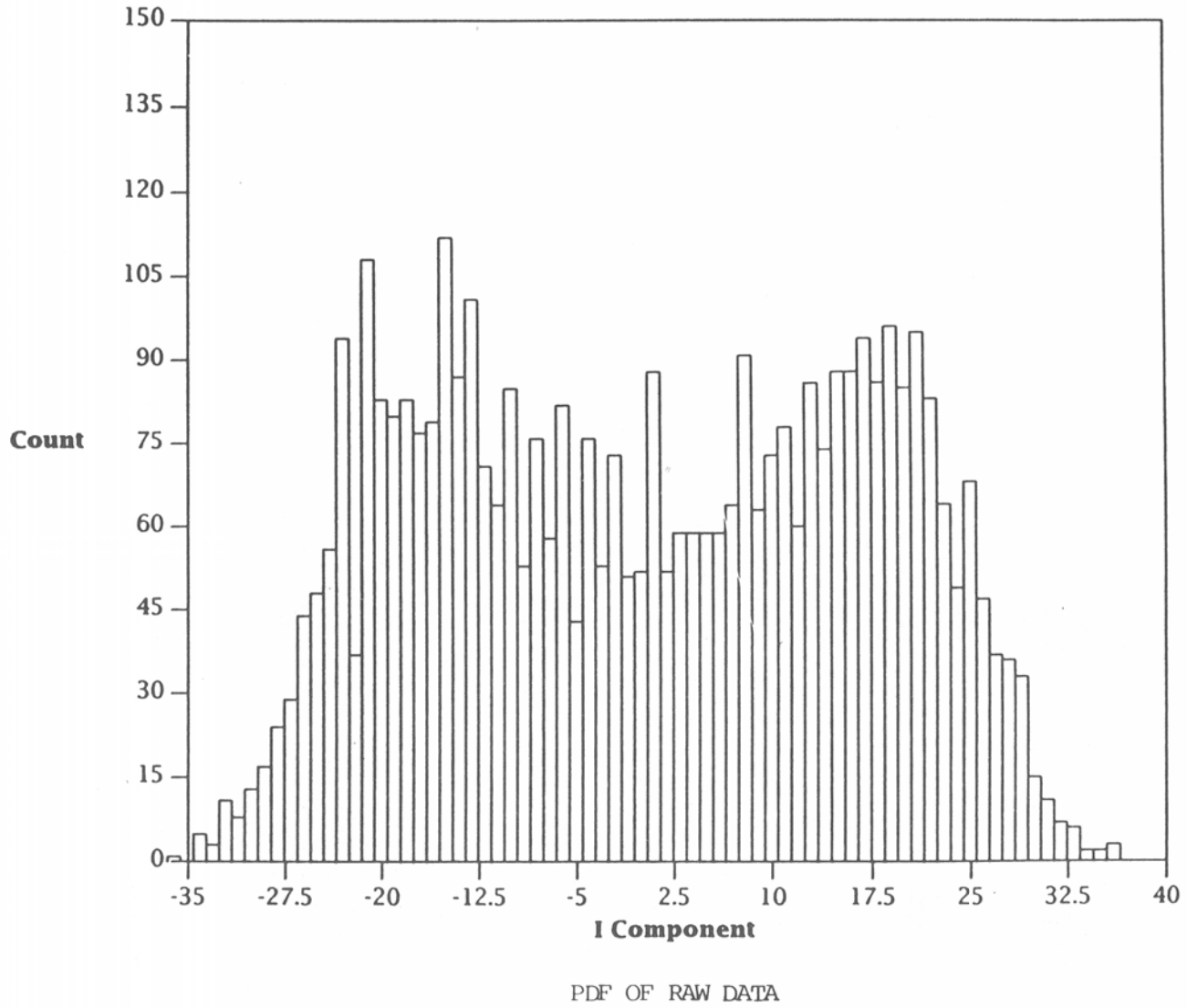

Figure 25. Probability density function of the I-channel data (case study 4).

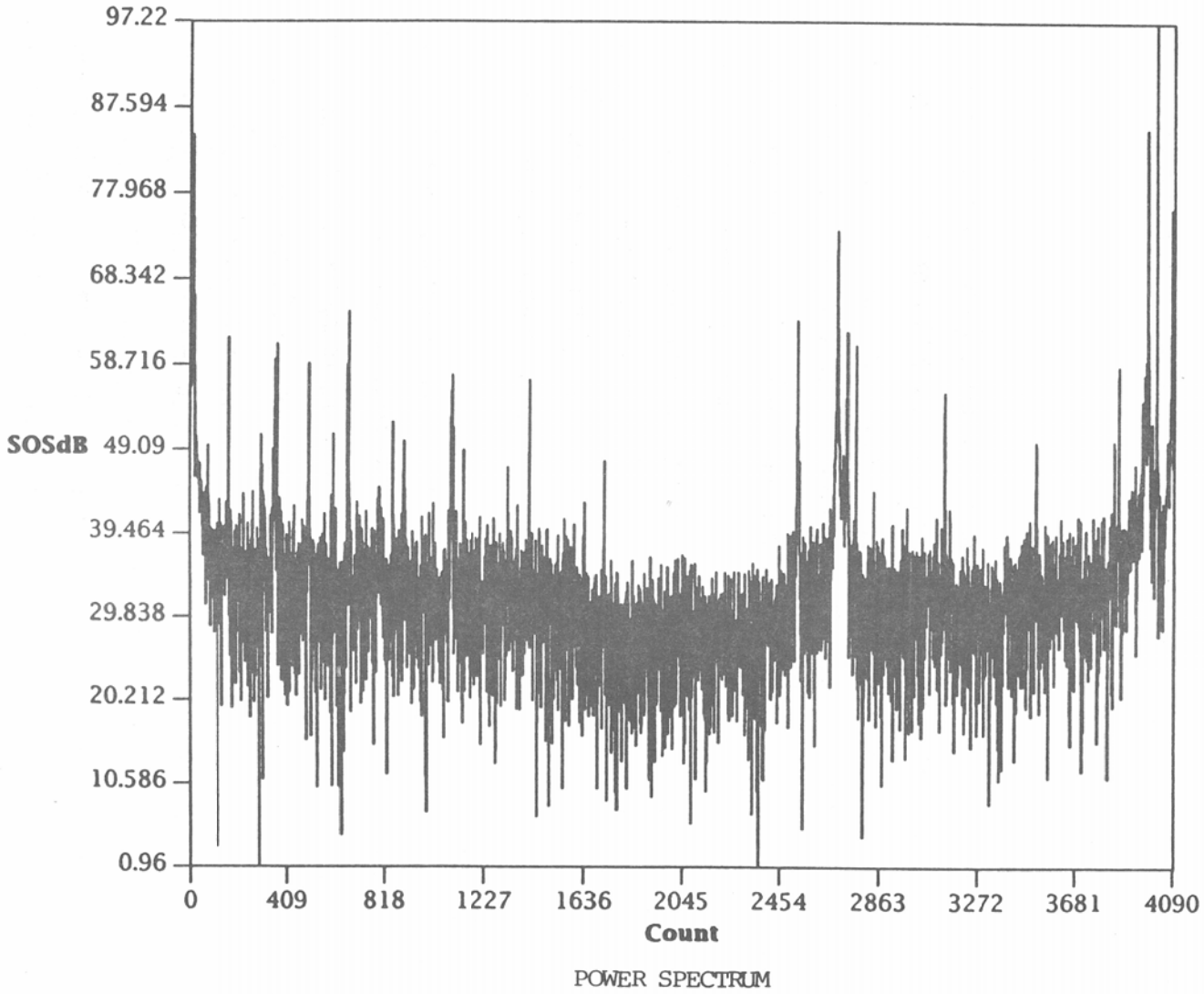

Figure 26. Power spectrum over a bandwidth of 1.024 MHz (case study 4).

of the noise/interference in the time and frequency domains are shown in Figures 27 and 28, respectively. These cdf's are clearly not step functions, and in fact resemble the cdf's of the previous case studies. In modeling the noise/interference it is therefore important to take into account the presence of the many narrowband interferers and the Gaussian noise even though the noise/interference power is dominated by a single interferer.

2.3.5 Case Study 5.

The data in this case study were obtained at 19:22:31 UT on 15 March 1989 at a center frequency of 23.862 MHz. A plot of the first 4 ms of the I-channel data is shown in Figure 29. This case was selected because of the impulsive nature of the noise. Of the 42 noise records examined in this study, this noise record is the only one that clearly exhibits impulsive noise in the raw data. The origin of the noise pulses is unknown, but is almost certainly not atmospheric noise. The reason is because the noise pulses do not occur randomly in time, but appear to occur in a quasi-periodic fashion. For example, Figure 30 shows 4 ms of the I-channel data from another part of the I-second noise record (not the first 4 ms shown in Figure 29). The noise pulses are not precisely periodic in time, but tend to be separated by approximately .5 ms; thus, the source of the impulses has been assumed to be of manmade origin.

In this particular noise record the quantization of the noise samples is apparent from inspection of Figures 29 and 30. The reason is presumably because the gain of the HF receiver was decreased to prevent the noise impulses from saturating the system, so that the voltage level of the noise floor was comparable to the resolution of the A/D converters.

The pdf's of the I-channel data and the power envelope for the first 4 ms of the noise record are shown in Figures 31 and 32, respectively. These results appear qualitatively similar to those of the previous case studies, except for the appearance of long tails in the distributions at high voltage (power) levels, which are the hallmark of an impulsive process. The tail in the power distribution is more readily apparent in the power cdf plotted on logarithmic scales, shown in Figure 33.

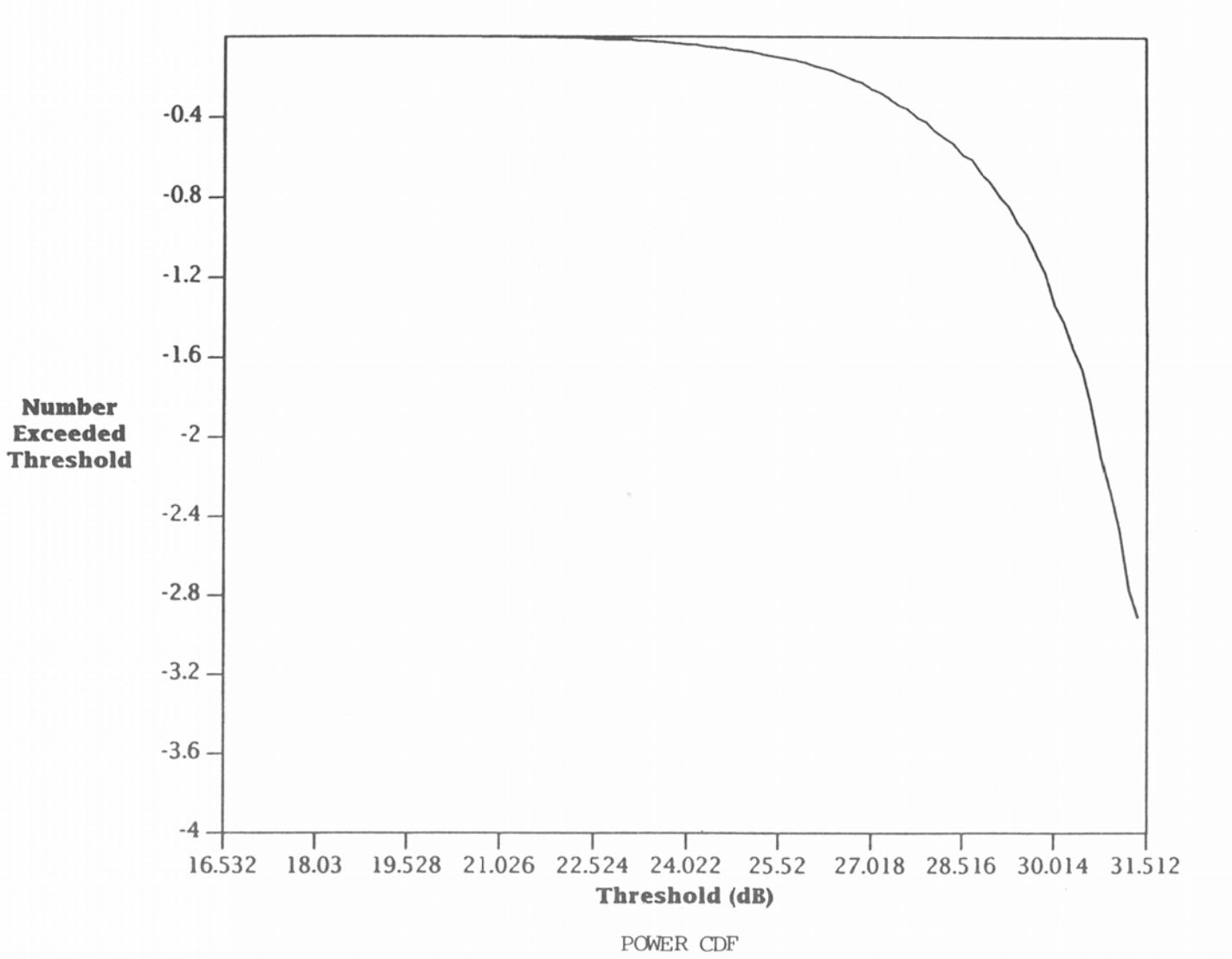

Figure 27. Cumulative distribution function of the power envelope in the time domain (case study 4).

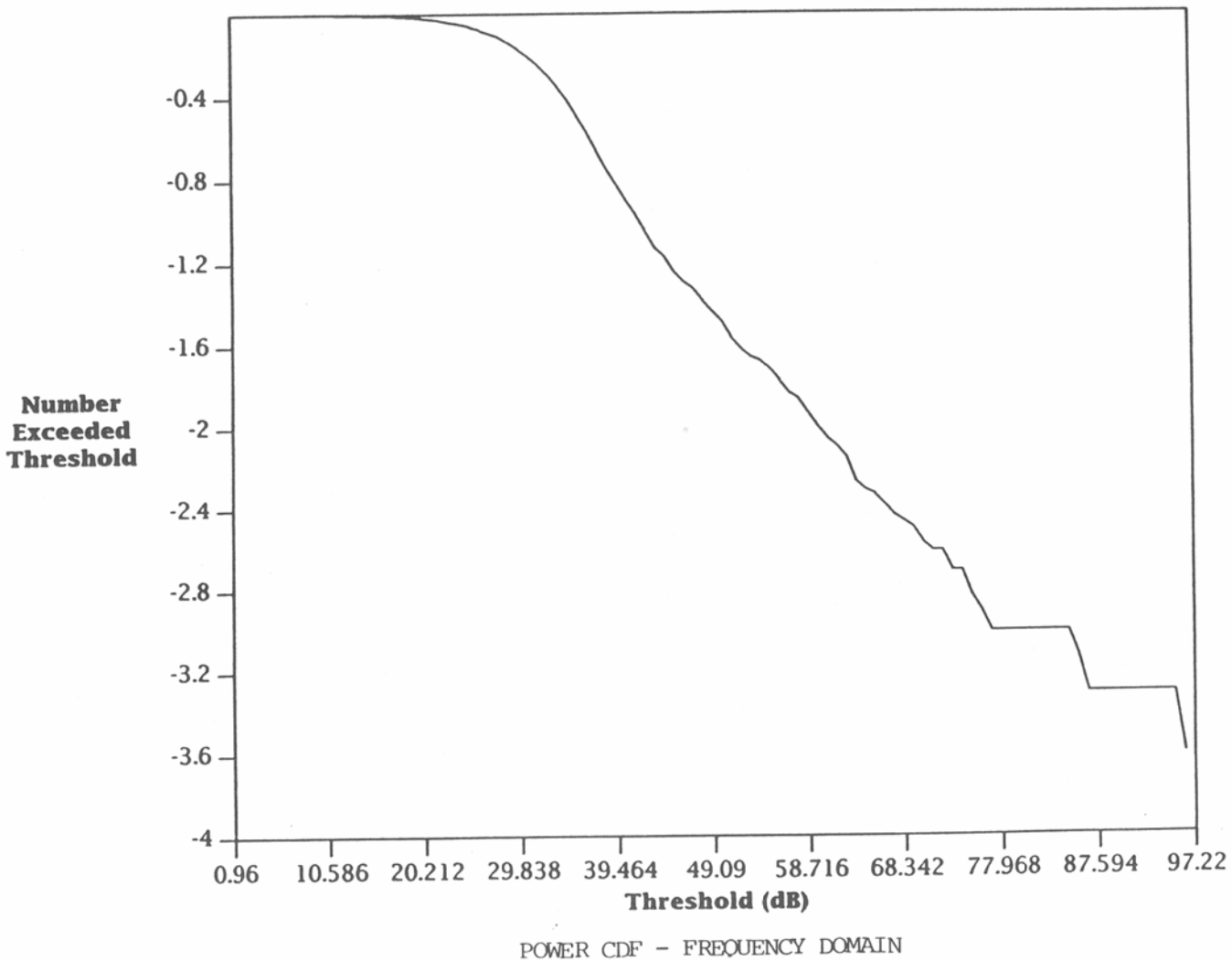

Figure 28. Cumulative distribution function of the power envelope in the frequency domain (case study 4).

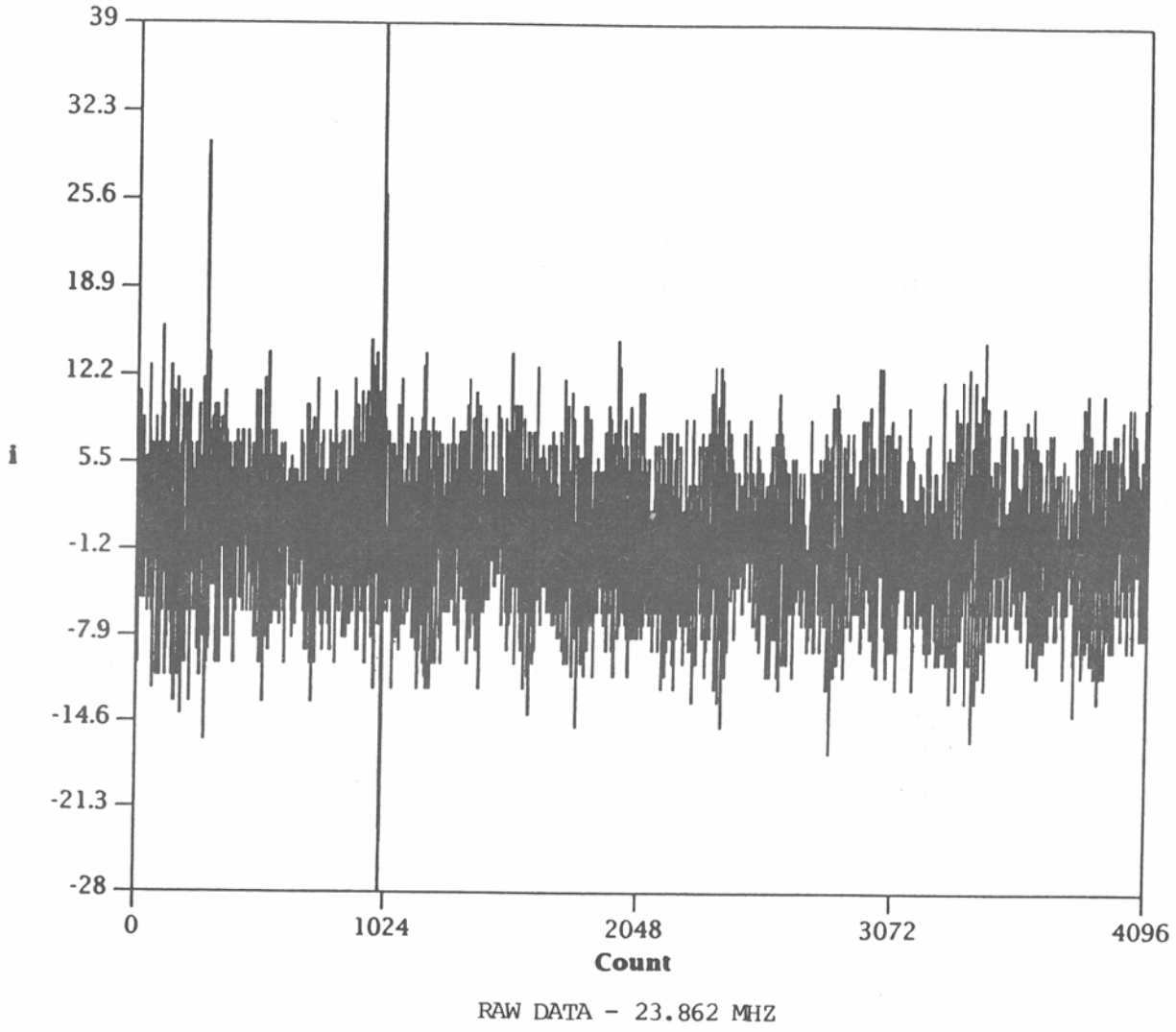

Figure 29. I-channel data at 23.862 MHz (case study 5).

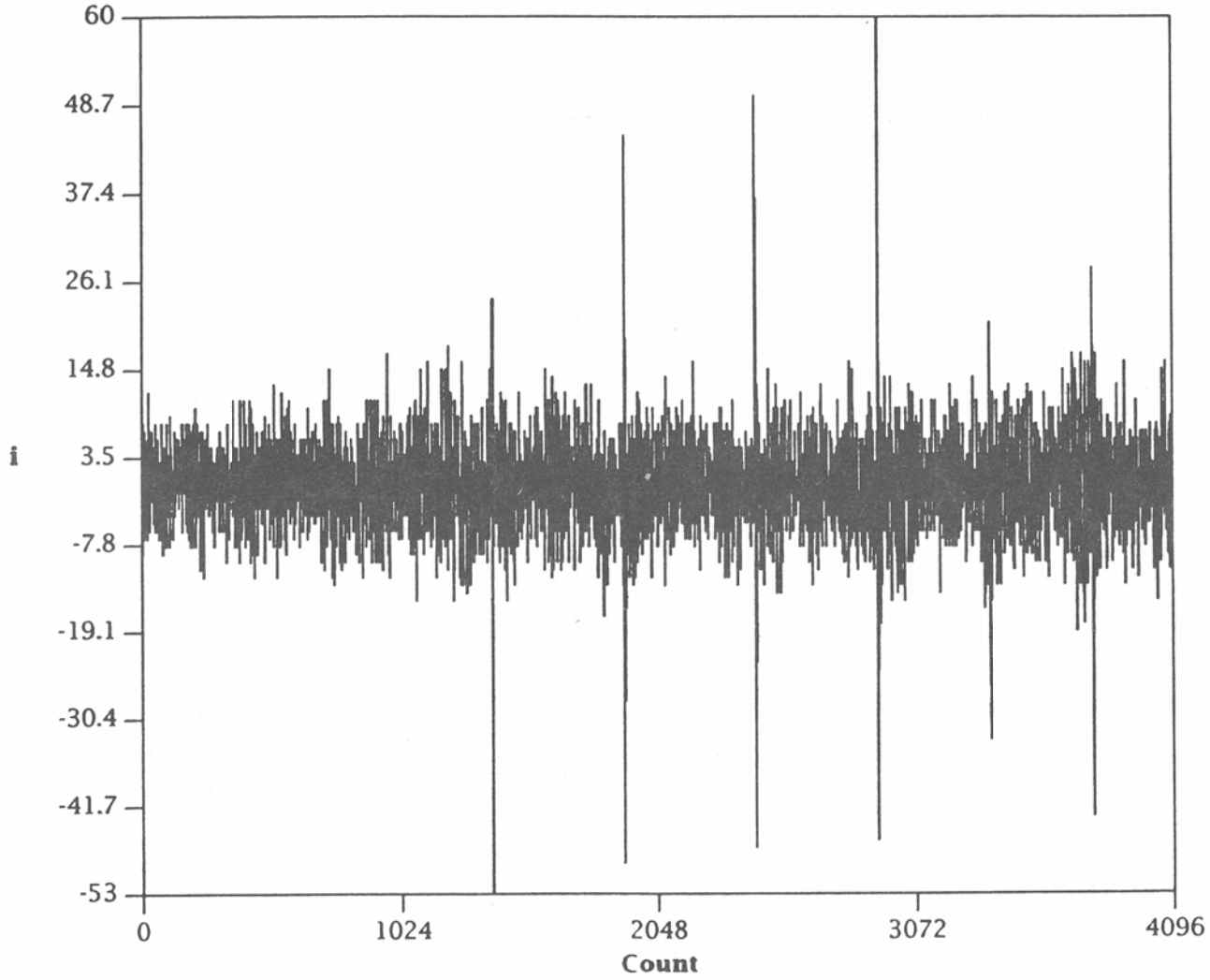

Figure 30. I-channel data at 23.862 MHz (case study 5).

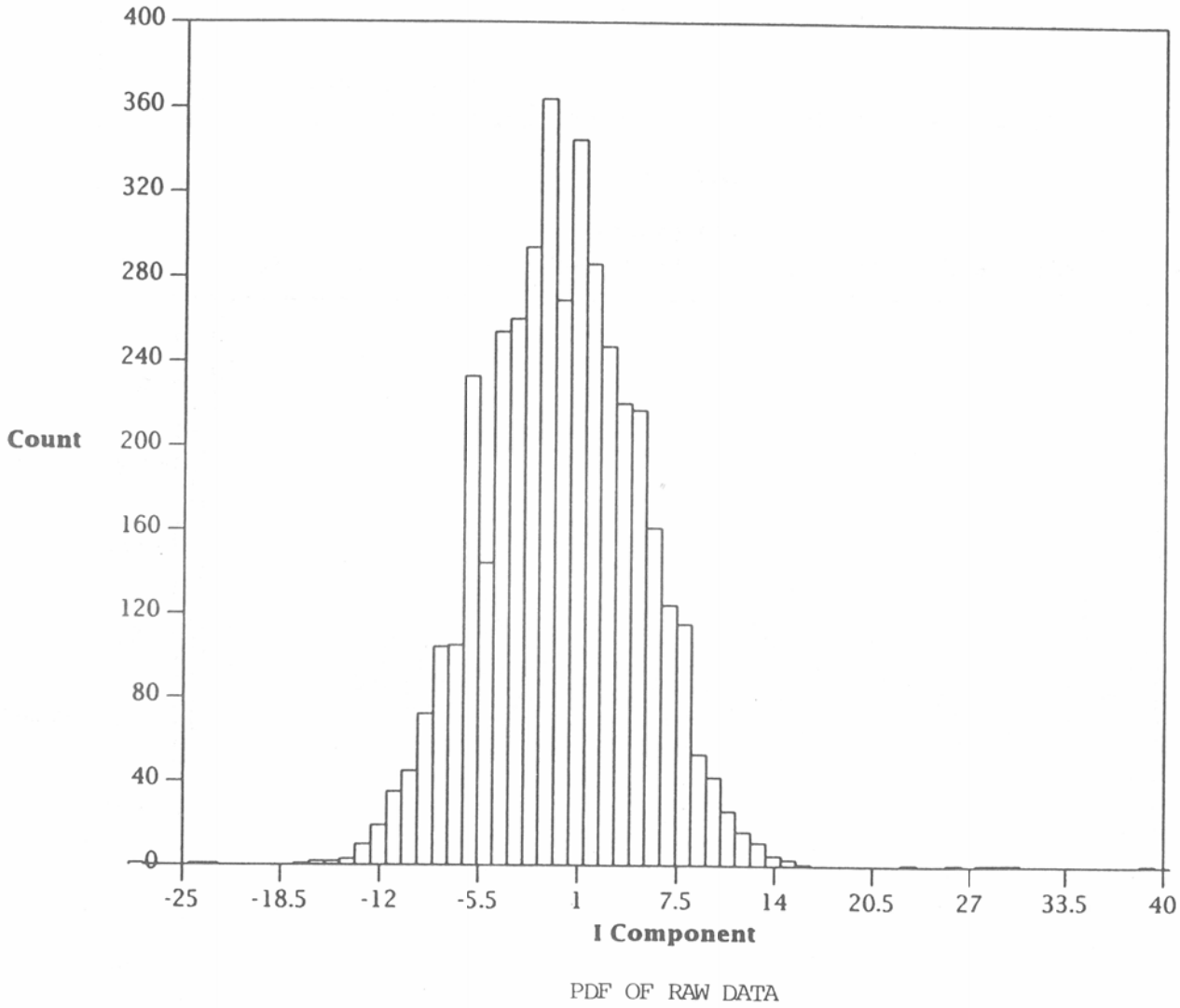

Figure 31. Probability density function of the I-channel data (case study 5).

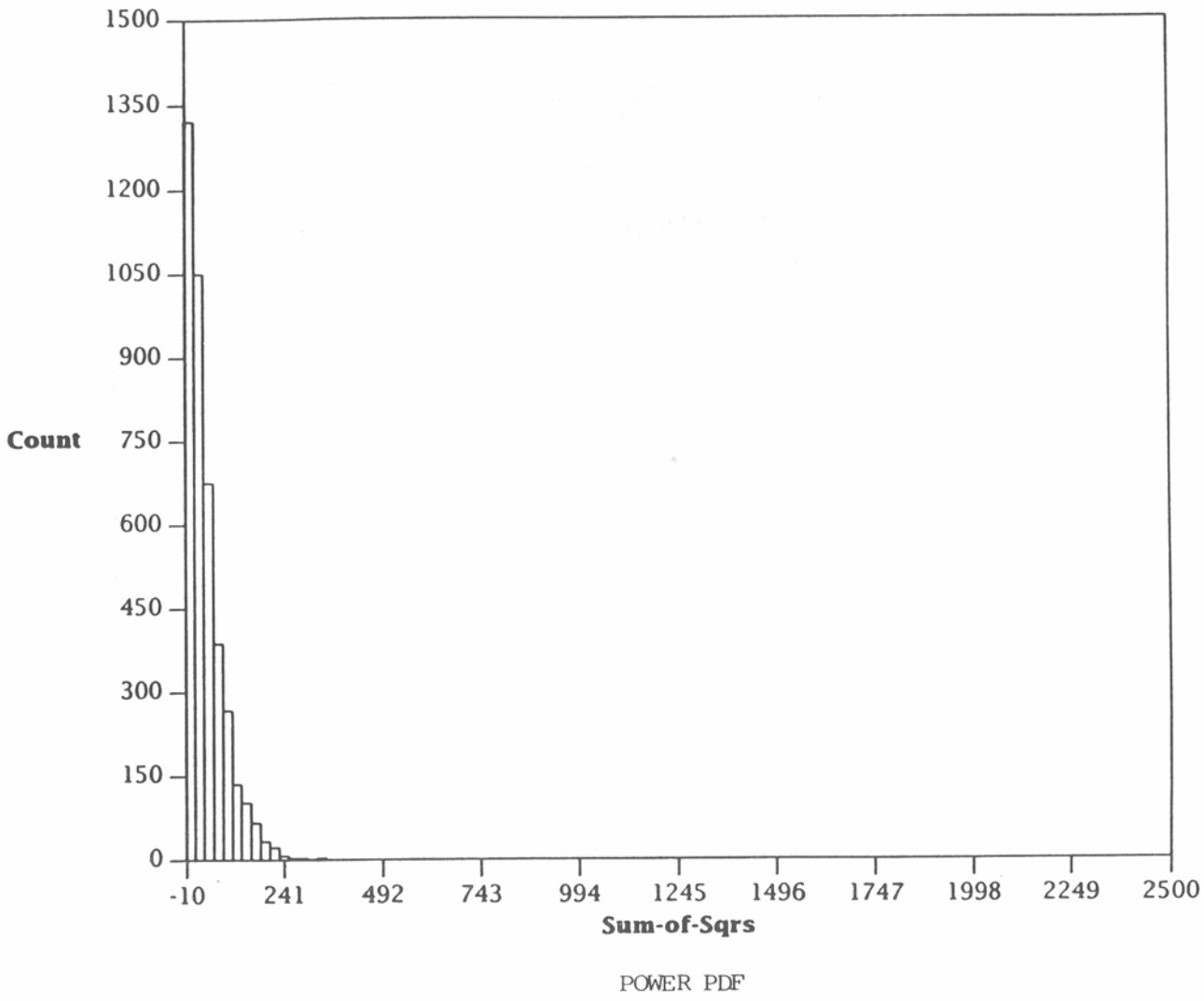

Figure 32. Probability density function of the power envelope in the time domain (case study 5).

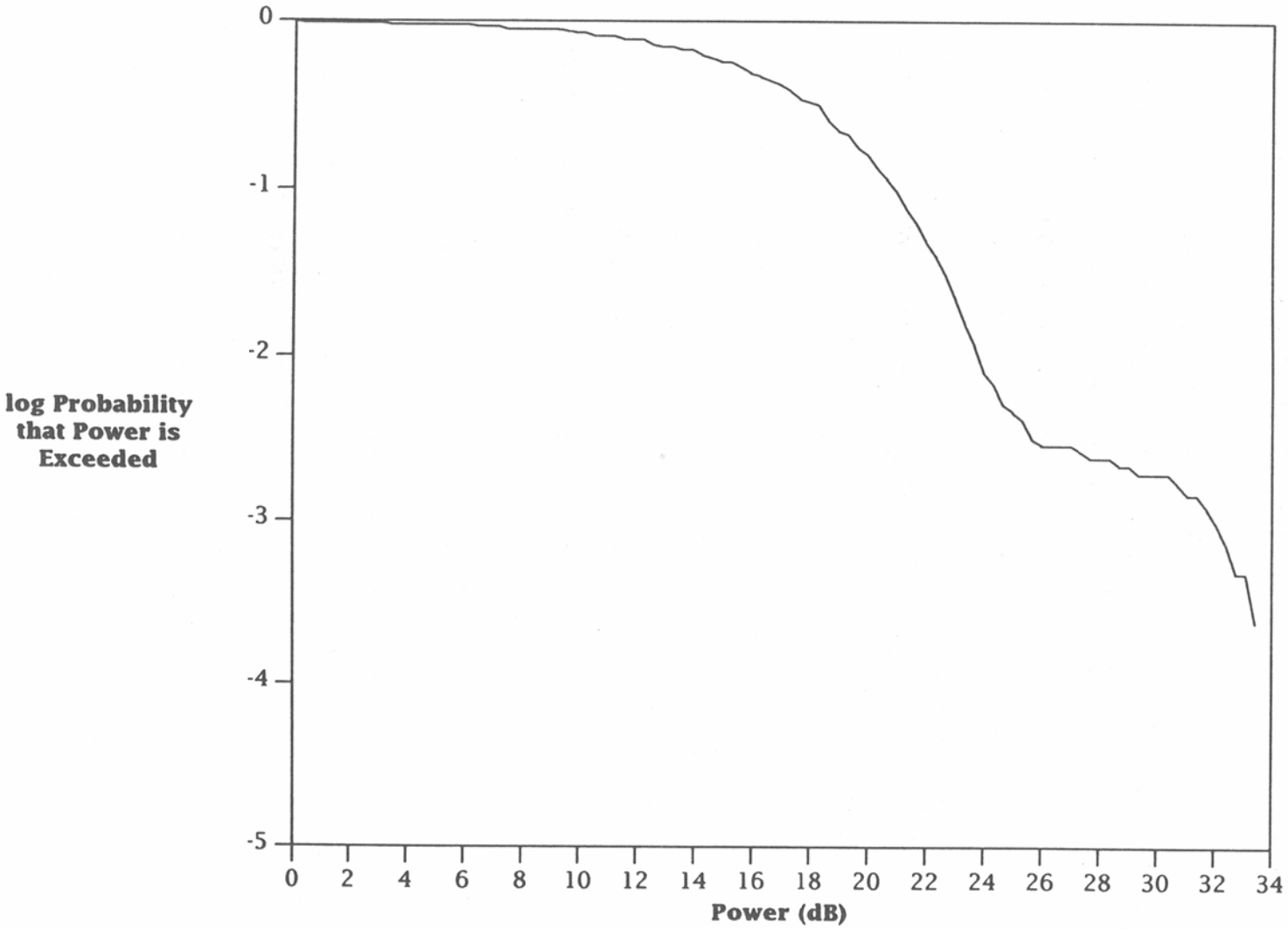

Figure 33. Cumulative distribution function of the power envelope in the time domain (case study 5).

The level crossing distribution of the voltage envelope is shown in Figure 34. Again, this distribution is similar to those of previous cases (see, for example, Figure 7), except for the long tail at high voltage levels.

The presence of impulsive noise is also apparent in the power spectrum, shown in Figure 35. The fact that the noise floor within the 400 kHz bandpass of the filters in the HF receiver is greater (by approximately 20 dB) than the noise floor outside the bandpass of the filters indicates that a broadband process (impulsive noise) is contributing to the power spectral density within the band.

The power spectrum also reveals the presence of numerous narrowband interferers, as in previous cases. The power distribution of these interferers can be obtained from the power cdf in the frequency domain, plotted in Figure 36, which is again similar to those of previous cases.

Because the data in this case study clearly reveal the presence of impulsive noise, which is not apparent in the previous cases, it is of interest to see what effect, if any, the impulsive noise has on the phase distributions. The pdf's of the phase in both the time and frequency domains are shown in Figures 37 and 38, respectively. Unlike the previous time domain phase distributions, which are uniform, the distribution in Figure 37 is clearly nonuniform, with spikes occurring at discrete values of phase. On the other hand, the frequency domain phase distribution in Figure 38 is qualitatively similar to those of the previous cases.

The peculiar spikes in the time domain phase distribution can be understood as an artifact which arises due to the aforementioned quantization of the raw data. Because the I- and Q-channel voltages are integral multiples of a fundamental voltage (the resolution of the A/D converters), it follows that the phase is discretized at values equal to the arctangent of the ratio of two integers. Thus, one expects peaks in the phase distribution at $\arctan(0/1)=0$, $\arctan(1/0)=\pi/2$, $\arctan(1/1)=\pi/4$, $\arctan(1/2)=0.46$, etc., and peaks at precisely these values of phase can be seen in Figure 37.

To summarize, it appears that the noise/interference in this case study can be described by a combination of Gaussian noise, narrowband interferers, and impulsive noise.

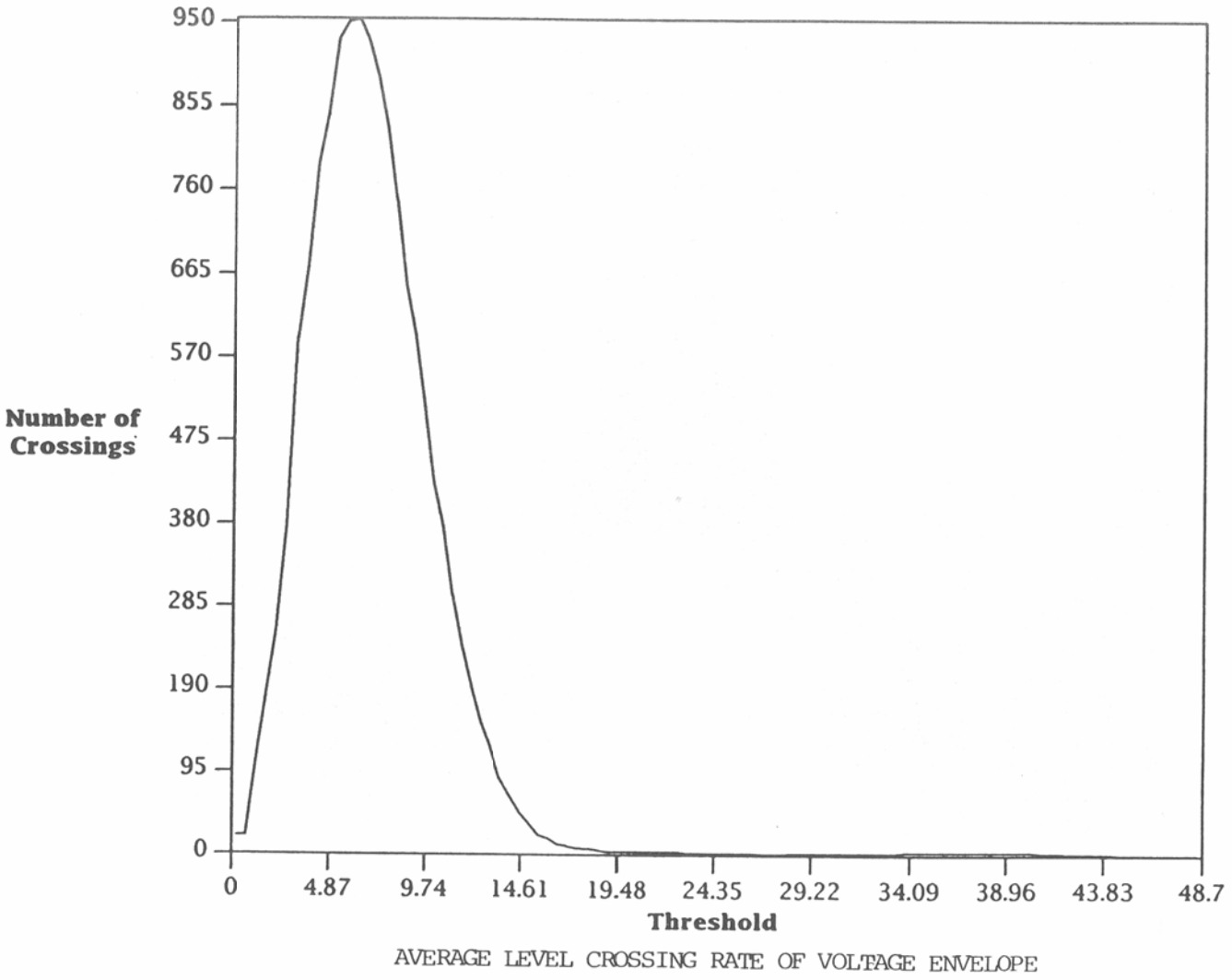

Figure 34. Level crossing distribution of the voltage envelope (case study 5).

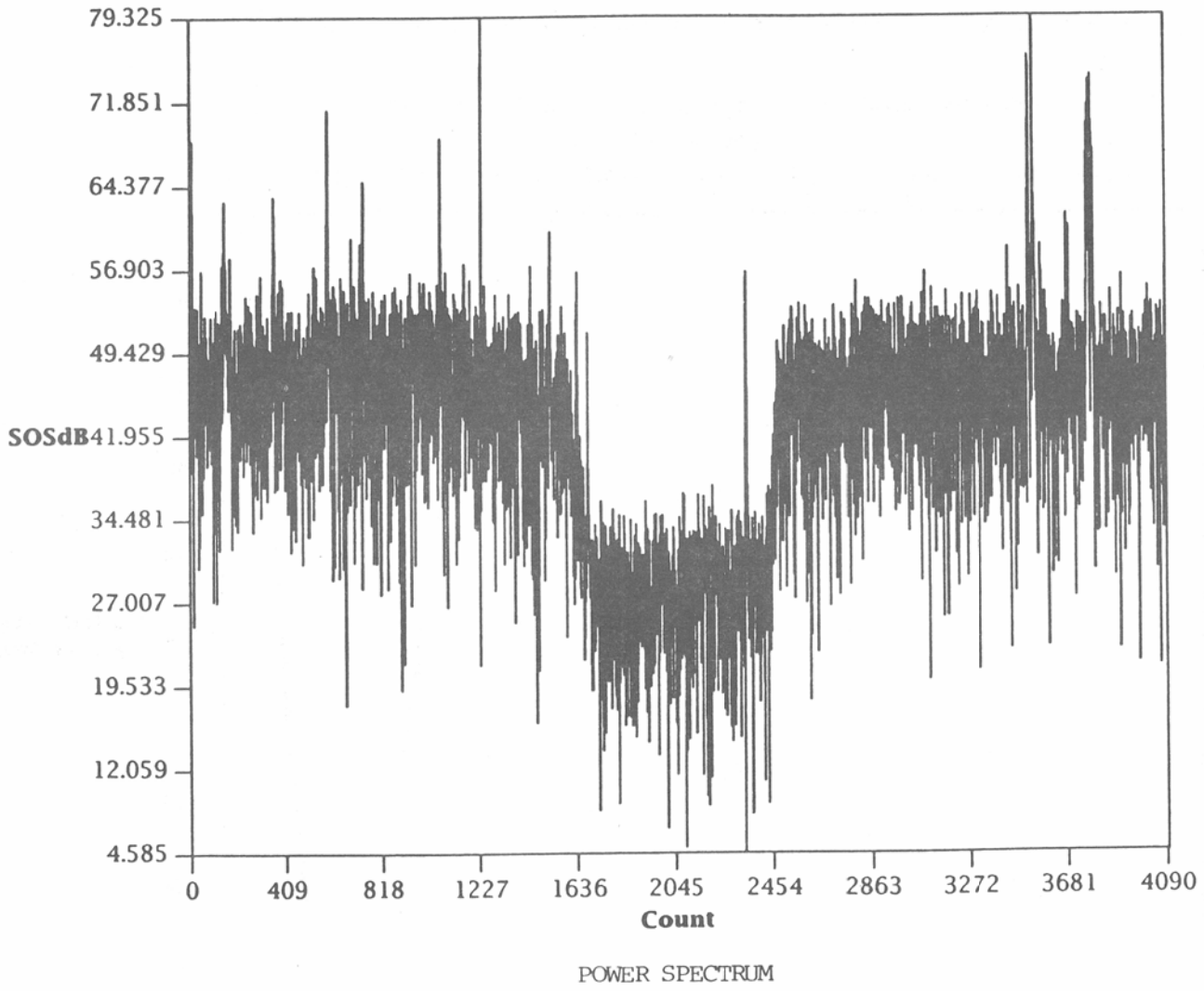

Figure 35. Power spectrum over a bandwidth of 1.024 MHz (case study 5).

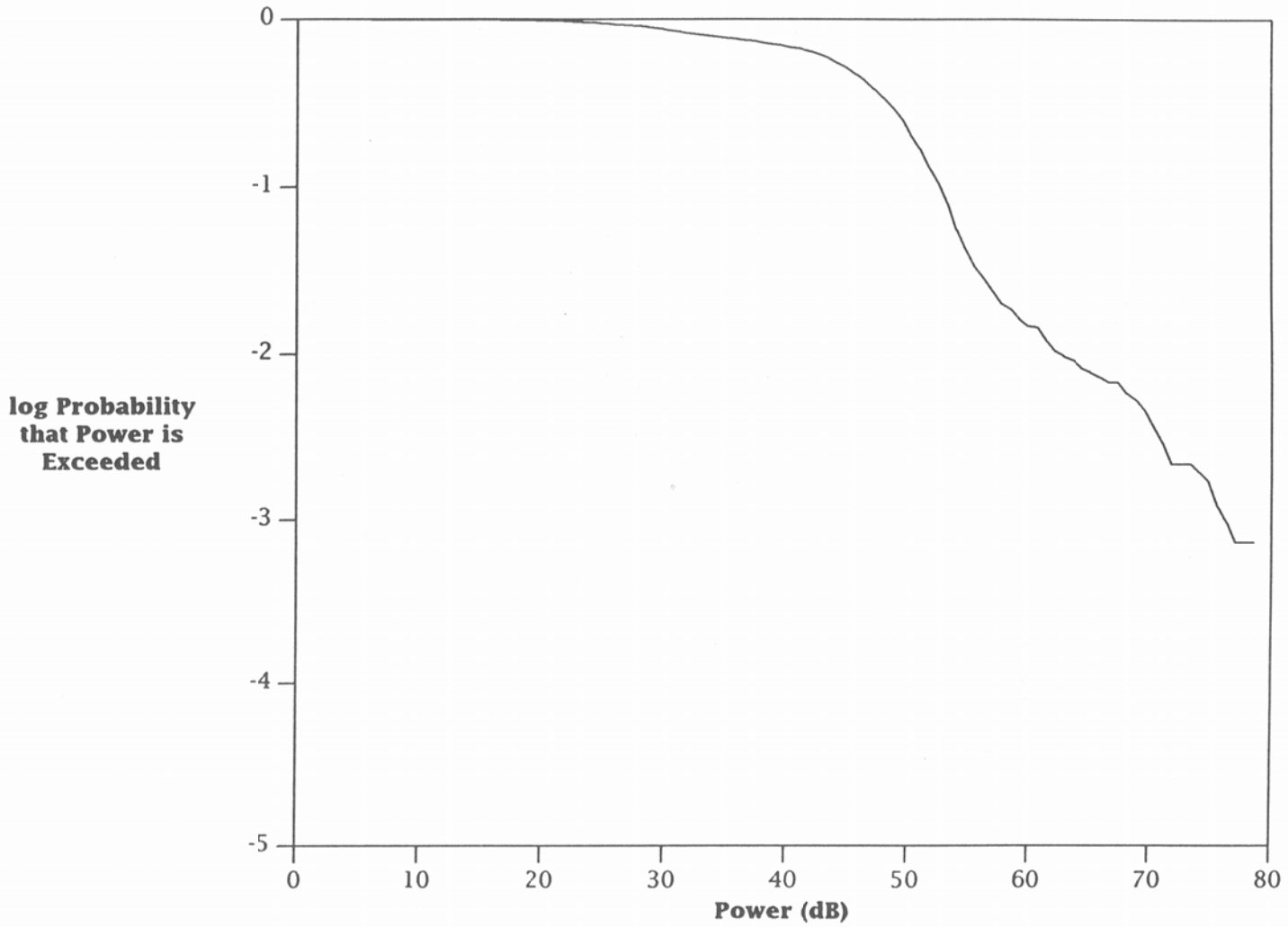

Figure 36. Cumulative distribution function of the power envelope in the frequency domain (case study 5).

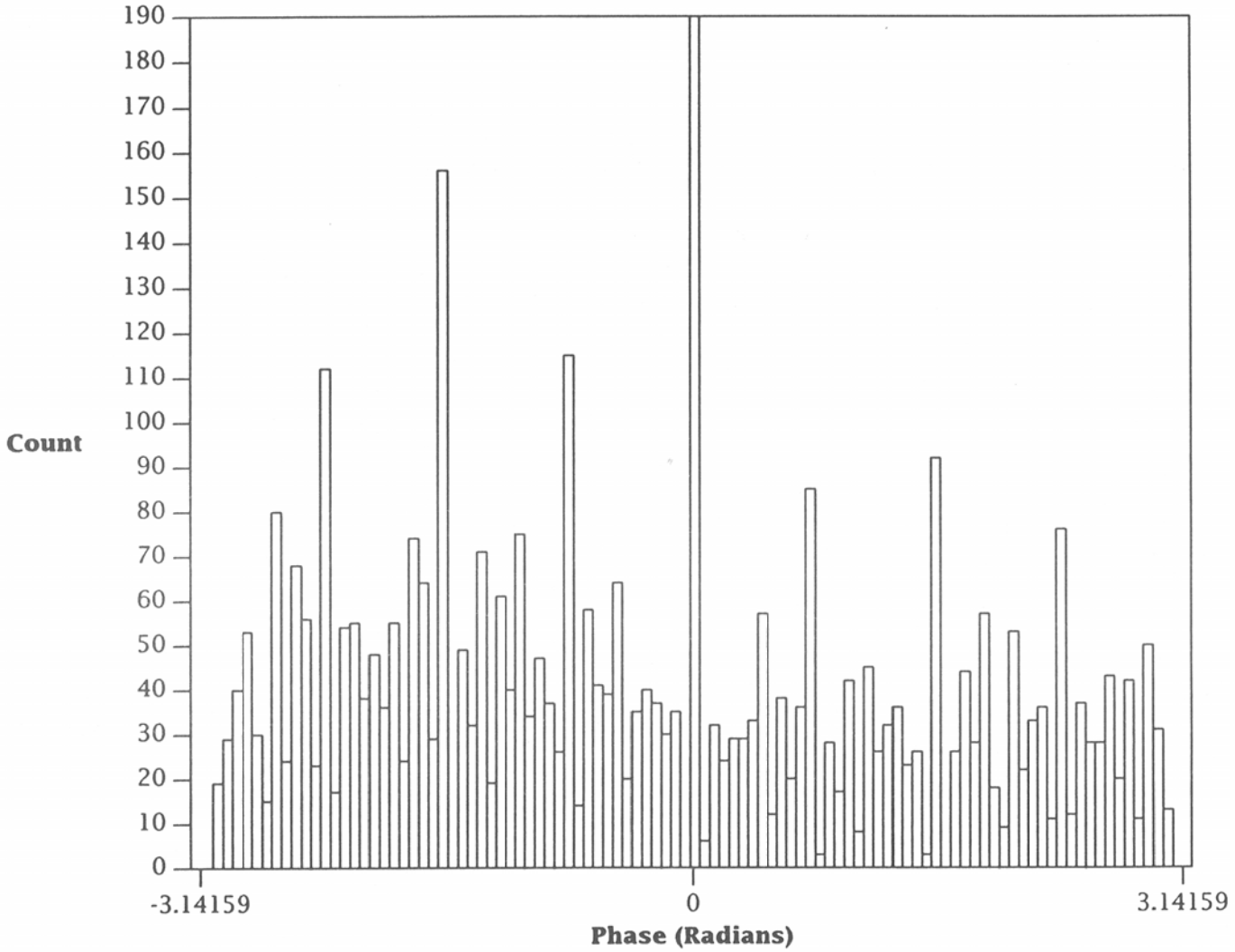

Figure 37. Probability density function of the phase in the time domain (case study 5).

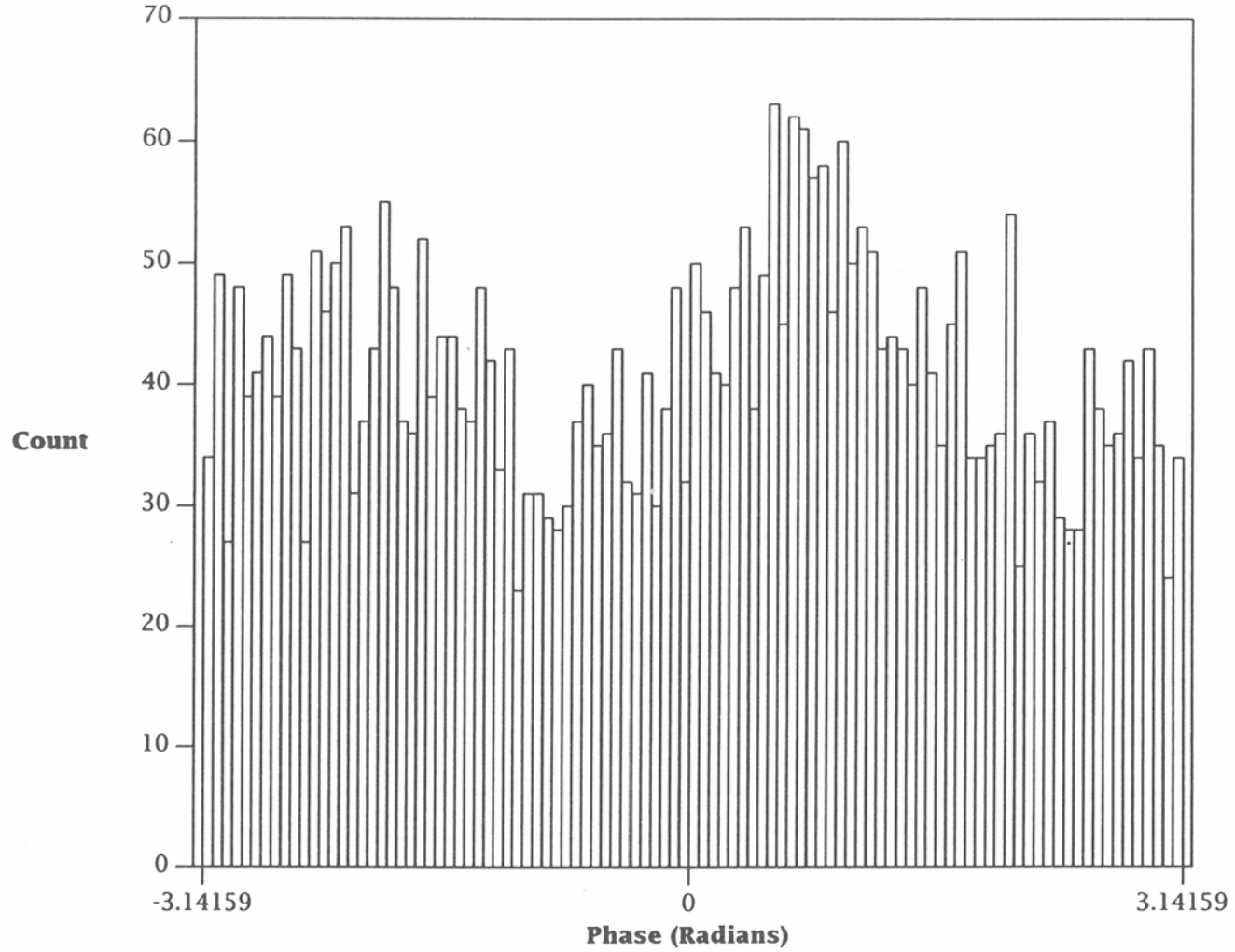

Figure 38. Probability density function of the phase in the frequency domain (case study 5).

The Gaussian noise and narrowband interferers have statistical properties similar to those of the previous cases. The impulsive noise must be modeled by a process which yields the aforementioned tails in the amplitude and crossing rate distributions, but not the spikes in the time domain phase distribution, which are an artifact of the A/D conversion.

3. NOISE/INTERFERENCE MODEL

3.1 Description of Model

Based on the case studies, a simple model of wideband HF noise/interference has been developed. The model is capable of describing the first-order statistics of all the aforementioned noise/interference data, and consists of three components:

- Gaussian noise
- Narrowband interferers (sine waves)
- Impulsive noise (filtered delta functions)

The presence of these three components is not unexpected, and is in accord with intuition. Within a bandwidth on the order of 1 MHz one expects contributions to the noise/interference from many independent sources, and hence, via the central limit theorem, a Gaussian component. On the other hand, one also expects many narrowband interferers, and if one or a few of these interferers are dominant, the central limit theorem no longer holds, so that these interferers must be included as a separate component of the model. Finally, it is well known that HF noise can be impulsive, due to atmospheric noise and other broadband manmade noise which is neither narrowband nor Gaussian, and must therefore be included as a third component of the model.

To make this precise, let x(t) denote the noise/interference signal at rf, and let the in-phase and quadrature components of the baseband signal be denoted by I(t) and Q(t), respectively. Then x(t) can be written as

$$x(t) = I(t)\cos\omega_0 t + Q(t)\sin\omega_0 t \qquad \textbf{(1)}$$

where ω_0 is the carrier frequency. The measured data correspond to I(t) and Q(t), which are the quantities we wish to model.

A sine wave of frequency ω can be written in the form of (1) by using the identity

$$\cos(\omega t + \phi) = \cos\omega_0 t\,\cos(\Delta\omega t + \phi) - \sin\omega_0 t\,\sin(\Delta t + \phi) \qquad \textbf{(2)}$$

where $\Delta\omega = \omega - \omega_0$ and φ is an arbitrary phase. The baseband components I and Q are the coefficients of $\cos\omega_0 t$ and $\sin\omega_0 t$, respectively.

Similarly, the baseband components of an impulse which arrives at time $t = t_0$ can be obtained by applying (2) to the Fourier integral representation of a delta function and transforming the variable of integration from ω to $\Delta\omega$:

$$\begin{aligned}\delta(t-t_0) &= \int_{-\infty}^{\infty} \cos\omega(t-t_0)\,d\omega \\ &= \cos\omega_0(t-t_0)\int_{-\infty}^{\infty}\cos\Delta\omega(t-t_0)\,d\Delta\omega \\ &= -\sin\omega_0(t-t_0)\int_{-\infty}^{\infty}\sin\Delta\omega(t-t_0)\,d\Delta\omega\end{aligned} \qquad \textbf{(3)}$$

Since we wish to model measured I and Q components which have been low-pass filtered, the upper and lower limits of the integrals in (3) should be replaced by $\pm 2\pi$ B, where B is the band-pass in Hz. The last integral in (3) vanishes because the $\sin\Delta\omega(t-t_0)$ is an odd function of $\Delta\omega$; evaluating the integral of $\cos\Delta\omega(t-t_0)$ and expanding $\cos\omega_0(t-t_0)$ enables one to express a filtered impulse $\delta_f(t-t_0)$ as

$$\delta_f(t-t_0) = \frac{\sin 2\pi B(t-t_0)}{t-t_0}\left(\cos\omega_0 t_0\,\cos\omega_0 t + \sin\omega_0 t_0\,\sin\omega_0 t\right) \qquad \textbf{(4)}$$

Again, the I and Q components correspond to the coefficients of $\cos\omega_0 t$ and $\sin\omega_0 t$, respectively. Combining results, the baseband components of the noise/interference model can be written as

$$I(t) = g_I(t) + \sum_{i=1}^{N_i} A_i\cos(\Delta\omega_i t + \phi_i + \sum_{j=1}^{N_j} B_j\frac{\sin 2\pi B(t-t_j)}{t-t_j}\cos\omega_0 t_j \qquad \textbf{(5)}$$

$$Q(t) = g_Q(t) - \sum_{i=1}^{N_i} A_i\sin(\Delta\omega_i t + \phi_i + \sum_{j=1}^{N_j} B_j\frac{\sin 2\pi B(t-t_j)}{t-t_j}\sin\omega_0 t_j \qquad \textbf{(6)}$$

where $g_I(t)$ and $g_Q(t)$ are independent, identically distributed zero-mean Gaussian processes, N_i is the number of narrowband interferers in the frequency band of interest, and N_j is the

number of impulses which occur during the time interval over which the noise/interference is being modeled.

Still to be specified are what fraction of the total noise/interference power is associated with each of the three components, how the narrowband interferers are distributed in amplitude, phase, and frequency, and how the noise impulses are distributed in amplitude and time. To do so, the results of the various case studies discussed above were examined.

It was concluded that the frequency and phase distributions of the narrowband interferers are uniform. As discussed in Section 2.3.1, the amplitude distribution of the narrowband interferers can be obtained from the cdf of the power envelope in the frequency domain. This has been shown by Lemmon (1989) to be well described by a combination of a Gaussian process and an impulsive process defined by a model developed by Hall (1966). It may seem inappropriate to use a model of impulsive phenomena to describe narrowband interferers; however, narrowband interferers are impulsive in the frequency domain, and it is the amplitude distribution of these frequency domain impulses that must be described. Thus, it was concluded that the pdf for the amplitudes A_i can be modeled by the amplitude pdf of the Hall model:

$$p(A) = \frac{(\theta - 1)\gamma^{\theta-1} A}{\left(A^2 + \gamma^2\right)^{(\theta+1)/2}} \qquad \textbf{(7)}$$

The model has two free parameters, θ and γ. Roughly speaking, the value of θ determines the slope of the power cdf at high power levels, where the cdf is approximately linear (on log-log scales), and the value of γ determines the overall power scale.

A possible objection to modeling the amplitude distribution as a pure "Hall" process is that although the power cdf in the frequency domain is well described by a combination of Gaussian and Hall processes, and although the noise/interference in the time domain is assumed to consist of a combination of a Gaussian process and narrowband interferers (in the absence of impulsive noise), it has not been shown that the Gaussian process in the time domain corresponds to a Gaussian process in the frequency domain. Thus, it has not been shown that the narrowband interferers in the time domain correspond to a Hall process in the frequency domain.

That this is indeed the case, however, can be seen by the following argument. The Rice representation for zero-mean Gaussian noise (Rice, 1944 and 1945) in a time interval of length T and in a frequency band from -B to B can be written as

$$g(t) = \sum_{n=1}^{BT_i} \left(a_n \cos \frac{2\pi nt}{T} + b_n \sin \frac{2\pi nt}{T} \right) \qquad \textbf{(8)}$$

where the Fourier coefficients a_n and b_n are independent random variables which are Gaussian distributed with zero means. Here the distribution of a given coefficient (fixed value of n) refers to the distribution of values of that coefficient obtained from an ensemble of noise records. Note that a_n and b_n correspond to the real and imaginary parts, respectively, of the Fourier transform of g(t).

Now consider a single noise record and the distribution p(a) of the set of values of a_n for n= 1,2,...,BT. We wish to determine under what circumstances p(a) is a Gaussian. Note that p(a) can be viewed as the probability that a given a_n is.sampled, times the pdf of a_n for that value of n, summed over n. The probability that a given a_n is sampled is 1/BT. Thus, p(a) can be written as

$$p(a) = \frac{1}{\sqrt{2\pi}BT} \sum_{n=1}^{BT} \frac{e^{-a^2/\sigma^2(a_n)}}{\sigma(a_n)} \qquad \textbf{(9)}$$

where $\sigma(a_n)$ is the standard deviation of the pdf of a_n. Since Gaussians with different standard deviations are linearly independent, and since (9) is a sum of Gaussians, it is easy to see that p(a) is a Gaussian if and only if the $\sigma(a_n)$ are equal to one another for all n. A similar argument holds for the b_n. Therefore, the Fourier transform of a (real) Gaussian process g(t) is a (complex) Gaussian process in the frequency domain if and only if g(t) is white Gaussian noise, that is, Gaussian noise whose spectral properties (i.e., the a_n and b_n) are independent of frequency.

The argument can be generalized to include the case of a complex Gaussian process g(t). Thus, the Fourier transform of a complex Gaussian process is a complex Gaussian process in the frequency domain if and only if g(t) is white. Although we have no proof that

the Gaussian component of actual noise/interference is white, the power spectra shown in the previous examples strongly suggest this to be the case.

It is of interest to see that modeling the noise/interference as a combination of Gaussian and "Hall" processes in the frequency domain leads to a nonuniform phase distribution in the. frequency domain, even though the Gaussian and Hall processes individually have uniform phase distributions. Let G(ω) and H(ω) denote the in-phase components. of a complex Gaussian and a complex "Hall" process, respectively, in the frequency domain, and let their corresponding quadrature components be denoted by $\widetilde{G}$ (ω) and $\widetilde{H}$(ω). Then the joint pdf $p_{x,\tilde{x}}(x,\tilde{x})$ for the combined process X = G + H, $\widetilde{X} = \widetilde{G} + \widetilde{H}$ can be written as a double convolution integral:

$$p_{x,\tilde{x}}(x,\tilde{x}) = \int_{-\infty}^{\infty}\int_{-\infty}^{\infty} p_{H,\tilde{H}}\left(x-z,\tilde{x}-\tilde{z}\right)p_{G,\tilde{G}}\left(z,\tilde{z}\right)dzd\tilde{z} \qquad \textbf{(10)}$$

where $p_{H,\tilde{H}}$ and $p_{G,\tilde{G}}$ denote the joint pdfs for the Hall and Gaussian processes, respectively. An expression for $p_{H,\tilde{H}}$ has been derived by Hall (1966):

$$p_{H,\tilde{H}}(x,\tilde{x}) \propto \frac{1}{\left(x^2+\tilde{x}^2+\gamma^2\right)^{(\theta+1)/2}} \qquad \textbf{(11)}$$

Since G and $\widetilde{G}$ are independent, identically distributed Gaussian processes, $p_{G,\tilde{G}}$ can be written as

$$p_{G,\tilde{G}}(x,\tilde{x}) \propto e^{-\left(x^2+\tilde{x}^2\right)/2\sigma^2} \qquad \textbf{(12)}$$

Substituting (11) and (12) into (10) gives

$$p_{x,\tilde{x}}(x,\tilde{x}) \propto \int_{-\infty}^{\infty}\int_{-\infty}^{\infty} \frac{e^{-\left(z^2+\tilde{z}^2\right)/2\sigma^2}}{\left[\left(x-z\right)^2+\left(\tilde{x}-\tilde{z}\right)^2+\gamma^2\right]^{(\theta+1)/2}}dzd\tilde{z} \qquad \textbf{(13)}$$

Making a transformation of variables from $(x,\tilde{x})$ to (V,φ) via

$$x^2 + \tilde{x}^2 = V^2 \tag{14}$$

$$x^2 + \tilde{x}^2 = V^2 \tag{15}$$

$$x^2 + \tilde{x}^2 = V^2 \tag{16}$$

results in the joint pdf $p_{v,\varphi}$ in amplitude V and phase φ for the combined process:

$$p_{v,\phi} = v p_{x,\tilde{x}} \propto \int_{-\infty}^{\infty}\int_{-\infty}^{\infty} v \frac{e^{-\left(z^2+\tilde{z}^2\right)/2\sigma^2}}{\left[V^2 - 2zV\cos\phi - 2\tilde{z}V\sin\phi + z^2 + \tilde{z}^2 + \gamma^2\right]^{(\theta+1)/2}} dz d\tilde{z} \tag{17}$$

Finally, the phase distribution p_φ is obtained from the joint distribution $p_{v,\varphi}$ by integrating over V,

$$p_\phi = \int_0^{\infty} p_{v,\phi} dV \tag{18}$$

so that

$$p_\phi \propto \int_0^{\infty} dV \int_{-\infty}^{\infty} dz \int_{-\infty}^{\infty} d\tilde{z} \frac{V e^{-\left(z^2+\tilde{z}^2\right)/2\sigma^2}}{\left[V^2 - 2zV\cos\phi - 2\tilde{z}V\sin\phi + z^2 + \tilde{z}^2 + \gamma^2\right]^{(\theta+1)/2}} \tag{19}$$

Although no attempt has been made to evaluate the triple integral in (19), it is clear that p_φ is not uniform, but is φ-dependent, and has a period of 2π.

Turning now to the impulsive noise, it was concluded from examination of the power cdf's in the time domain that the amplitude distribution of the impulses can also be described by that of the Hall model for amplitudes B_j which are less than some maximum value B_{max}. At larger values of amplitude, the distribution appears to be cut off (relative to that of the Hall model). Whether this is due to some intrinsic property of the noise pulses or is due to the limited dynamic range of the receiving and data acquisition systems remains unclear at this time; the resolution of this question will require additional data

obtained with a system that has greater dynamic range. In any case, based upon these observations, it is proposed that the amplitude distribution p(B) of the impulses in the time domain be modeled by that of a cutoff Hall model:

$$p(B) = \left\{ 0 \frac{1-\theta}{\left(B_{\max}^2 + \gamma^2\right)^{(1-\theta)/2} - \gamma^{2(1-\theta)/2}} \cdot \frac{B}{B>B_{\max}} \left(B^2 + \gamma^2\right)^{(\theta+1)/2}, 0 \le B \le B_{\max} \right\} \qquad \textbf{(20)}$$

The expression in the first line of (20) differs from that in (7) because cutting off the distribution results in a different normalization constant.

As discussed in Section 2.3.5, in the one noise record which clearly exhibits impulsive noise, the noise impulses do not occur randomly in time, but tend to occur in a quasi-periodic fashion. However, quantitatively modeling the arrival time distribution requires investigation of the noise pulse spacing distribution, and this, as well as investigation of the other higher-order statistics, is beyond the scope of the present work, and will not be further discussed in this report. For the present purposes of modeling the first-order statistics, the pulse arrival distribution will therefore be assumed to be uniform.

3.2 Comparisons of Model with Measurements

To demonstrate the usefulness of the model for simulation purposes, noise/interference has been simulated, analyzed, and compared to the corresponding analyses of measured data for two particular noise/interference environments: the case study discussed in Section 2.3.1, which is typical of the data examined in the 42 noise records, and the case study discussed in Section 2.3.5, which exhibits impulsive noise, in addition to the Gaussian and narrowband components. The purpose of these comparisons is not to exhibit simulated results which are identical to the corresponding measured results, but rather to demonstrate that the model generates noise/interference with the same statistical characteristics as the measured data.

In the first case, the simulated noise/interference consists of a combination of Gaussian noise and 40 sine waves. Each sample of the Gaussian noise was generated by summing 12 random variables, uniformly distributed between -0.5 and 0.5. Since the mean and variance of each of the random variables are 0 and 1/12, respectively, the mean and variance of the composite process are 0 and 1, respectively. The central limit theorem

implies that the composite process is (approximately) Gaussian, as discussed, for example, by Mihram (1972). Moreover, because each sample was generated independently of the others, the autocorrelation function of the process is impulsive; thus, its Fourier transform (the power spectrum) is flat, and the noise is therefore white.

The model specifies that the amplitudes A_i of the sine waves are distributed according to (7). A set of amplitudes so distributed can be generated by integrating (7) to obtain the cumulative probability P(A),

$$P(A) = 1 - \frac{\gamma^{\theta-1}}{\left(A^2 + \gamma^2\right)^{(\theta-1)/2}} \tag{21}$$

inverting the result to obtain A(P),

$$A(P) = \gamma\left[\frac{1}{(1-P)^{2/(\theta-1)}} - 1\right]^{1/2} \tag{22}$$

and viewing the cumulative probability P as a random variable uniformly distributed between 0 and 1. Thus, random values of P, uniformly distributed between 0 and 1, were generated and substituted into (22) to obtain values of A_i. The values of the parameters γ and θ were chosen to be $\gamma = 0.3$ and $\theta = 2.0$.

The phases φ_i of the sine waves are uniformly distributed between 0 and 2π, and the baseband frequencies $\Delta\omega_i$ are uniformly distributed between -400 kHz and +400 kHz.

Plots of the I-channel data, both measured and simulated, over an interval of 4 ms, are shown in Figure 39. Although the measured and simulated data are qualitatively similar, the simulated data appears to have more high frequency noise than the measured data. However, this is due to the fact that the frequency of the dominant narrowband interferer in the simulated data happens to be higher than that in the measured data in this particular case. Because the frequencies and amplitudes of the narrowband interferers are treated as random variables in the simulation, it is unlikely that the measured and simulated data will exhibit identical sets of narrowband interferers. Nevertheless, the statistical properties of the measured and simulated data are quite similar, as can be seen by comparing the measured and simulated pdf's of the I-channel data, the power envelope, and the phase, which are shown in Figures 40, 41, and 42, respectively.

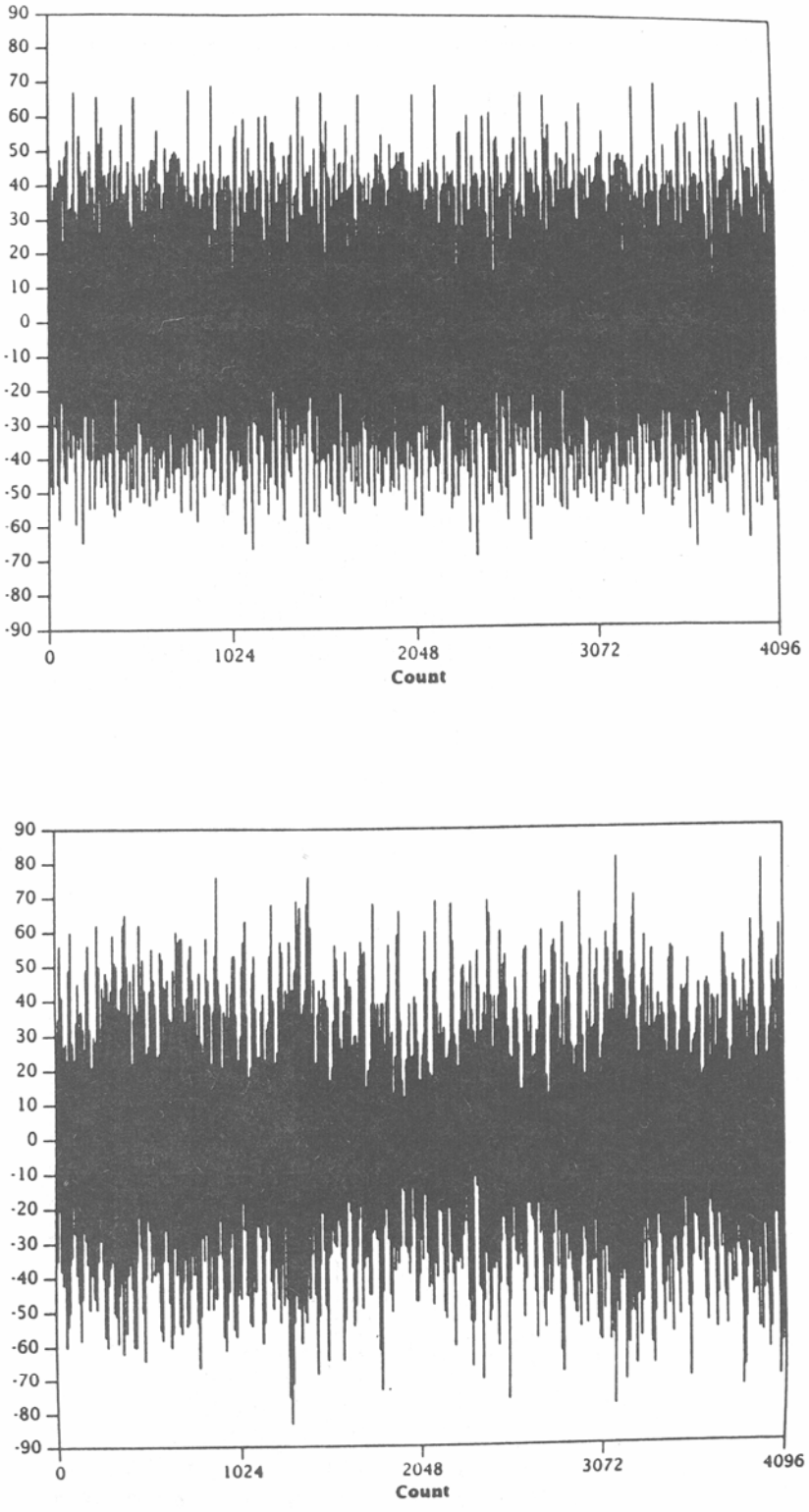

Figure 39. Comparison of (a) simulated and (b) measured (case study 1) noise/interference in the I-channel data.

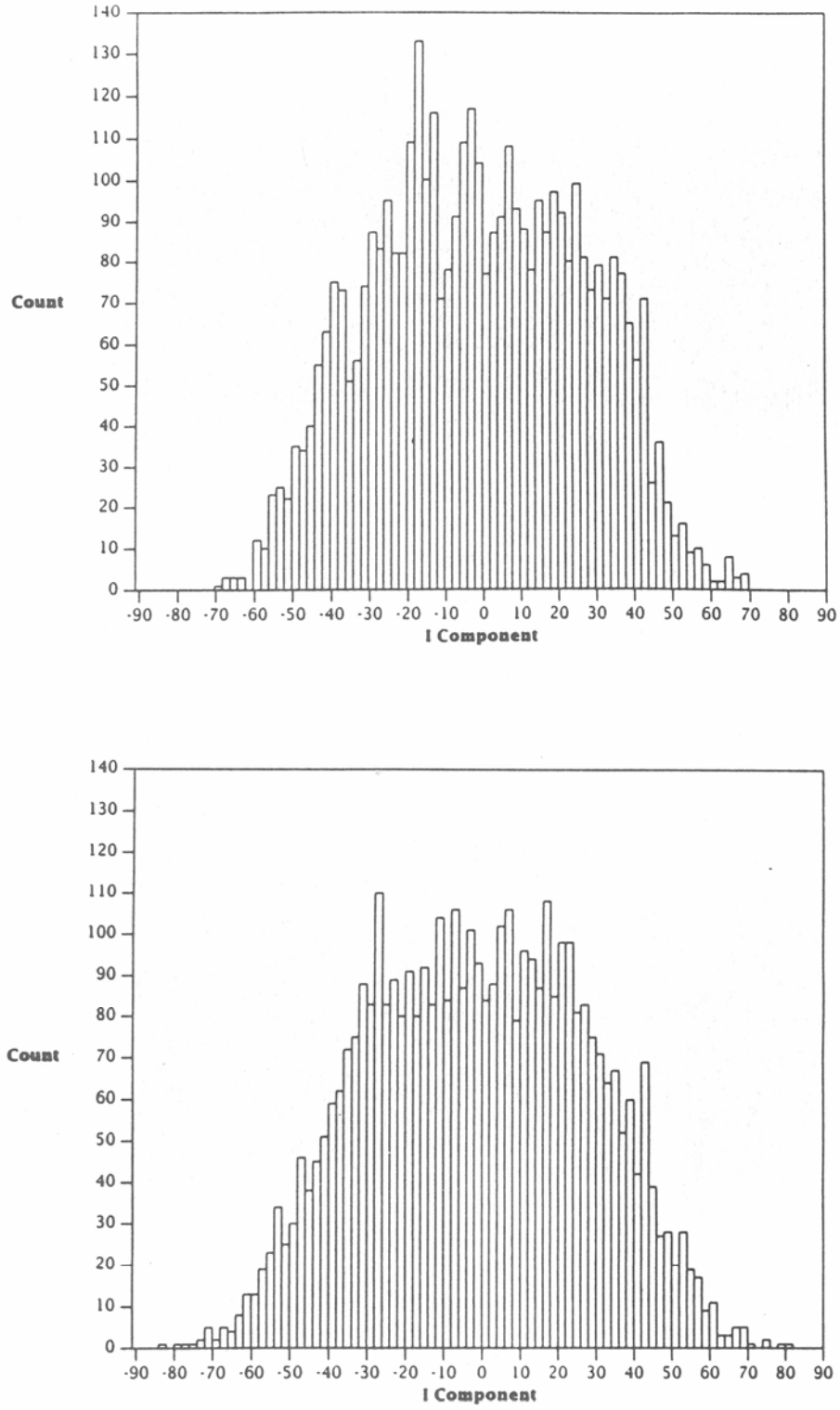

Figure 40. Comparison of (a) simulated and (b) measured (case study 1) probability density functions of the I-channel data.

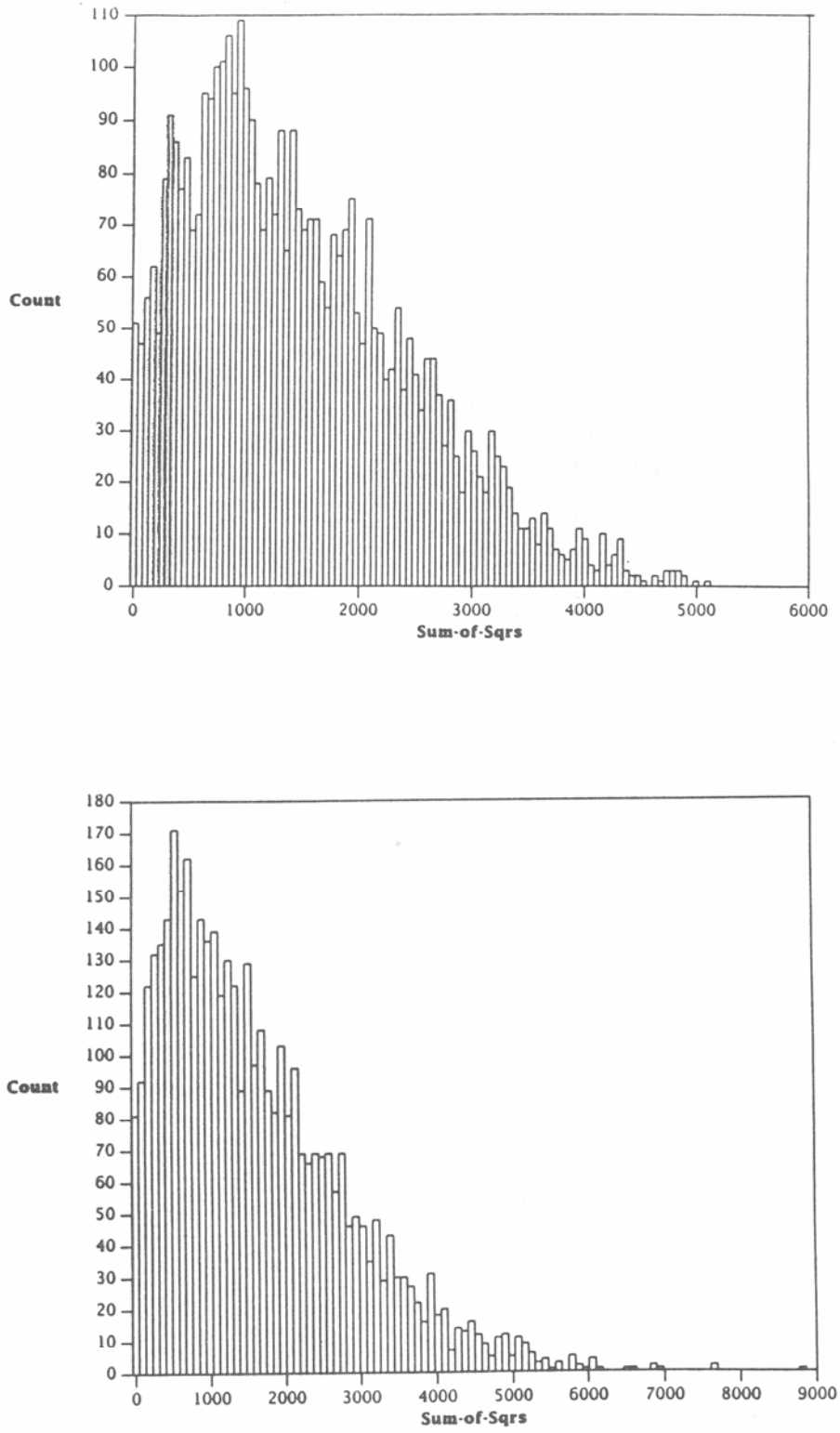

Figure 41. Comparison of (a) simulated and (b) measured (case study 1) probability density functions of the power envelope in the time domain.

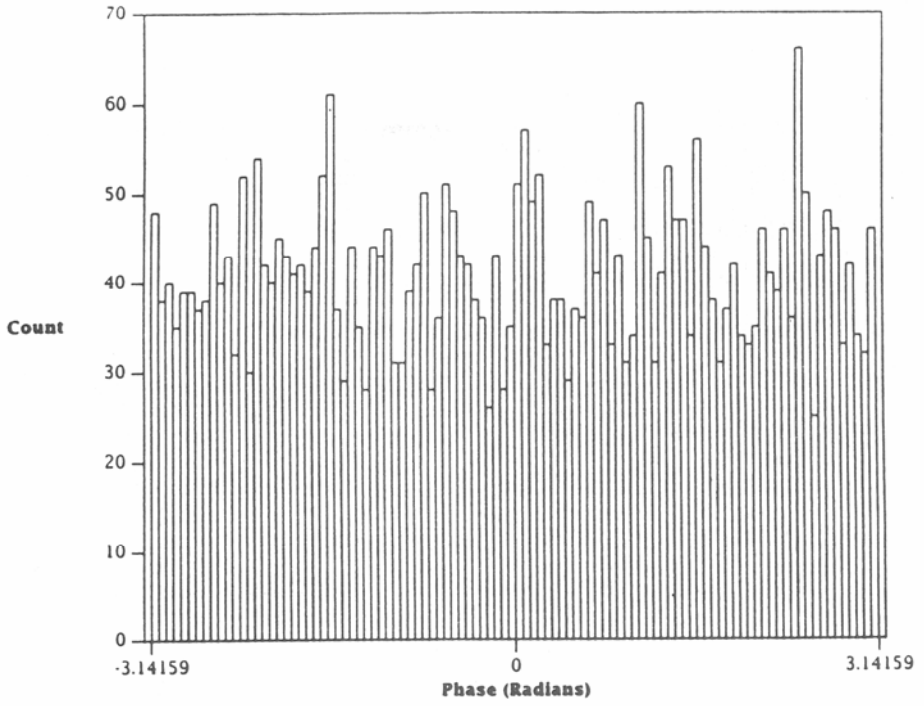

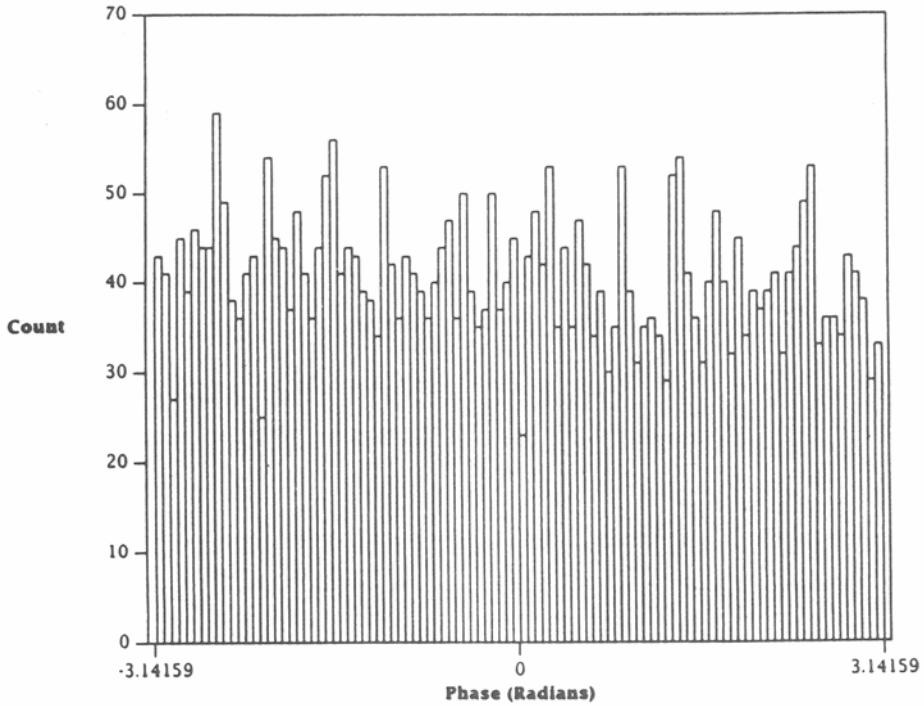

Figure 42. Comparison of (a) simulated and (b) measured (case study 1) probability density functions of the phase in the time domain.

65

The level crossing distributions of the voltage envelope are shown in Figure 43. Again, the measured and simulated distributions are qualitatively similar, although the scale of the simulated distribution is nearly three times larger than that of the measured distribution. This is to be expected if the frequency of the dominant narrowband interferer in the simulated data is several times greater than that in the measured data.

That this is indeed the case can be seen by comparing the measured and simulated power spectra, shown in Figure 44. Whereas the frequency of the dominant interferer in the simulated data is approximately 350 kHz, the frequencies of the dominant interferers in the measured data tend to cluster around -125 kHz. Also note that the spectral lines corresponding to the dominant interferers have a finite width, even though they have been modeled by zero bandwidth sine and cosine waves. The reason is because the power spectrum is the square of the Fourier transform of a noise record of finite length (4 ms) and the Fourier transform of a complex exponential $e^{i\Delta\omega t}$ of finite time duration is a linear combination of a filtered impulse and its Hilbert transform:

$$\int_0^T e^{-i\Delta\omega t} e^{i\omega t}\, dt = \frac{1}{\omega - \Delta\omega}\left\{\sin\left(\omega - \Delta\omega\right)T - i\left[\cos\left(\omega - \Delta\omega\right)T - 1\right]\right\} \qquad \textbf{(23)}$$

Thus, the structure of the spectral lines in the power spectrum corresponds to the logarithm of the envelope $1/(\omega\text{-}\Delta\omega)^2$.

The cdf's of the power envelope in the frequency domain and the pdf's of the phase in the frequency domain are shown in Figures 45 and 46, respectively. The similarity of the measured and simulated power envelope cdf's is to be expected, because the amplitude distribution of the sine waves in the simulation was chosen to reproduce the measured distribution. The simulated phase distribution is nonuniform, as expected based on the discussion in Section 3.1, and also is qualitatively similar to the measured distribution, although shifted in phase. However, a relative phase shift in the frequency domain corresponds to a relative time shift of the noise record, which is of no physical significance.

The noise/interference discussed in Section 2.3.5 was simulated by combining Gaussian noise, 40 sine waves, and 50 impulses. The Gaussian noise and sine waves were

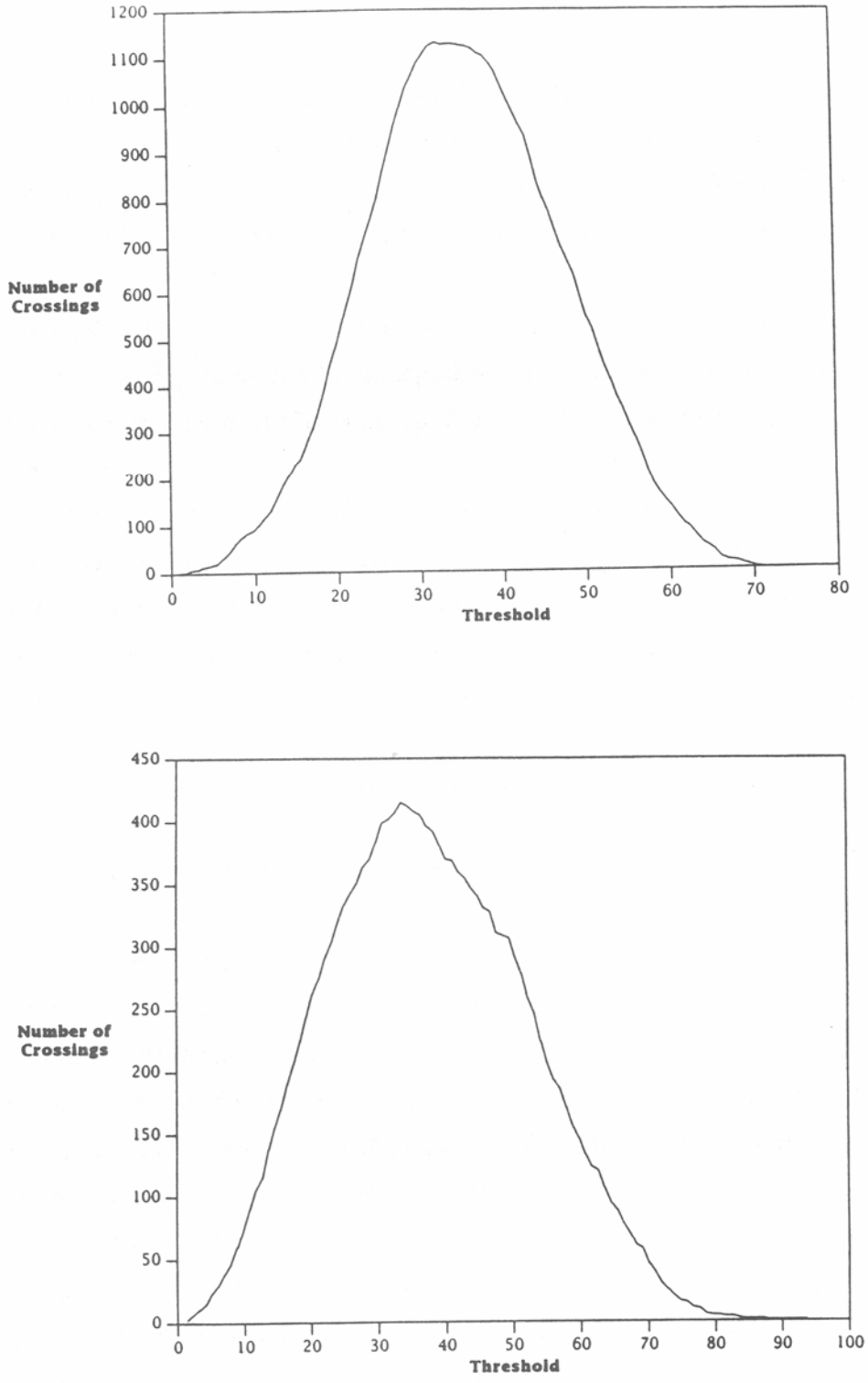

Figure 43. Comparison of (a) simulated and (b) measured (case study 1) level crossing distributions of the voltage envelope.

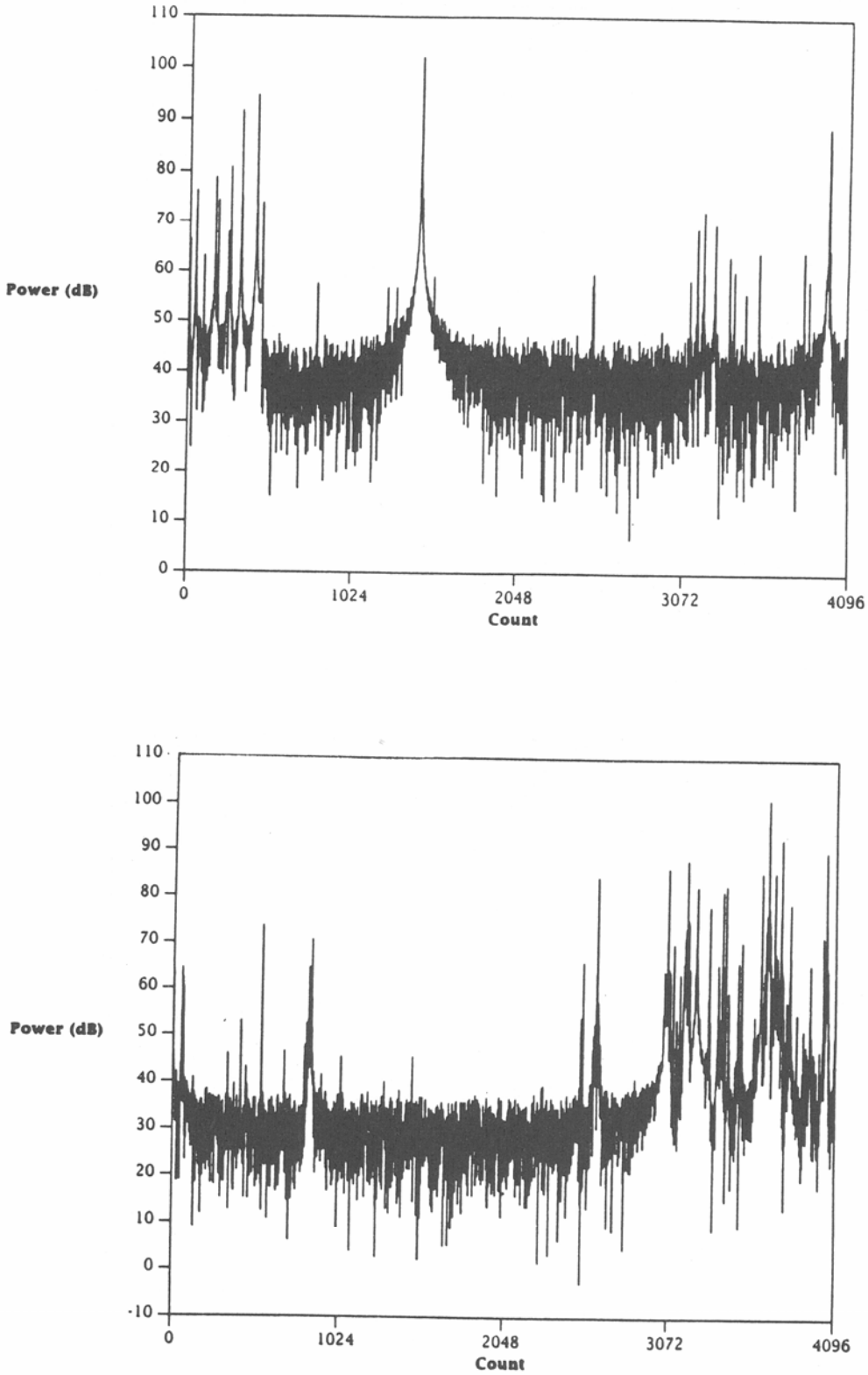

Figure 44. Comparison of (a) simulated and (b) measured (case study 1) power spectra.

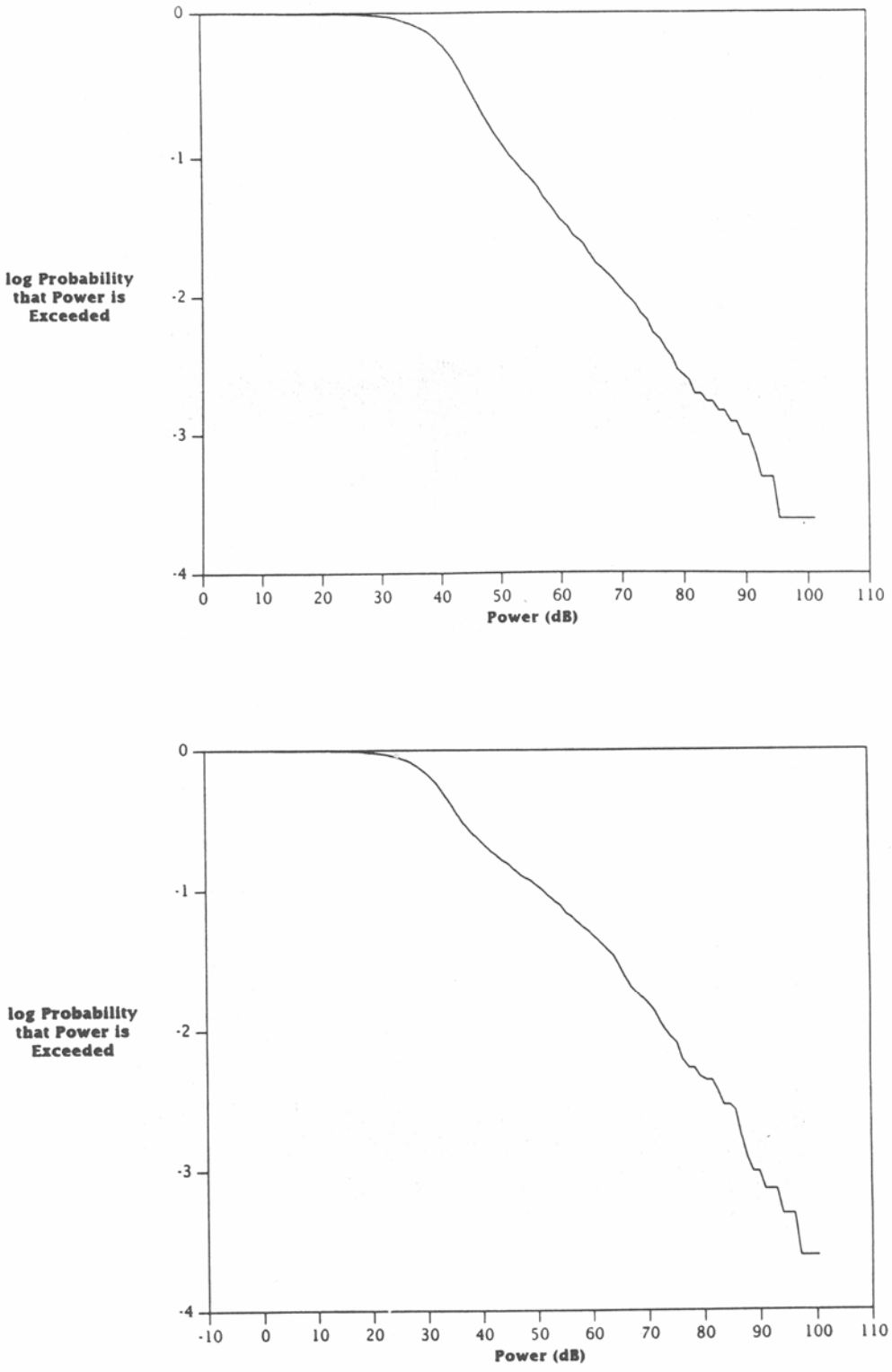

Figure 45. Comparison of (a) simulated and (b) measured (case study 1) cumulative distribution functions of the power envelope in the frequency domain.

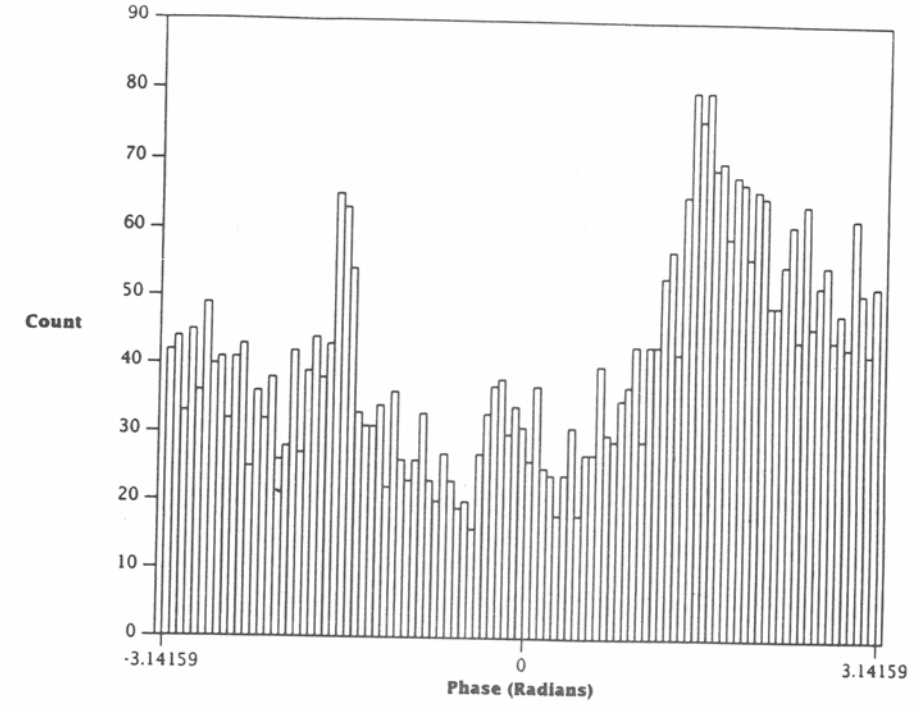

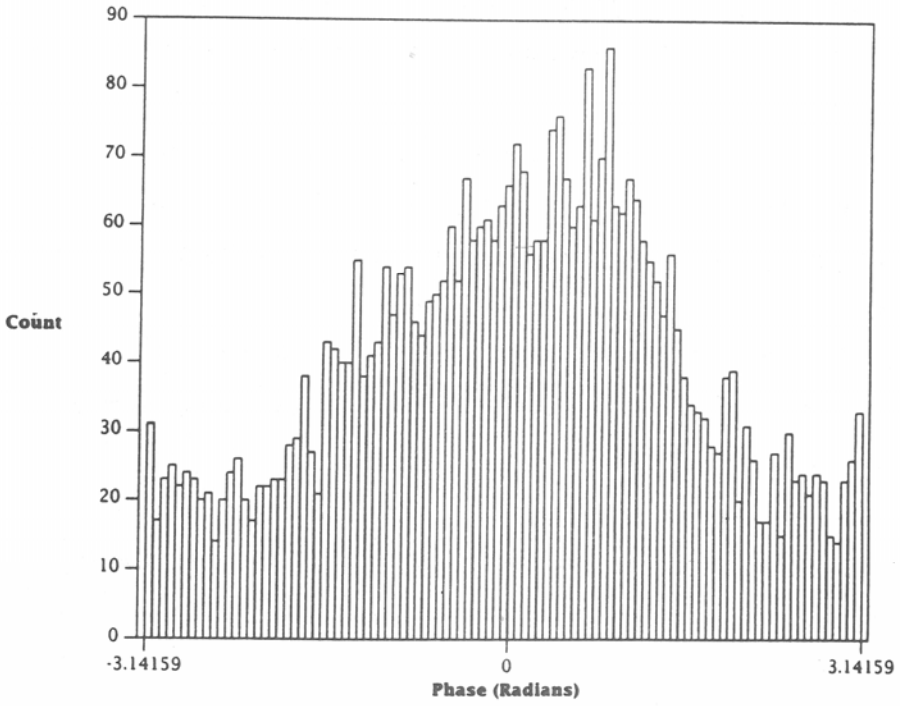

Figure 46. Comparison of (a) simulated and (b) measured (case study 1) probability density functions of the phase in the frequency domain.

generated by the techniques discussed in the previous example, except that the Gaussian noise samples were multiplied by a factor of 0.12, so that $g_I(t)$ and $g_Q(t)$ each have a variance σ^2=0.0144, and the parameters γ and θ in the amplitude distribution of the sine waves were chosen to be $\gamma = 0.2$ and $\theta = 2.0$.

The amplitudes B_j of the impulses are distributed according to (20) and were generated by a technique analogous to that used to generate the A_i. Integrating (20) to obtain the cumulative distribution P(B),

$$P(B) = \frac{\left(B^2 + \gamma^2\right)^{(1-\theta)/2} - \gamma^{2(1-\theta)/2}}{\left(B_{\max}^2 + \gamma^2\right)^{(1-\theta)/2} - \gamma^{2(1-\theta)/2}} \tag{24}$$

and inverting to obtain B(P),

$$B(P) = \gamma\left\{\left[P\left[\left(\frac{B_{\max}^2}{\gamma^2}+1\right)^{(1-\theta)/2} - 1\right]+1\right]^{2/(1-\theta)} - 1\right\}^{1/2} \tag{25}$$

values of B_j were obtained by generating random values of P**,** uniformly distributed between 0 and 1, and substituting into (25). The parameters were chosen to be $B_{max}=2\text{x}10^{-5}$, $\gamma = 1.0\text{x}10^{-8}$, and $\theta = 1.2$.

The arrival times t_j of the impulses are uniformly distributed between 0 and 4 ms.

Plots of the I-channel data and pdf's of these data are shown in Figures 47 and 48, respectively. The presence of impulses in the raw data results in the long tails in the pdf's, which otherwise are typical of those of previous case studies.

The pdf's of the power envelope, which are shown in Figure 49, also exhibit long tails, which are more readily apparent in the cdf of the power envelope plotted on log-log scales, as shown in Figure 50.

The pdf's of the phase in the time domain are shown in Figure 51. As discussed above, the spikes in the measured distribution are an artifact of the A/D conversion, and are intentionally not being simulated.

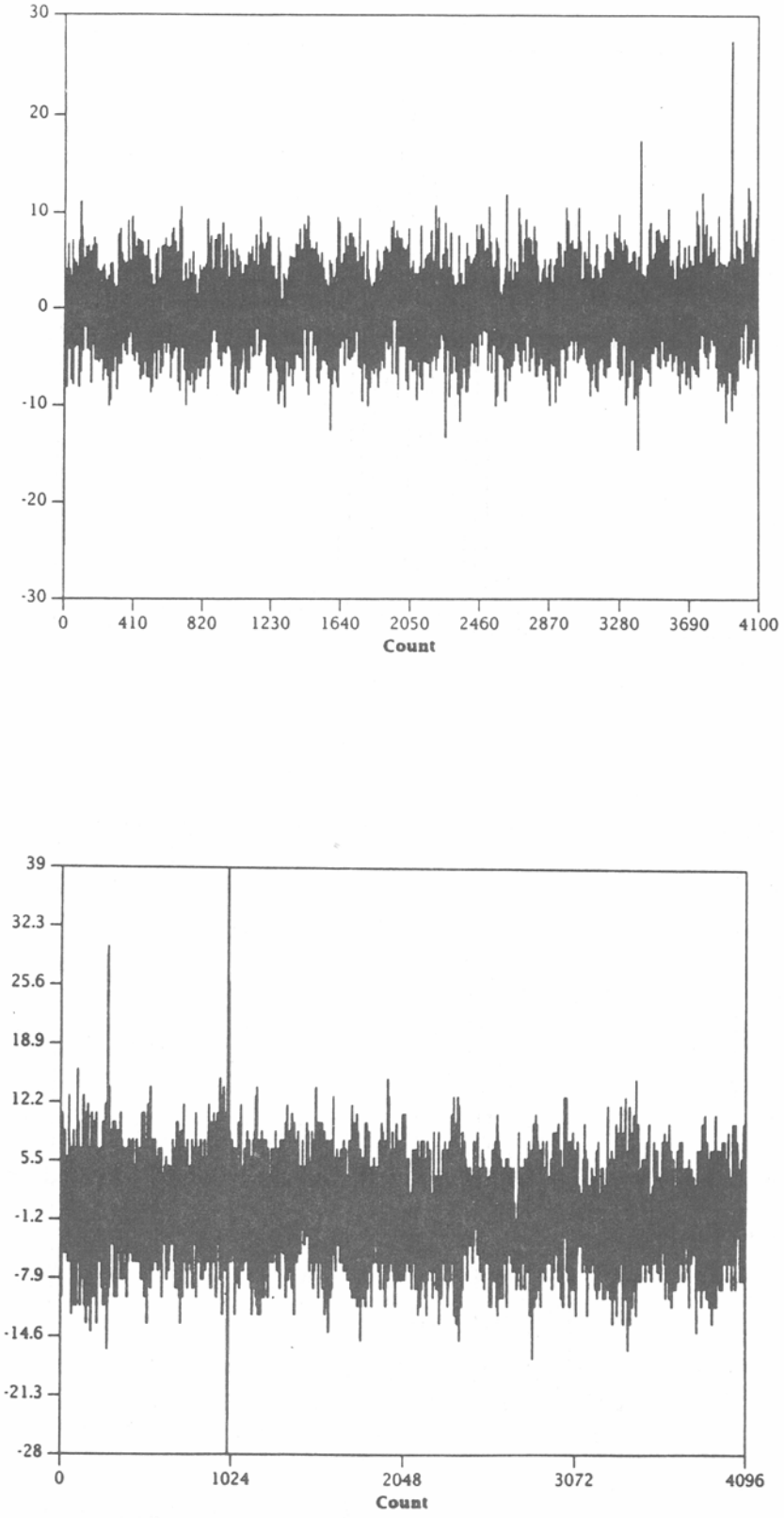

Figure 47. Comparison of (a) simulated and (b) measured (case study 5) I-channel data.

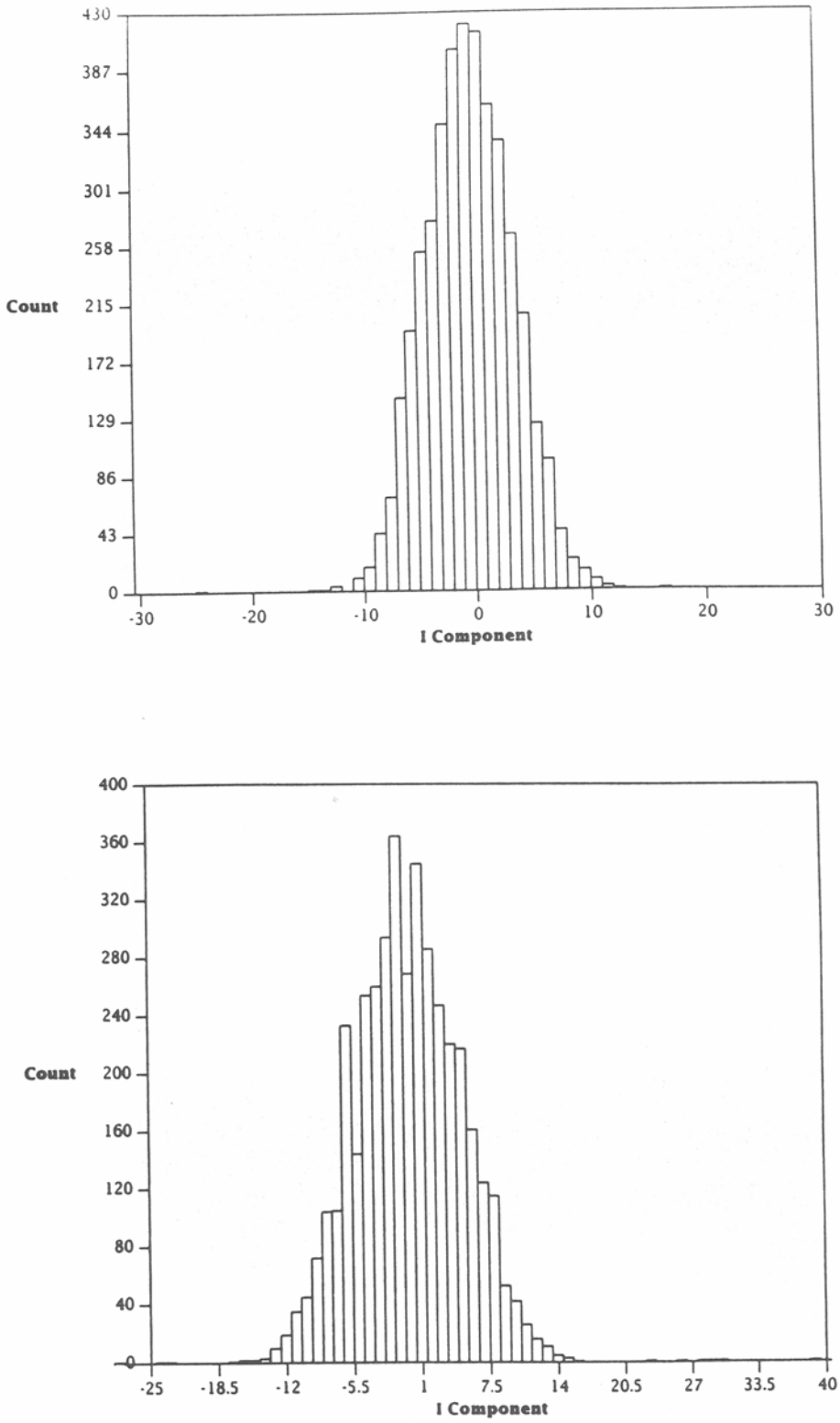

Figure 48. Comparison of (a) simulated and (b) measured (case study 5) probability density functions of the I-channel data.

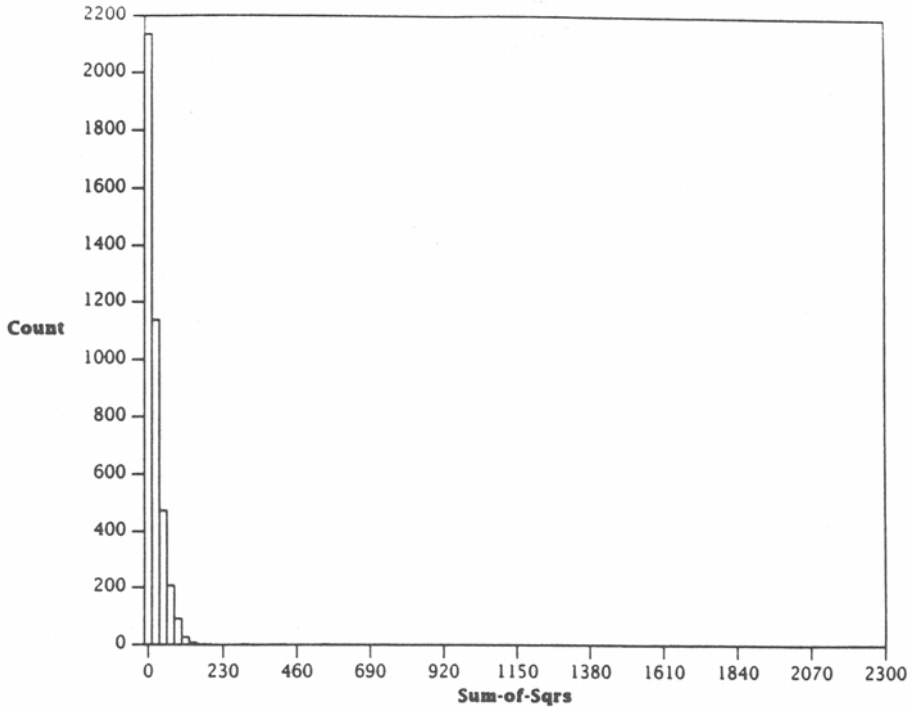

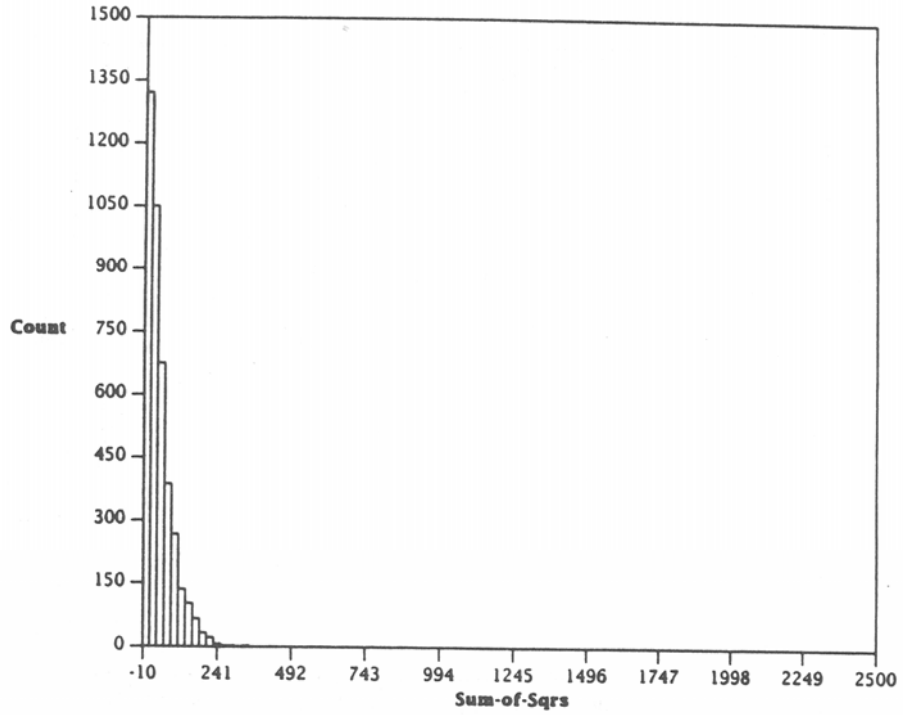

Figure 49. Comparison of (a) simulated and (b) measured (case study 5) probability density functions of the power envelope in the time domain.

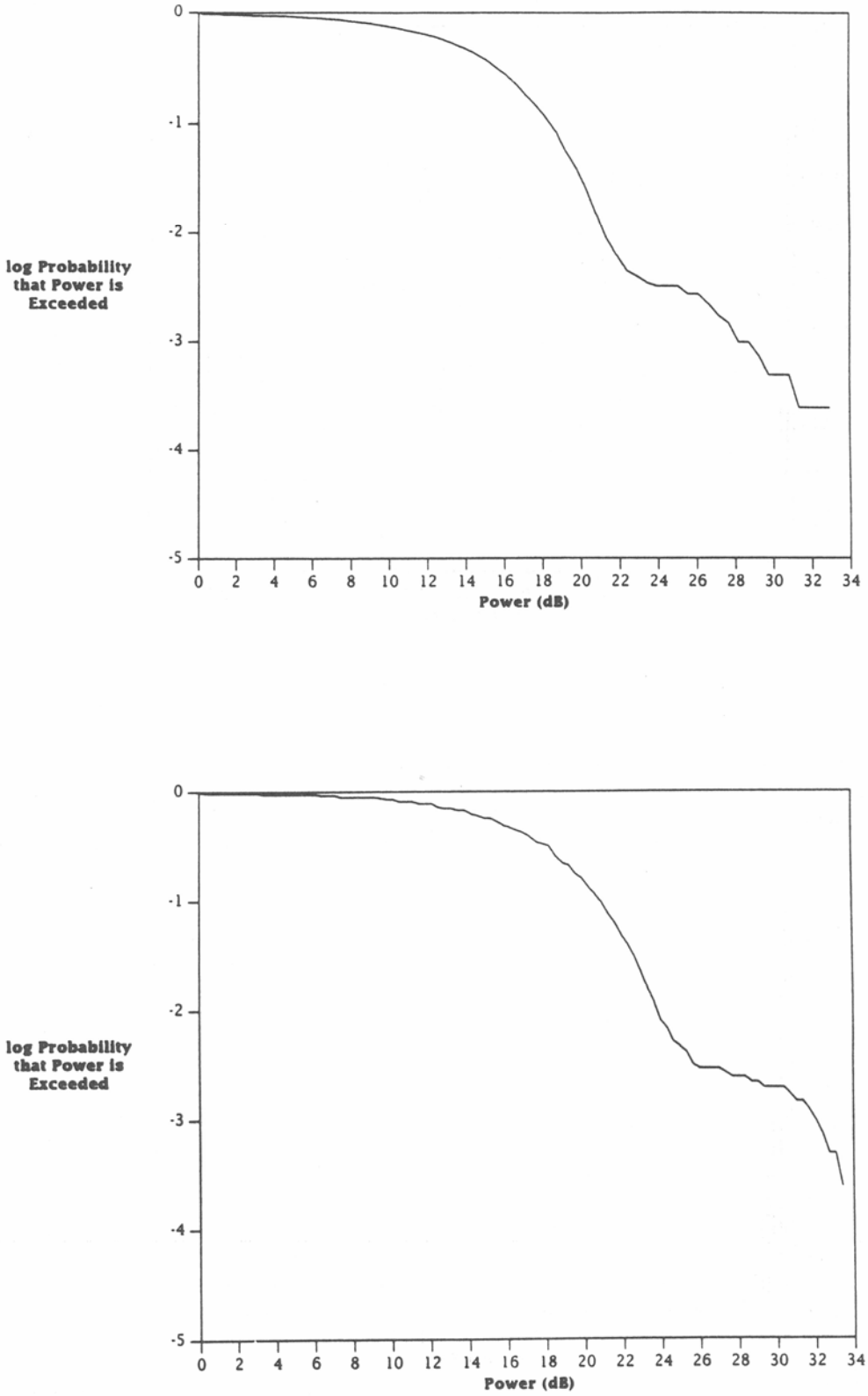

Figure 50. Comparison of (a) simulated and (b) measured (case study 5) cumulative distribution functions of the power envelope in the time domain.

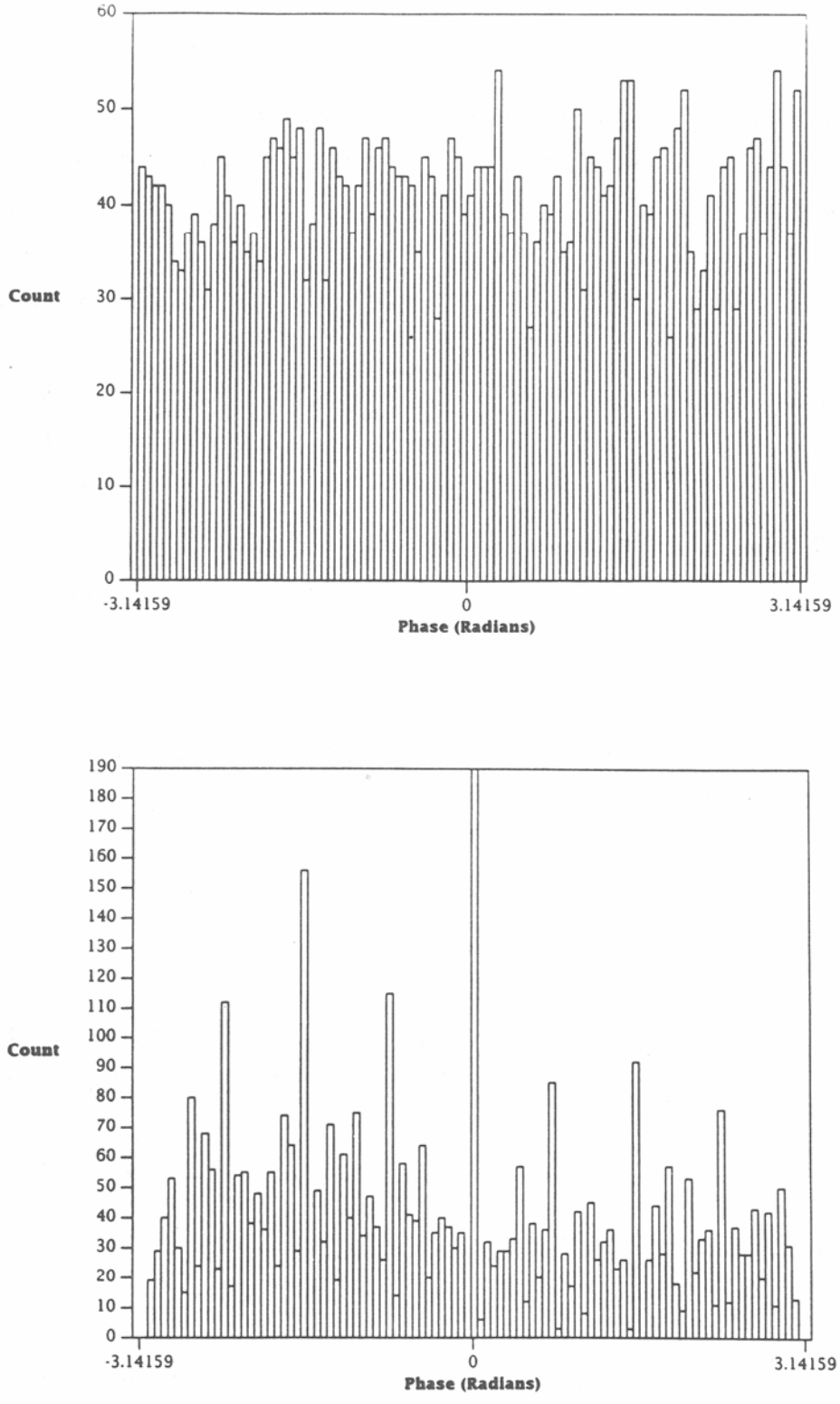

Figure 51. Comparison of (a) simulated and (b) measured (case study 5) probability density functions of the phase in the time domain.

The level crossing distributions of the voltage envelope are shown in Figure 52, and again resemble those of previous case studies, except for the long tails in the distributions.

The power spectra, power cdf's in the frequency domain, and phase pdf's in the frequency domain are shown in Figures 53, 54, and 55, respectively. These quantities resemble those of previous cases, except for the difference of approximately 20 dB in the noise floor of the power spectra between the portions of the band which are inside and outside the bandpass of the filters in the HF receiver. As pointed out above, this difference can be attributed to the presence of a filtered, broadband process (filtered impulses).

It is of interest to compute the relative power of the Gaussian, narrowband, and impulsive components of the noise/interference. Since the power is $I^2 + Q^2$, the average power in the Gaussian component is

$$P_G = \frac{1}{T}\int_0^T \left[g_I^2(t) + g_Q^2(t)\right]dt = \sigma_I^2 + \sigma_Q^2 \qquad \textbf{(26)}$$

where σ_I and σ_Q are the standard deviations of g_I and g_Q, respectively. The power in the narrowband component is

$$\begin{aligned} P_{NB} &= \frac{1}{T}\int_0^T \left\{\left[\sum_i A_i \cos\left(\Delta\omega_i t + \varphi_i\right)\right]^2 + \left[\sum_i A_i \sin\left(\Delta\omega_i t + \varphi_i\right)\right]^2\right\}dt \\ &= \sum_i A_i^2 \end{aligned} \qquad \textbf{(27)}$$

where the integral over the cross-terms in (27) vanishes due to the orthogonality of sines and cosines of different frequencies. The average power of the impulsive component is

$$\begin{aligned} P_{IMP} &= \frac{1}{T}\int_0^T \left\{\left[\sum_j B_j \frac{\sin 2\pi B\left(t - t_j\right)}{t - t_j}\cos\omega_0 t_j\right]^2 + \left[\sum_j B_j \frac{\sin 2\pi B\left(t - t_j\right)}{t - t_j}\sin\omega_0 t_j\right]^2\right\}dt \\ &\approx \frac{\pi B}{T}\sum_j B_j^2 \int_{-\infty}^{\infty} \frac{\sin^2 \pi x}{(\pi x)^2 dx} = \frac{\pi B}{T}\sum_j B_j^2 \end{aligned} \qquad \textbf{(28)}$$

where the cross-terms in (28) which arise from the products of two distinct impulses are assumed to approximately vanish, and where the integral from 0 to T has been approximated by the integral from $-\infty$ to $+\infty$.

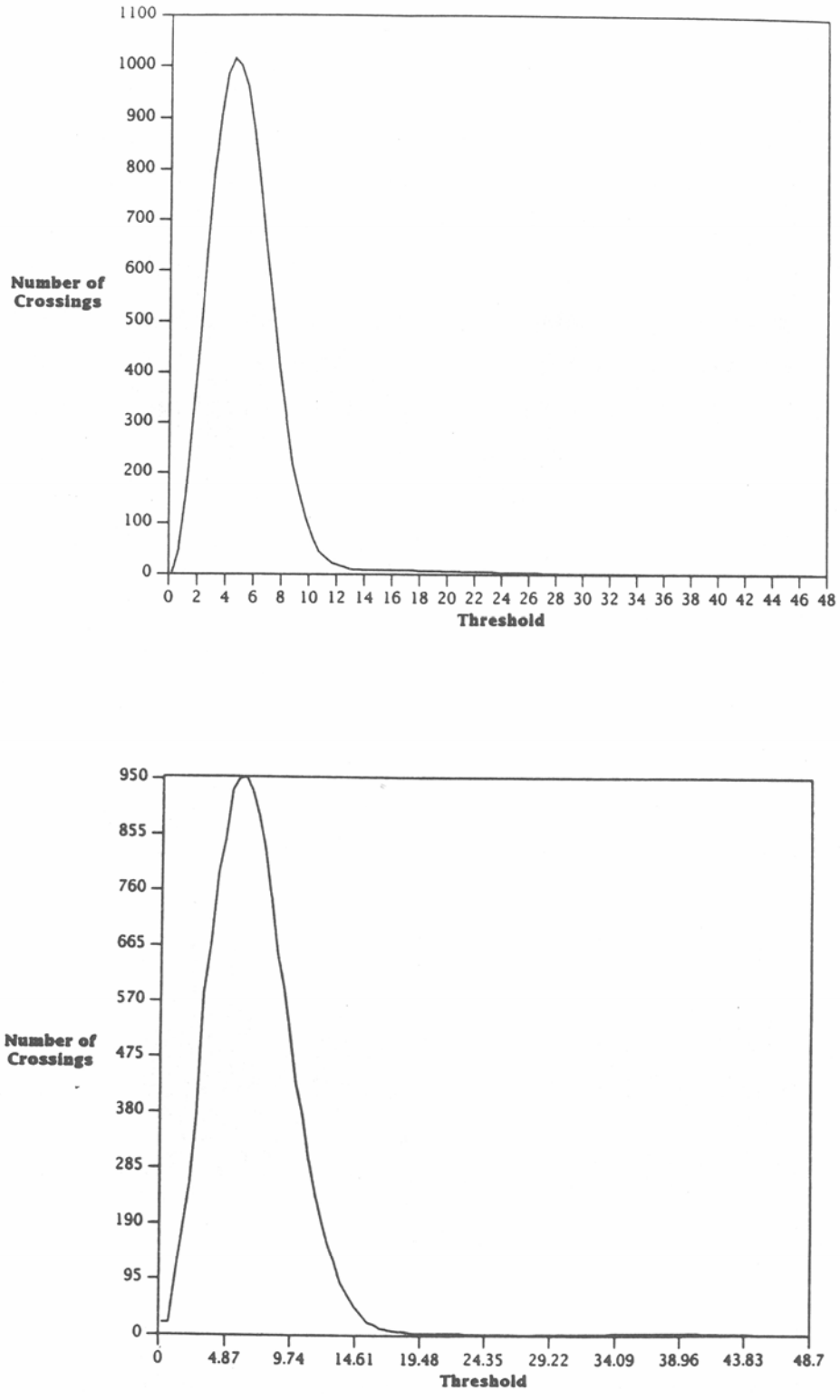

Figure 52. Comparison of (a) simulated and (b) measured (case study 5) level crossing distributions of the voltage envelope.

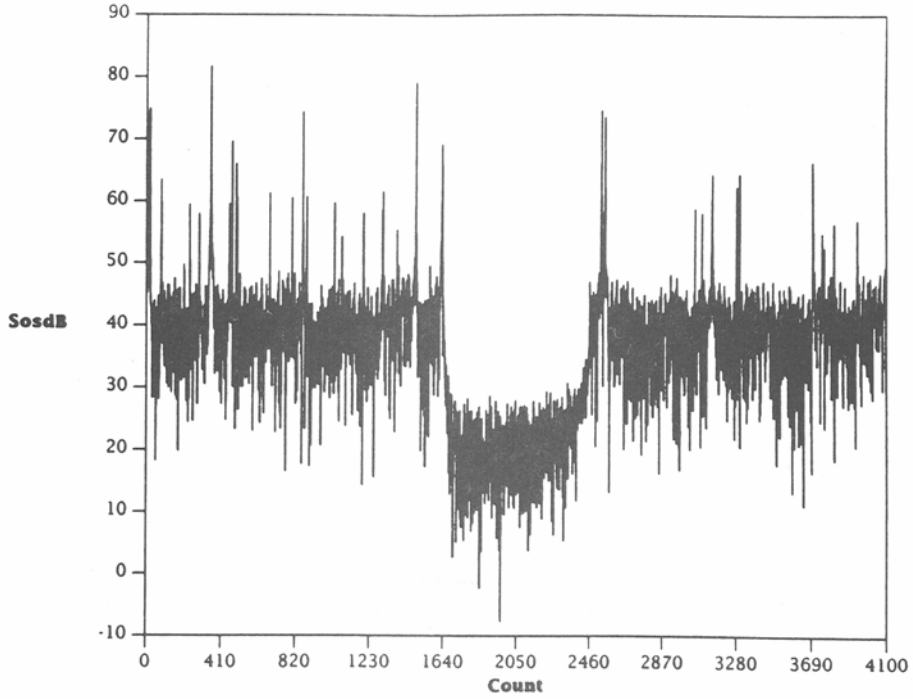

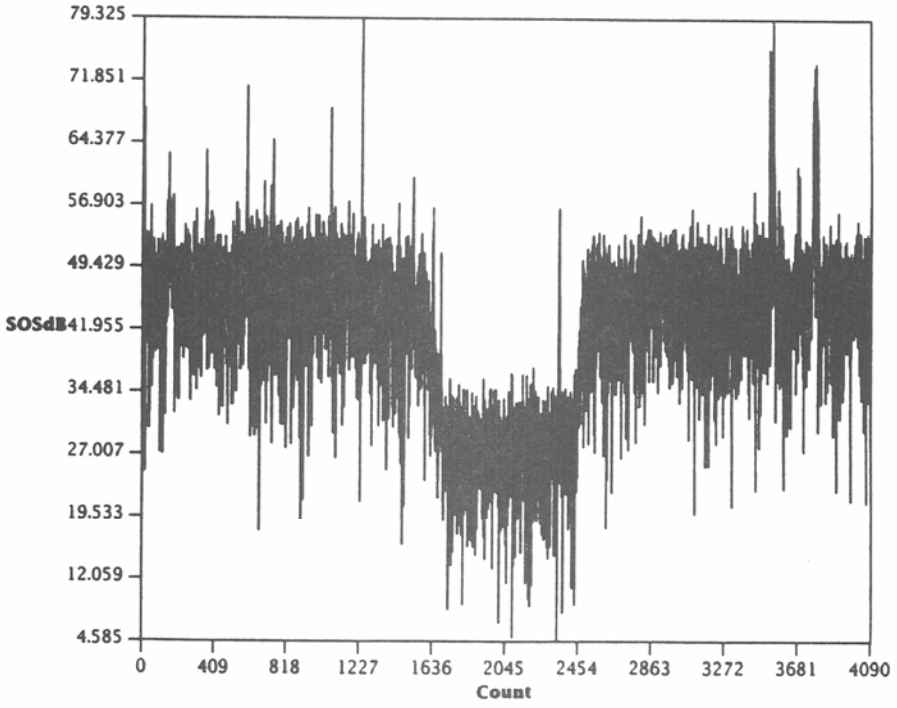

Figure 53. Comparison of (a) simulated and (b) measured (case study 5) power spectra.

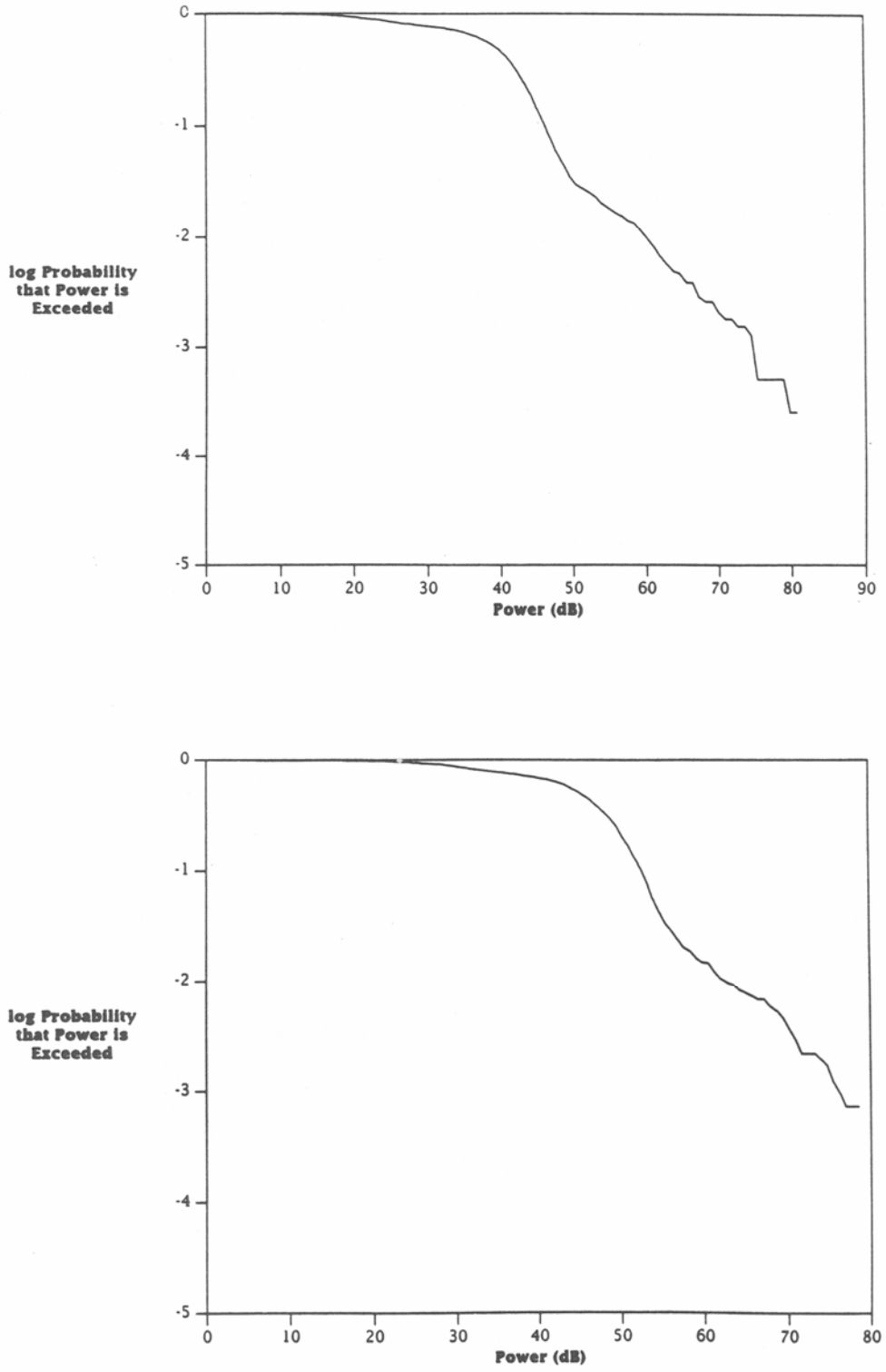

Figure 54. Comparison of (a) simulated and (b) measured (case study 5) cumulative distribution functions of the power envelope in the frequency domain.

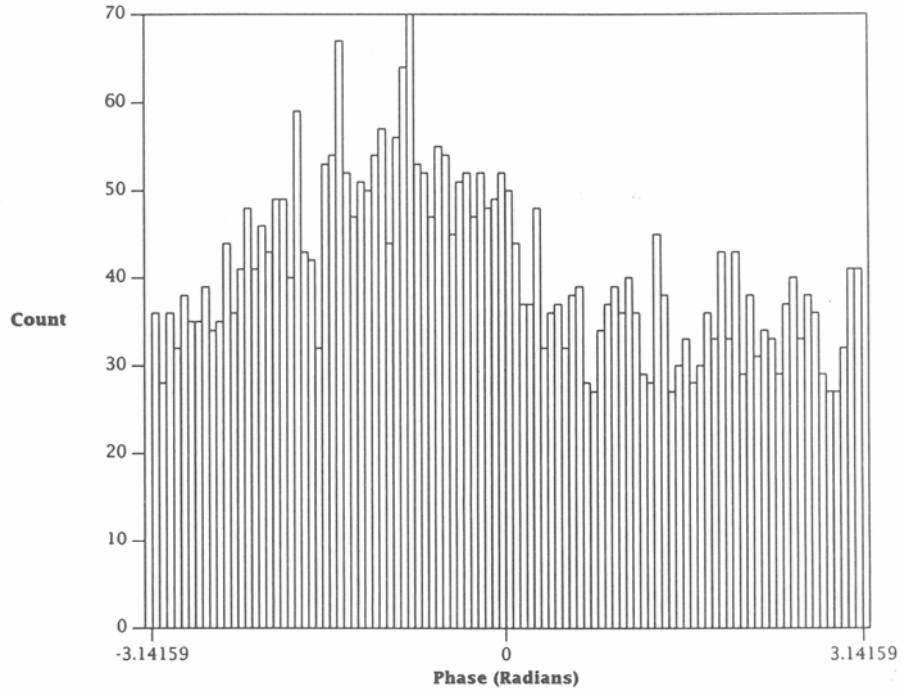

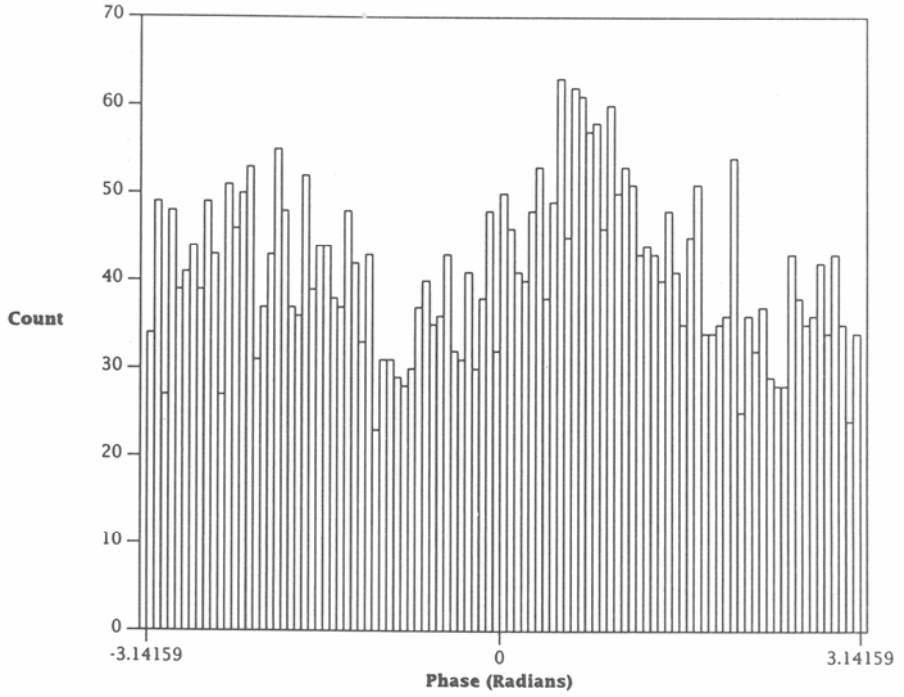

Figure 55. Comparison of (a) simulated and (b) measured (case study 5) probability density functions of the phase in the frequency domain.

In the simulation of noise/interference containing impulsive noise, $\sigma_I = \sigma_Q = 0.12$, $\sum A_i^2 = 28.13$, $\sum B_j^2 = 1.26 \times 10^{-9}$, $B = 2\pi \times 400$ kHz, and $T = 4$ ms. Substituting these values into (26)-(28), one finds that $P_G = 0.0288$, $P_{NB} = 28.13$, and $P_{IMP} = 2.52$. Thus, relative to the Gaussian noise power, the narrowband power is approximately 30 dB and the impulsive power is approximately 19 dB.

4. SUMMARY AND CONCLUSIONS

A simple physical model of wideband HF noise/interference has been developed, based on analyses of measured data. Unlike previously developed models, which have generally consisted of descriptions of the statistical characteristics of the received noise/interference (for example, the amplitude probability distribution), the present model provides a description of the received noise/interference waveform, and therefore can be used to simulate the noise/interference process. The statistical characteristics of the process have been investigated to guide the model development and to check the validity of the proposed model. In particular, we have examined the raw data, pdf's of the raw data, pdf's of the voltage and power envelopes, pdf's of the phase, and level crossing distributions of the voltage envelope. In addition, we have examined characteristics of the noise/interference in the frequency domain, including power spectra, cdf's of the power envelope in the frequency domain, and pdf's of the phase in the frequency domain. Every one of these quantities generated from the simulated data closely resembles the corresponding measured quantity for a variety of measured data. However, the model developed thus far is incomplete for several reasons.

First, in its present form the model provides no way of specifying values of the model parameters. For the simulations discussed in this report, values of the parameters were determined by examining the results of analyses of measured data. However, it would be desirable to have the capability to specify values of the parameters which are appropriate for a given environment (location, time of day, etc.) in the absence of measured data. Empirical noise models have been developed, for example the model for atmospheric noise specified by the CCIR (1986) and discussed by Spaulding and Washburn (1985), which could be of use in determining parameter values. However, combining such models with the present model to provide this capability has yet to be accomplished.

Second, the higher-order statistics, which describe the relationships between the noise/interference process at different instants in time, need to be examined and modeled. For example, distributions of pulse width and pulse spacing (essential for modeling the arrival time distribution of noise impulses) and the nonstationarity of the noise/interference need to be investigated.

Finally, the measured data analyzed thus far comprise a limited data base obtained during March 1989 at Bedford, MA. More data with impulsive noise, and atmospheric noise in particular, need to be analyzed and modeled, as do data obtained at different receive sites, at different times of year, with different antennas, and with appropriate dynamic range (greater than eight bits). These investigations are currently under way and will be reported elsewhere.

5. ACKNOWLEDGMENTS

The authors wish to thank Mr. Marc N. Richard of the Mitre Corporation for his generosity in sharing noise/interference data collected with the Mitre WBHF test facility. The authors also thank Messrs. J. McEvoy and W. Bonser of the Rome Air Development Center, Messrs. D. Bodson and G. Rekstad of the National Communication System, and LTC Robert Oldham of the U.S. Army Communications/Electronics Command for their funding support of the work reported herein.

6. REFERENCES

CCIR (1986), Characteristics and applications of atmospheric radio noise data, CCIR Report 322-3, Intl. Radio Consultive Committee, Itnl. Telecommun. Union, Geneva, Switzerland.

Dixon, R.C. (1984), Spread Spectrum Systems (John Wiley and Sons, New York, NY).

Giordano, A.A. (1970), Modeling of atmospheric noise, Ph.D. dissertation, University of Pennsylvania, Philadelphia, P A.

Hall, H.M. (1966), A new model of "impulsive" phenomena: application to atmospheric noise communications channels, Electron. Lab., Stanford Univ., Stanford, CA, Tech. Rep. 3412-8 and 7050-7, SU-SEL-66-052, Aug.

Hoffmeyer, J.A and M. Nesenbergs (1987), Wideband HF modeling and simulation, NTIA Report 87-221, July (NTIS Order No. PB 88-116116/AS).

Hoffmeyer, J.A. and L.E. Vogler (1987), Measurement, modeling, and simulation of LOS microwave channels, NATO AGARD Conf. Proc., No. 419, Scattering and Propagation in Random Media, Rome, Italy, May, Paper No. 31.

Ibukun, O. (1966), Structural aspects of atmospheric noise in the tropics, Proc. IEEE, 54, 361-367.

Lemmon, J.J. (1989), Wideband HF noise and interference modeling, IEEE 1989 Military Commun. Conf., Boston, MA, Paper No. 48.4.

Mihram, G.A. (1972), Simulation: Statistical foundations and methodology (Academic Press, Inc., New York, NY).

Perry, B.D. and L.G. Abraham (1988), Wideband HF interference and noise model based on measured data, IEE Conf. Publication 284: Fourth Intl. Conf. on HF Radio Systems and Techniques, London, U.K..

Perry, B.D. and R. Rifkin (1989), Measured wideband HF mid-latitude channel characteristics, IEEE 1989 Military Commun. Conf., Boston, MA, Paper No. 48.1.

Rice, S.O. (1944 and 1945), Mathematical analysis of random noise, Bell System Tech. J., 23, 282-332, July 1944; 24, 46-156, January 1945.

Spaulding, A.D. (1977), Stochastic modeling of the electromagnetic interference environment, Conf. Record, Intl. Conf. on Commun., ICC '77, Chicago, IL, June, pp. 43.4-114-123 (IEEE Catalog No. 77CH-1209-GCSCB).

Spaulding, A.D. (1982), Atmospheric noise and its effects on telecommunication system performance, Chapter 7, Handbook of Atmospherics, Vol. 1, H. Volland, Ed. (CRC Press, Boca Raton, FL).

Spaulding, A.D. and D. Middleton (1975), Optimum reception in an impulsive interference environment, OT Report 75-67 (NTIS Order No. COM 75-11097/AS).

Spaulding, A.D. and J.S. Washburn (1985), Atmospheric radio noise: worldwide levels and other characteristics, NTIA Report 85-173, April (NTIS Order No. PB 85-212942).

Vogler, L.E. and J.A Hoffmeyer (1988), A new approach to HF channel modeling and simulation, Part I: Deterministic model, NTIA Report 88-240, Dec. (NTIS Order No. PB 89-203962/AS).

Vogler, L.E. and J.A. Hoffmeyer (1990), A new approach to HF channel modeling and simulation, Part II: Stochastic model, NTIA Report 90-255, Feb. (NTIS Order No. PB 90-200338/AS).

Vogler, L.E., J.A. Hoffmeyer, J.J. Lemmon, and M. Nesenbergs (1988), Progress and remaining issues in the development of a wideband HF channel model and simulator, NATO AGARD Conf. Proc., Propagation Effects and Circuit Performance of Modern Military Radio Systems with Particular Emphasis on those Employing Bandspreading, Paris, France, Oct., Paper No.6.

Appendix

Table 1 displays the measurement parameters that were used to obtain the noise/interference records discussed in this report. Listed are the times, dates, center frequencies, and values of the variable attenuation that were used to record these data. Each record is identified by a record number. The following plots display the first 4 ms of both the Q- and I-channel data for each of the records.

Table A-1. Measurement Characteristics of Wideband HF Noise/Interference Records

Record Number	Date (1989)	Time (UT)	Center Frequency (MHz)	Variable Attenuation (dB)
1	15 March	04:01:22	9.244	24
2	15 March	05:50:42	7.844	21
3	15 March	06:22:00	10.662	16
4	15 March	07:48:05	7.844	29
5	15 March	09:46:34	5.936	22
6	15 March	11:57:02	7.844	21
7	15 March	15:15:59	19.29	6
8	15 March	19:22:32	23.862	6
9	15 March	20:06:49	15.848	26
10	22 March	22:21:16	19.29	27
11	15 March	22:34:52	19.29	6
12	10 March	00:29:22	19.29	6
13	10 March	00:39:19	18.718	24
14	17 March	00:57:51	15.848	29
15	17 March	03:20:34	10.662	11
16	10 March	03:41:19	13.666	12
17	10 March	03:48:17	13.666	18
18	17 March	04:45:19	9.244	28

Table A-1.(Cont.)

Record Number	Date (1989)	Time (UT)	Center Frequency (MHz)	Variable Attenuation (dB)
19	10 March	06:25:57	10.662	18
20	10 March	06:25:57	9.244	30
21	17 March	07:08:11	10.662	11
22	17 March	08:47:51	5.936	21
23	10 March	09:51:21	7.844	31
24	10 March	19:58:11	5.936	27
25	10 March	17:37:32	23.862	6
26	27 March	23:37:48	19.29	12
27	28 March	02:05:34	15.848	25
28	28 March	03:27:56	13.666	25
29	28 March	05:59:35	15.848	6
30	28 March	08:13:01	15.848	29
31	28 March	10:26:48	13.666	20
32	28 March	12:07:27	18.718	17
33	28 March	19:04:31	19.29	16
34	28 March	22:10:40	19.29	17
35	28 March	23:39:48	15.848	26
36	29 March	02:31:34	13.666	27
37	29 March	03:28:33	10.662	27
38	29 March	14:53:31	25.885	6
39	29 March	16:27:07	23.862	6
40	29 March	18:51:19	25.885	6
41	29 March	20:37:32	19.29	16
42	29 March	20:45:25	19.29	16

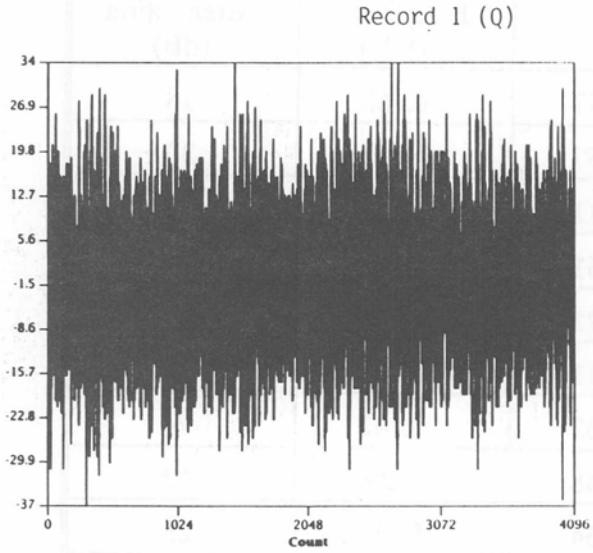
Record 1 (Q)
34
26.9
19.8
12.7
5.6
-1.5
-8.6
-15.7
-22.8
-29.9
-37
0
1024
2048
3072
4096
Count

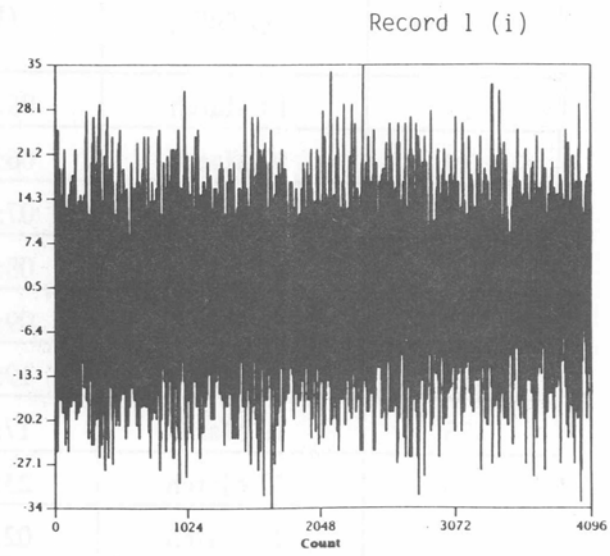
Record 1 (i)
35
28.1
21.2
14.3
7.4
0.5
-6.4
-13.3
-20.2
-27.1
-34
0
1024
2048
3072
4096
Count

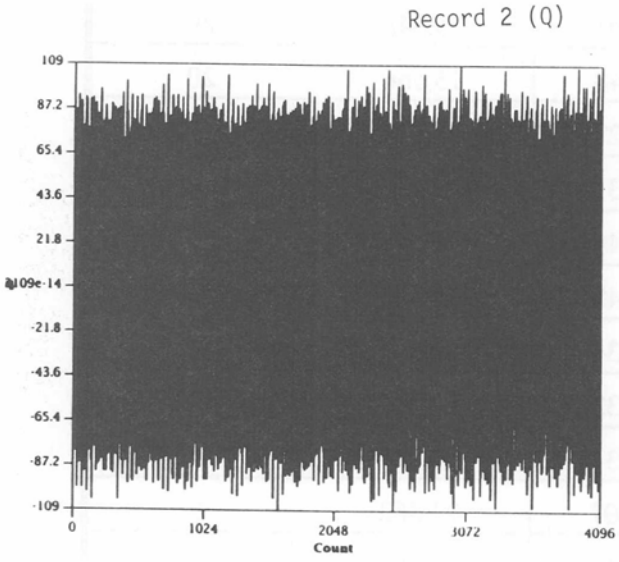
Record 2 (Q)
109
87.2
65.4
43.6
21.8
-1.09e-14
-21.8
-43.6
-65.4
-87.2
-109
0
1024
2048
3072
4096
Count

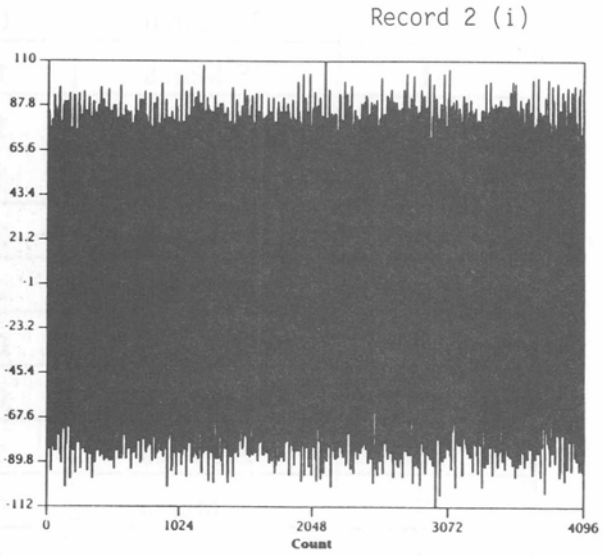
Record 2 (i)
110
87.8
65.6
43.4
21.2
-1
-23.2
-45.4
-67.6
-89.8
-112
0
1024
2048
3072
4096
Count

Record 3 (Q)

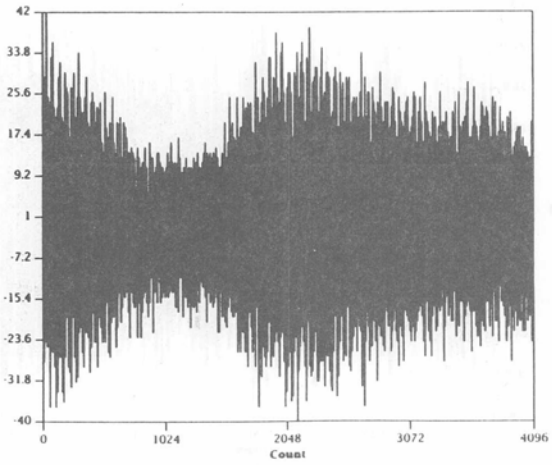

Record 3 (i)

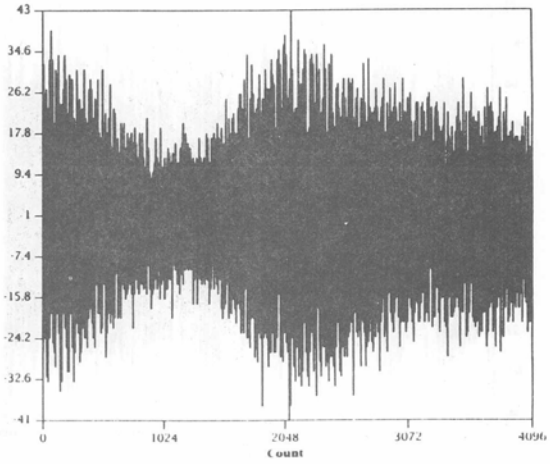

Record 4 (Q)

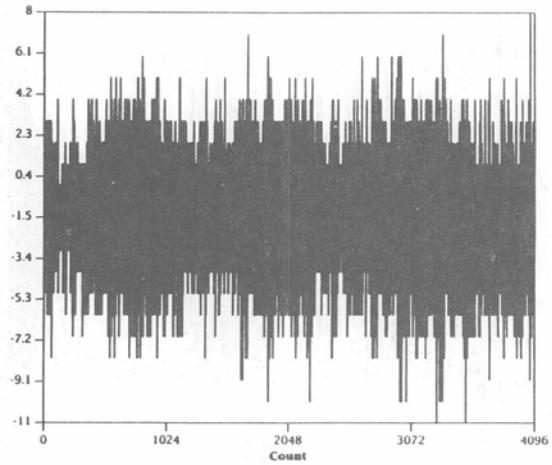

Record 4 (i)

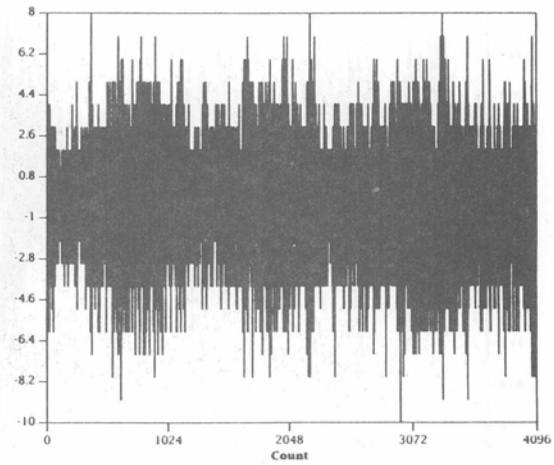

Record 5 (Q)

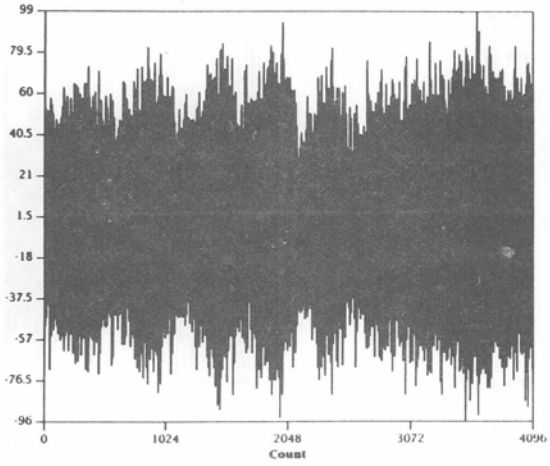

Record 5 (i)

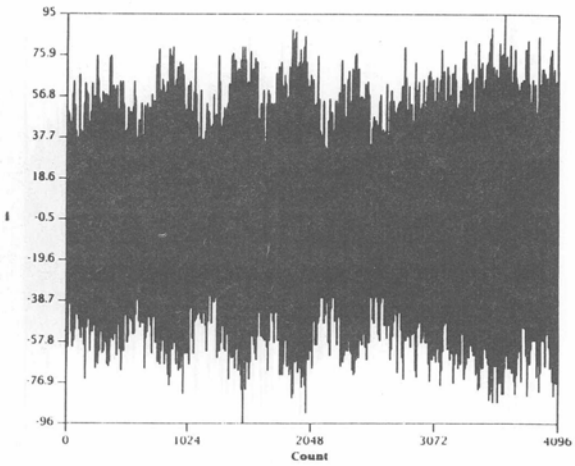

Record 6 (Q)

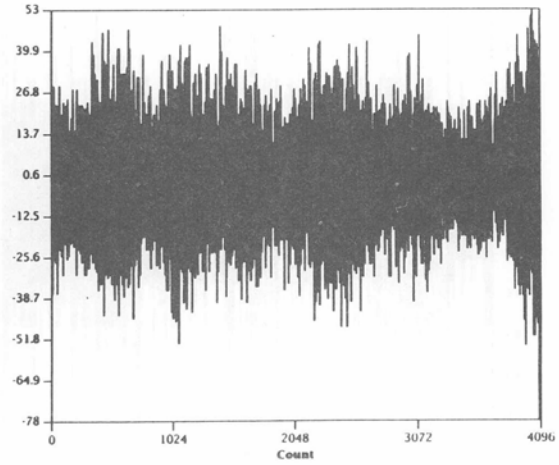

Record 6(i)

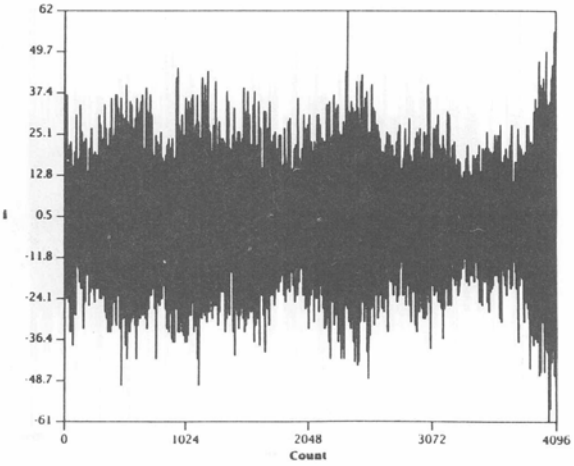

Record 7 (Q)

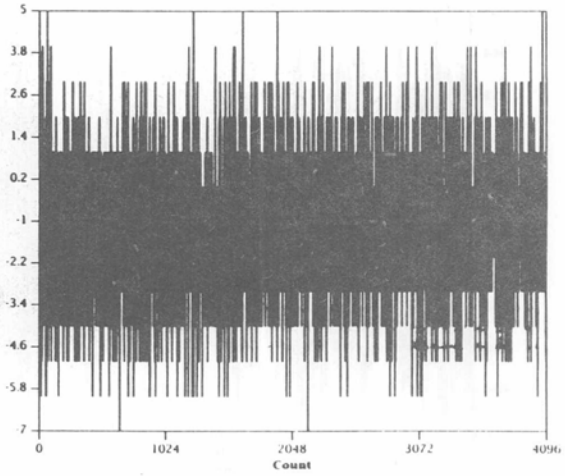

Record 7 (i)

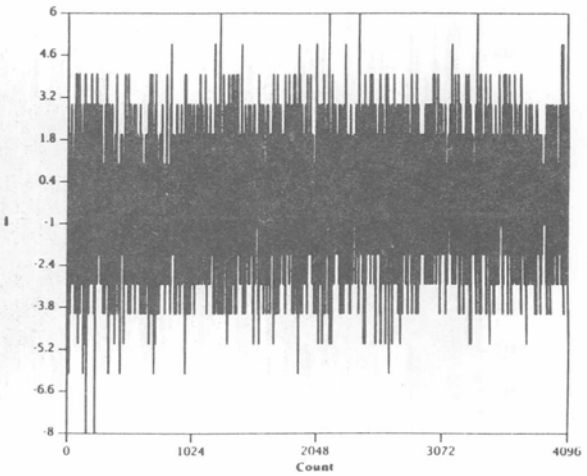

Record 8 (Q)

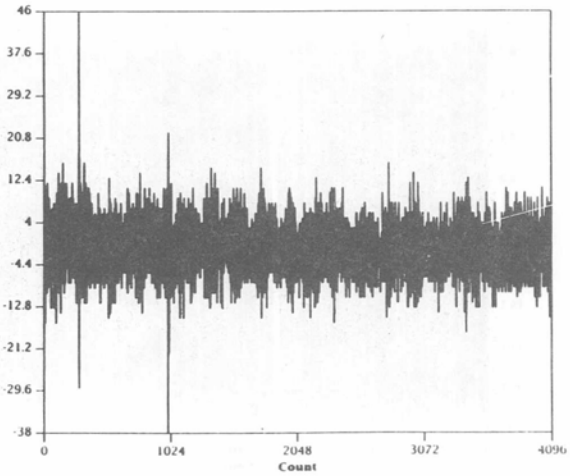

Record 8 (i)

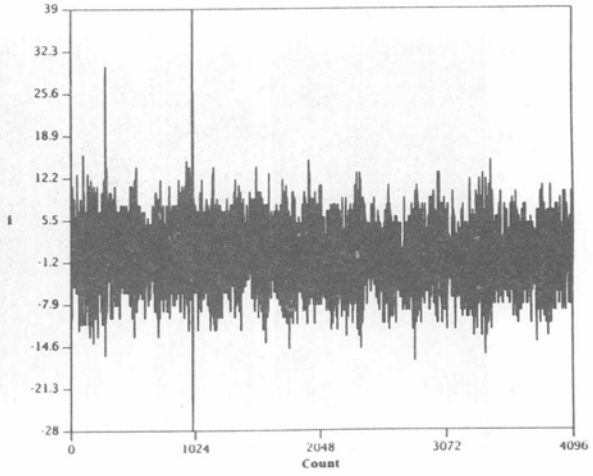

Record 9 (Q)

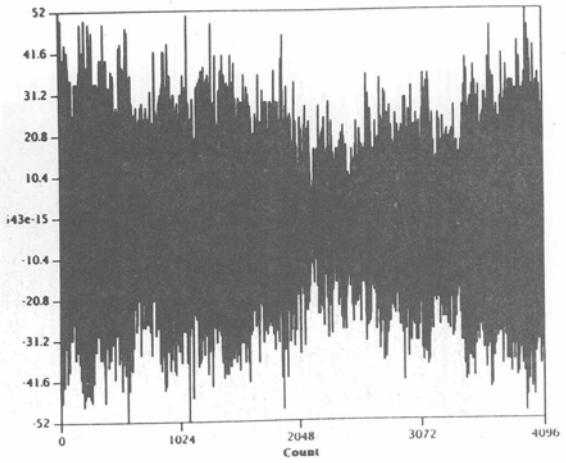

Record 9 (i)

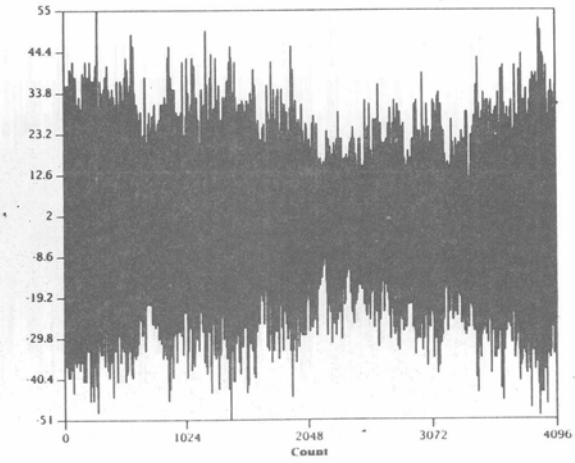

Record 10 (Q)

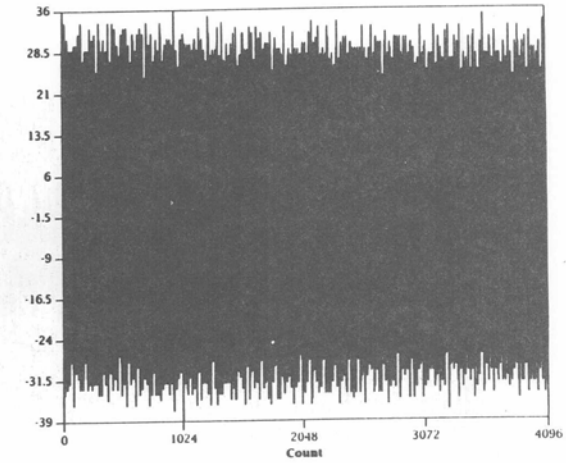

Record 10 (i)

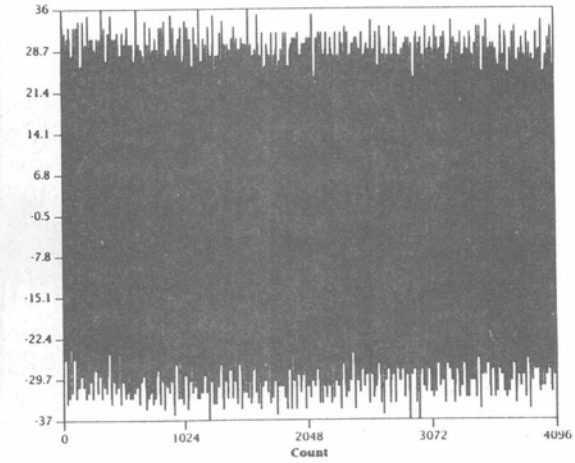

Record 11 (Q)

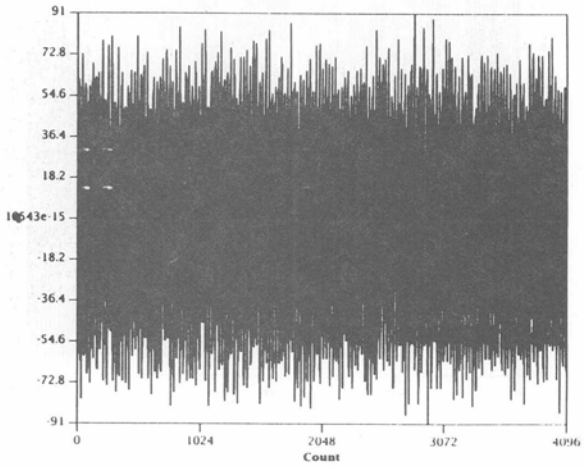

Record 11 (i)

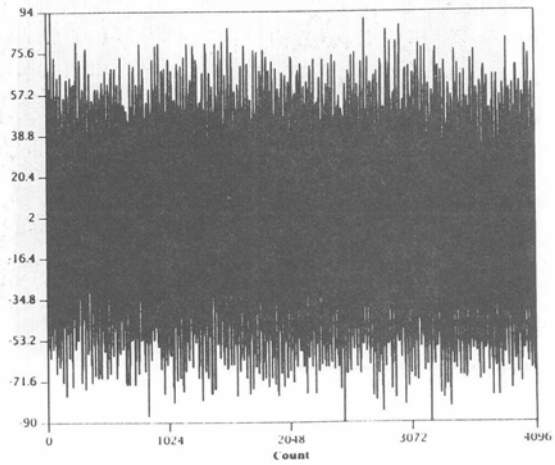

Record 12 (Q)

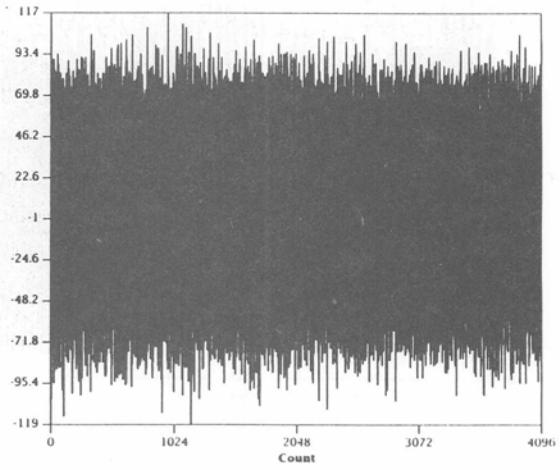

Record 12 (i)

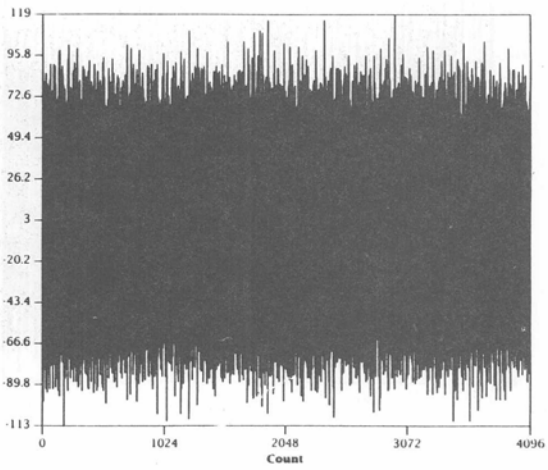

Record 13 (Q)

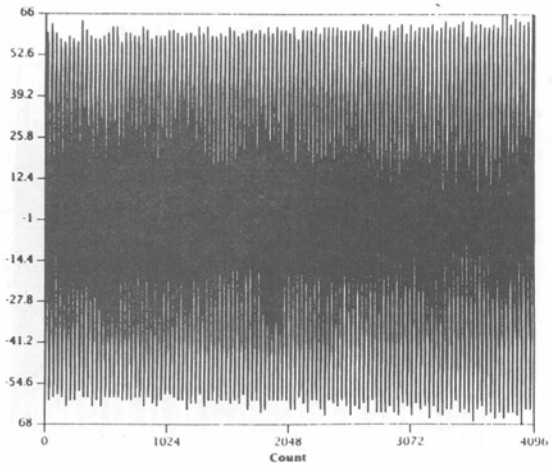

Record 13 (i)

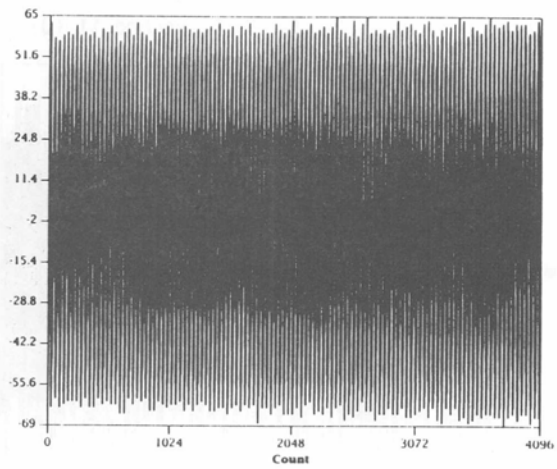

Record 14 (Q)

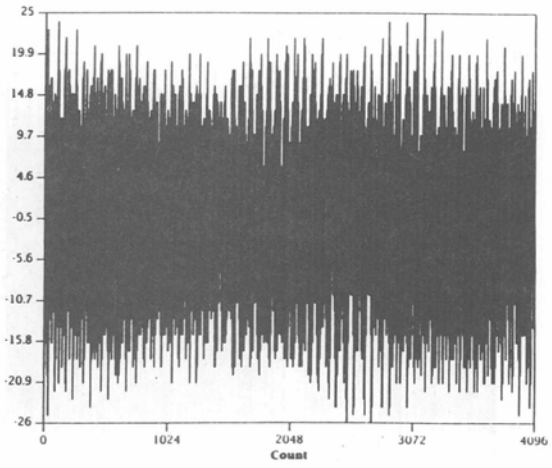

Record 14 (i)

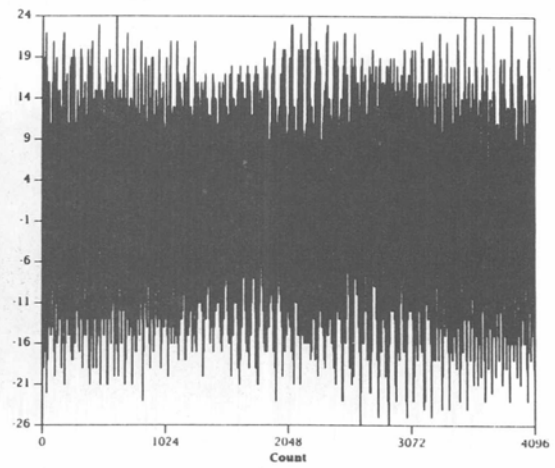

Record 15 (Q)

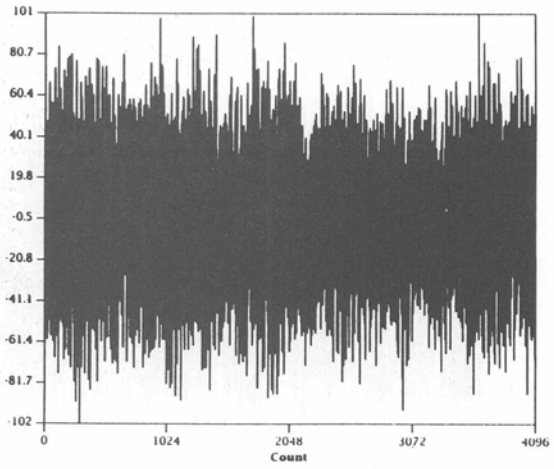

Record 15 (i)

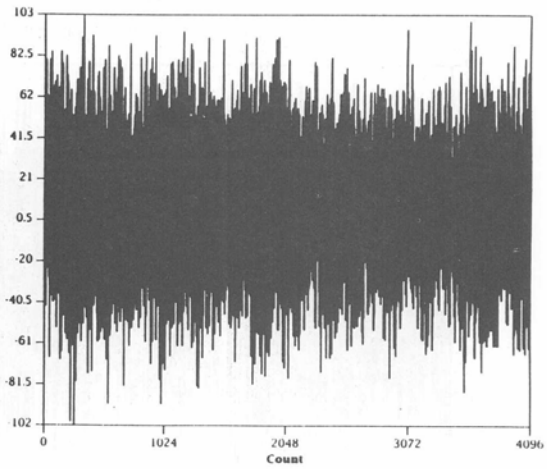

Record 16 (Q)

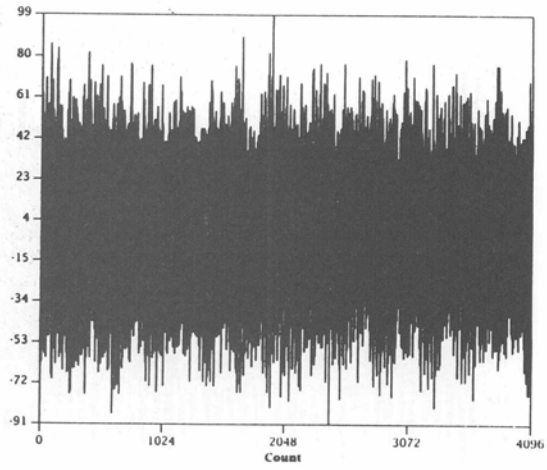

Record 16 (i)

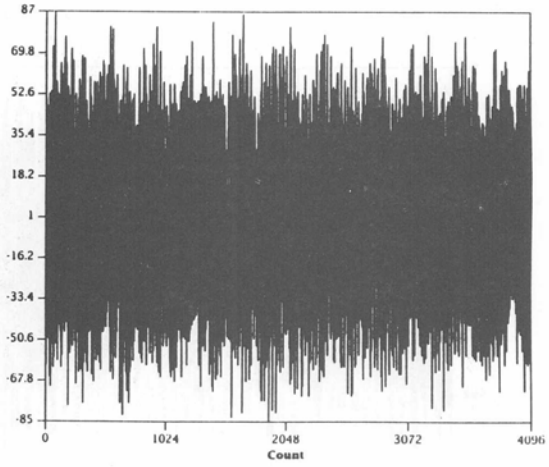

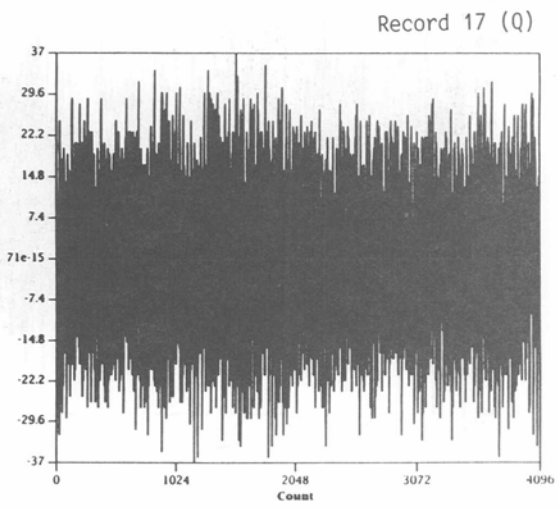
Record 17 (Q)
37
29.6
22.2
14.8
7.4
71e-15
-7.4
-14.8
-22.2
-29.6
-37
0
1024
2048
3072
4096
Count

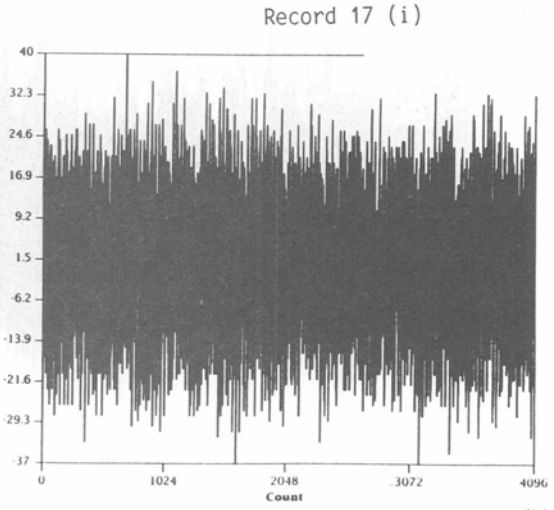
Record 17 (i)
40
32.3
24.6
16.9
9.2
1.5
-6.2
-13.9
-21.6
-29.3
-37
0
1024
2048
3072
4096
Count

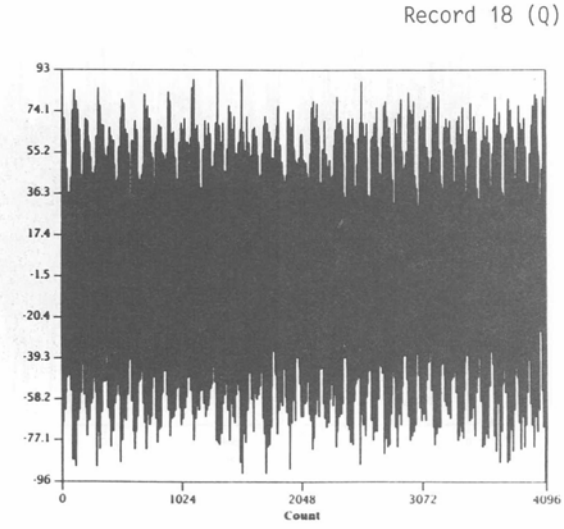
Record 18 (Q)
93
74.1
55.2
36.3
17.4
-1.5
-20.4
-39.3
-58.2
-77.1
-96
0
1024
2048
3072
4096
Count

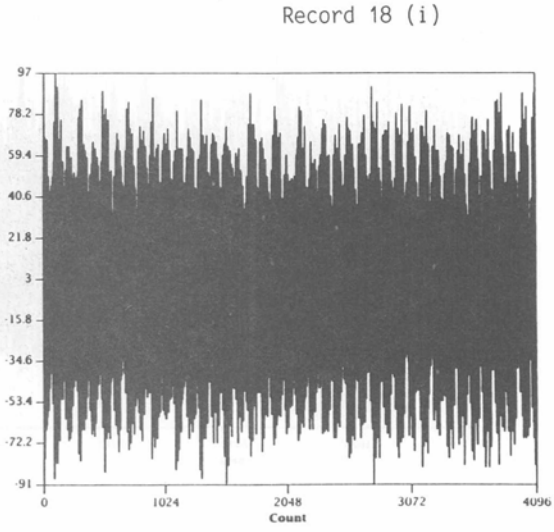
Record 18 (i)
97
78.2
59.4
40.6
21.8
3
-15.8
-34.6
-53.4
-72.2
-91
0
1024
2048
3072
4096
Count

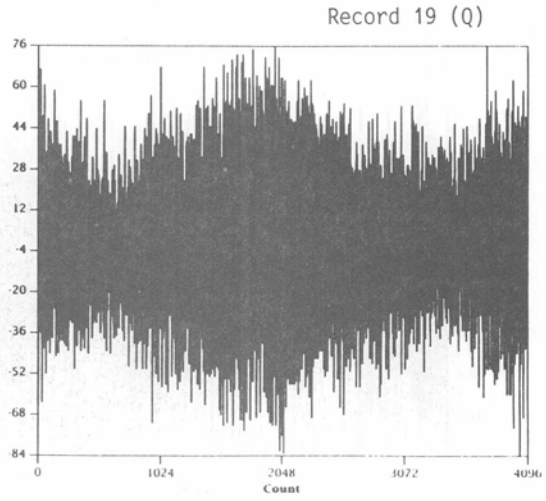
Record 19 (Q)
76
60
44
28
12
-4
-20
-36
-52
-68
-84
0
1024
2048
3072
4096
Count

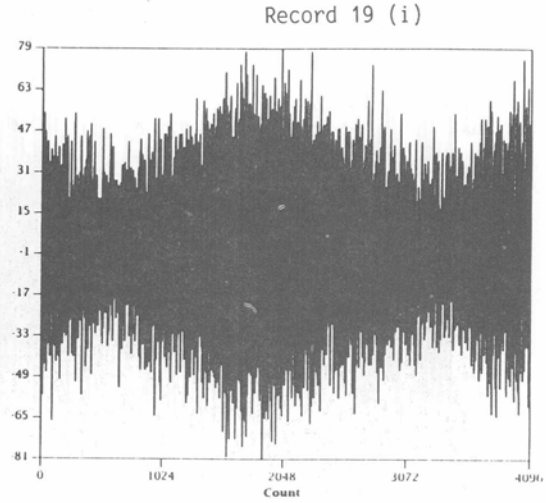
Record 19 (i)
79
63
47
31
15
-1
-17
-33
-49
-65
-81
0
1024
2048
3072
4096
Count

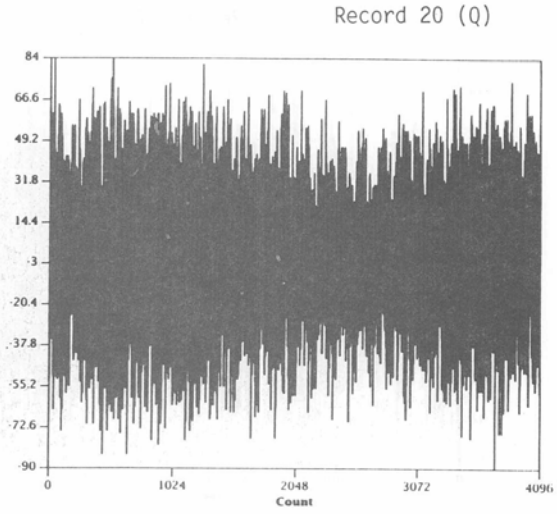
Record 20 (Q)
84
66.6
49.2
31.8
14.4
-3
-20.4
-37.8
-55.2
-72.6
-90
0
1024
2048
3072
4096
Count

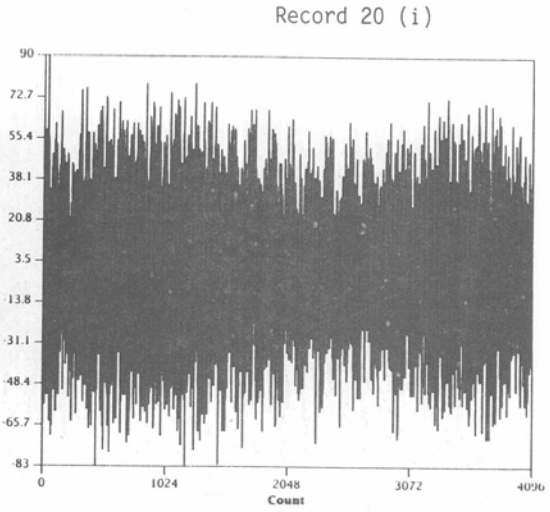
Record 20 (i)
90
72.7
55.4
38.1
20.8
3.5
-13.8
-31.1
-48.4
-65.7
-83
0
1024
2048
3072
4096
Count

Record 21 (Q)

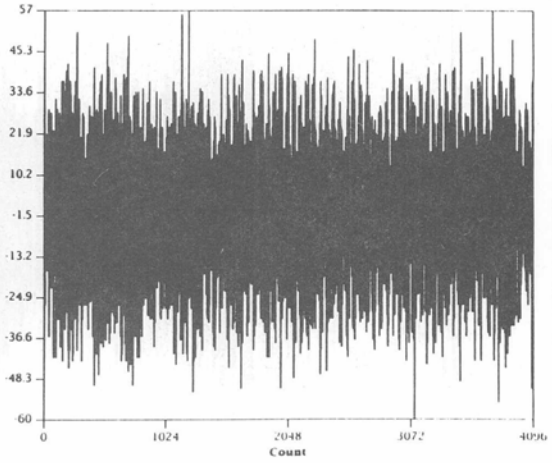

Record 21 (i)

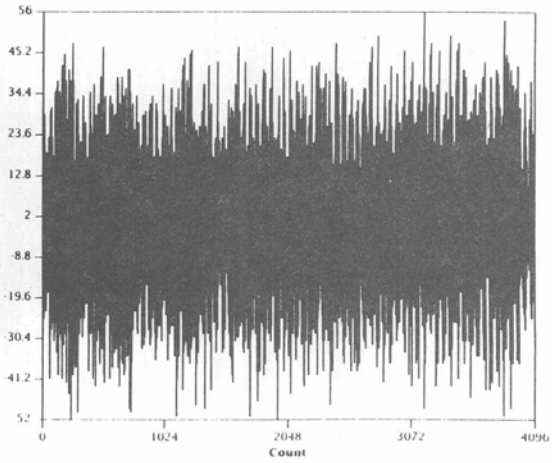

Record 22 (Q)

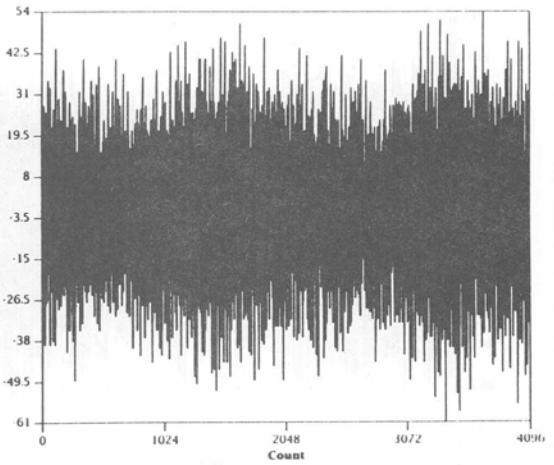

Record 22 (i)

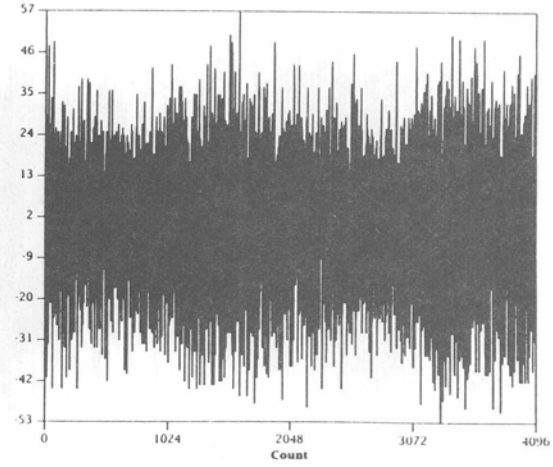

Record 23 (Q)

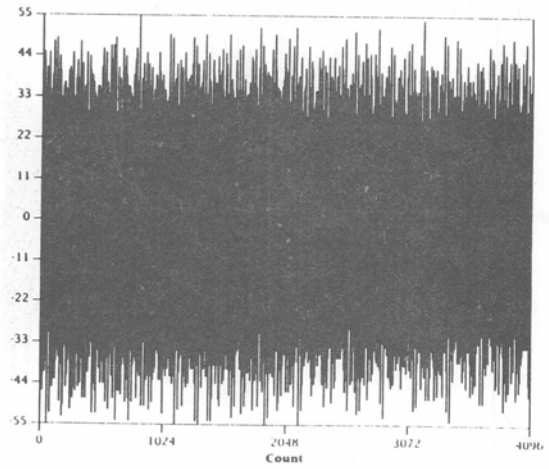

Record 23 (i)

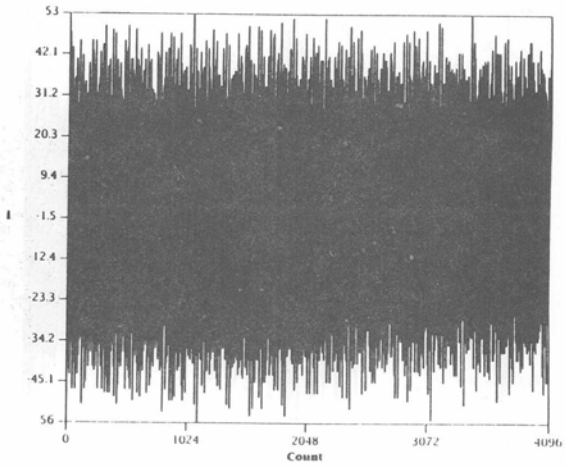

Record 24 (Q)

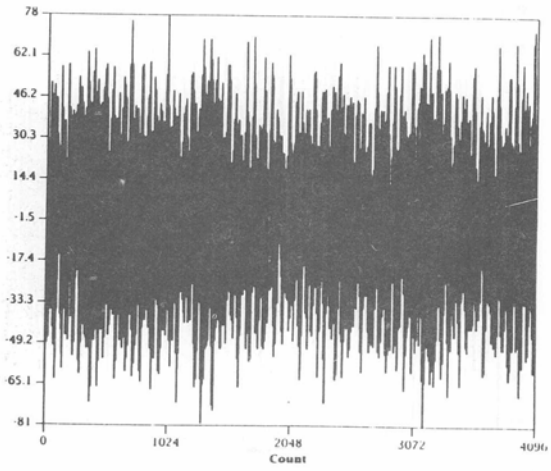

Record 24 (i)

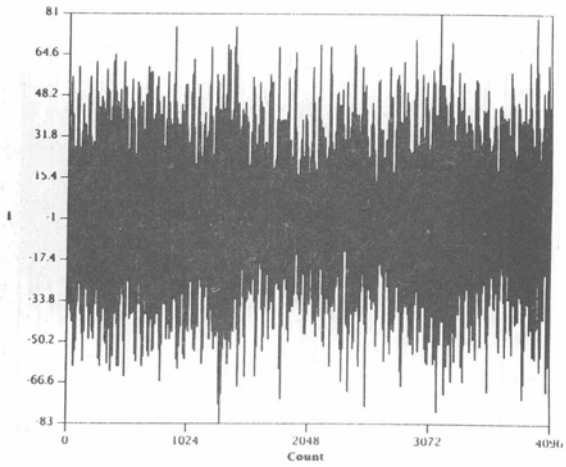

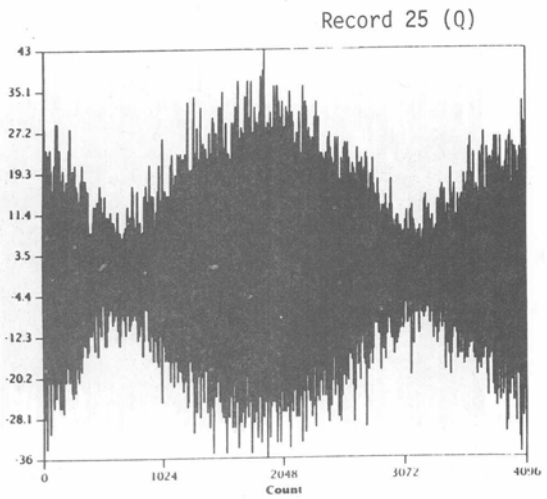
Record 25 (Q)
43
35.1
27.2
19.3
11.4
3.5
-4.4
-12.3
-20.2
-28.1
-36
0
1024
2048
3072
4096
Count

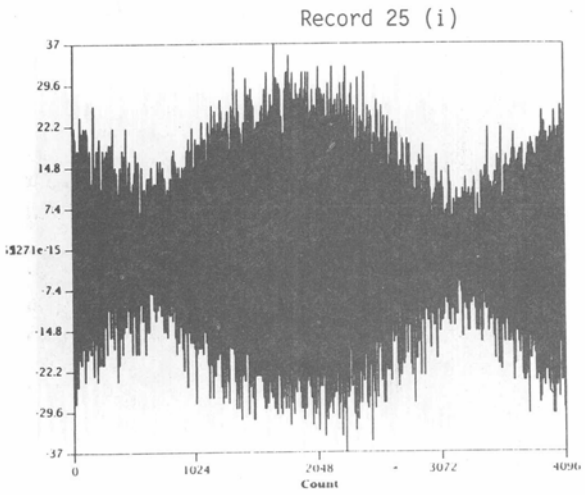
Record 25 (i)
37
29.6
22.2
14.8
7.4
-7.4
-14.8
-22.2
-29.6
-37
0
1024
2048
3072
4096
Count

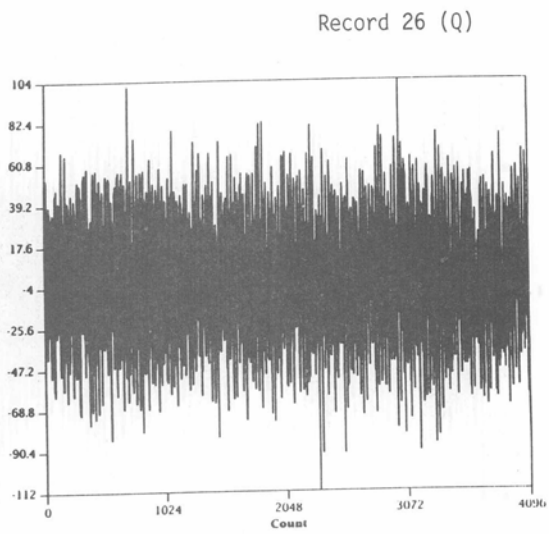
Record 26 (Q)
104
82.4
60.8
39.2
17.6
-4
-25.6
-47.2
-68.8
-90.4
-112
0
1024
2048
3072
4096
Count

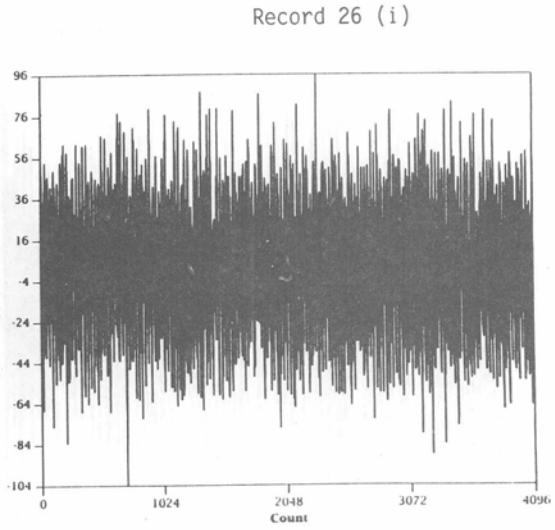
Record 26 (i)
96
76
56
36
16
-4
-24
-44
-64
-84
-104
0
1024
2048
3072
4096
Count

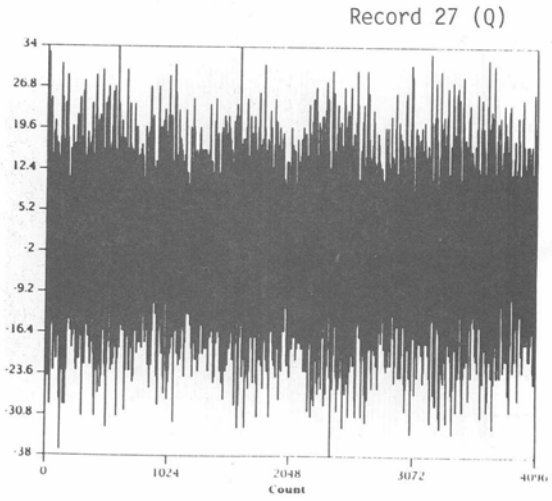
Record 27 (Q)
34
26.8
19.6
12.4
5.2
-2
-9.2
-16.4
-23.6
-30.8
-38
0
1024
2048
3072
Count

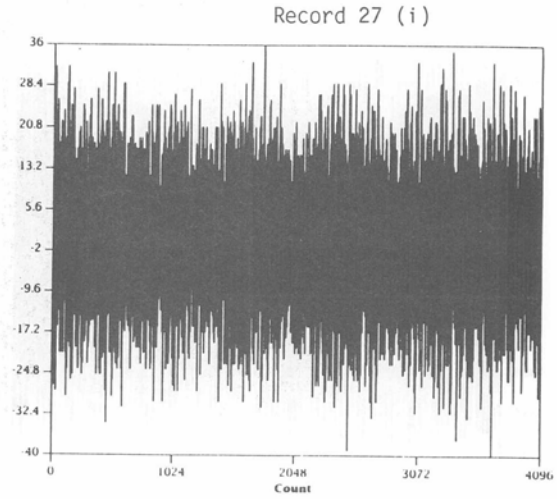
Record 27 (i)
36
28.4
20.8
13.2
5.6
-2
-9.6
-17.2
-24.8
-32.4
-40
0
1024
2048
3072
4096
Count

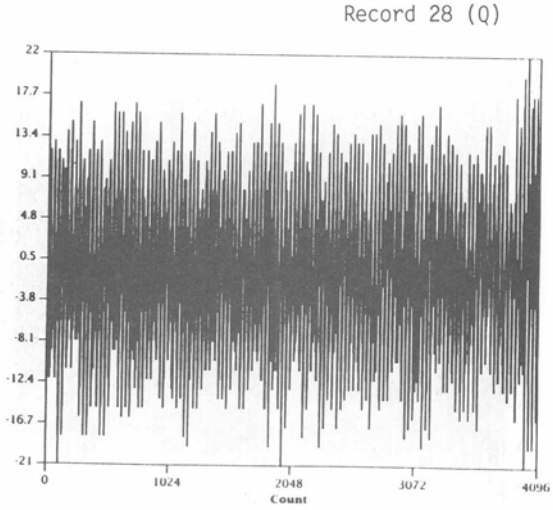
Record 28 (Q)
22
17.7
13.4
9.1
4.8
0.5
-3.8
-8.1
-12.4
-16.7
-21
0
1024
2048
3072
4096
Count

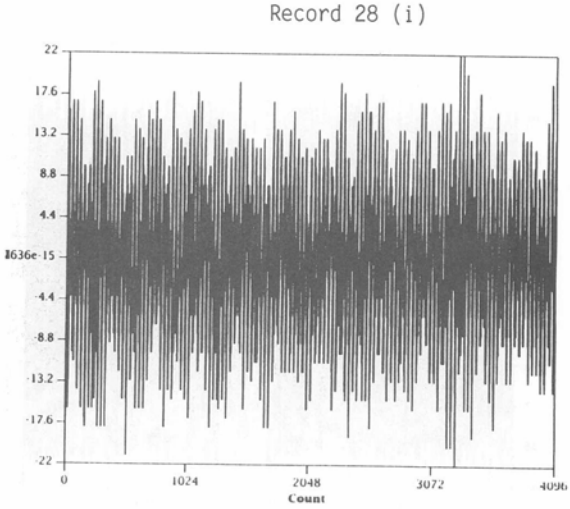
Record 28 (i)
22
17.6
13.2
8.8
4.4
1636e-15
-4.4
-8.8
-13.2
-17.6
-22
0
1024
2048
3072
4096
Count

Record 29 (Q)

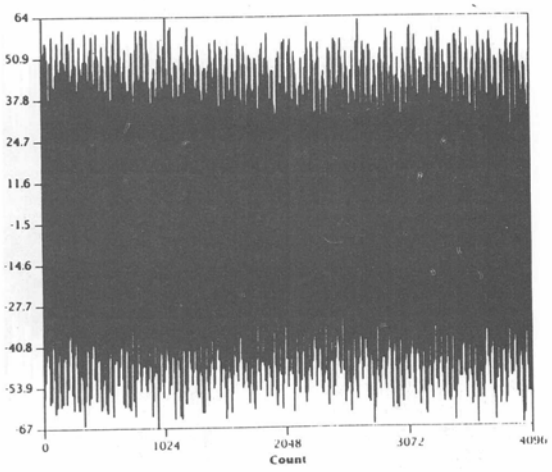

Record 29 (i)

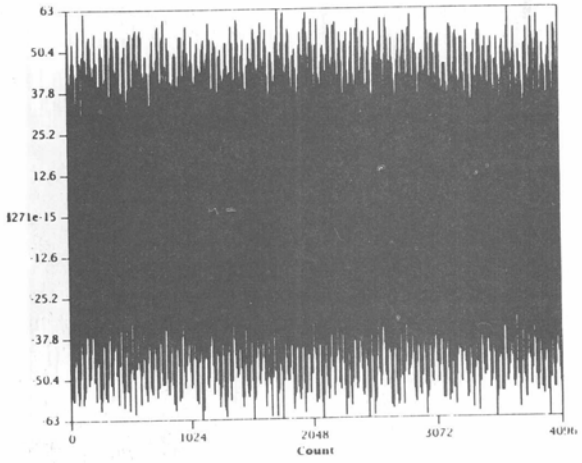

Record 30 (Q)

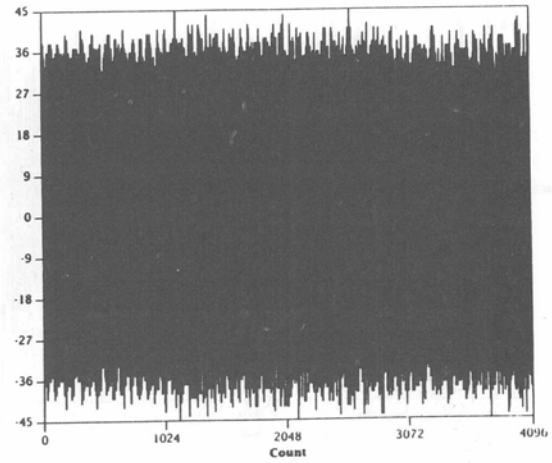

Record 30 (i)

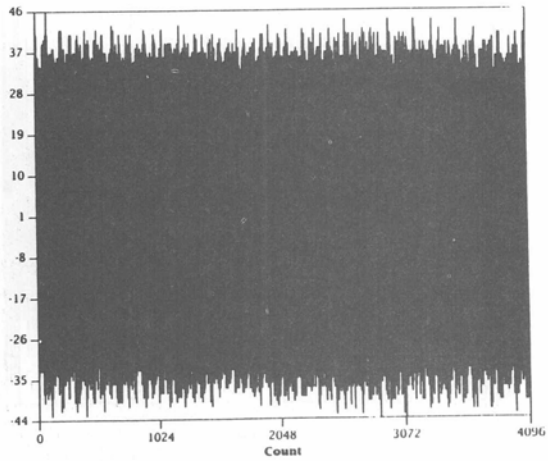

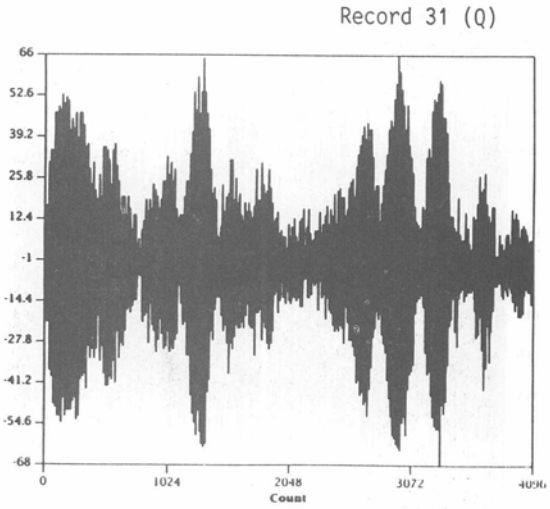
Record 31 (Q)
66
52.6
39.2
25.8
12.4
-1
-14.4
-27.8
-41.2
-54.6
-68
0
1024
2048
3072
Count

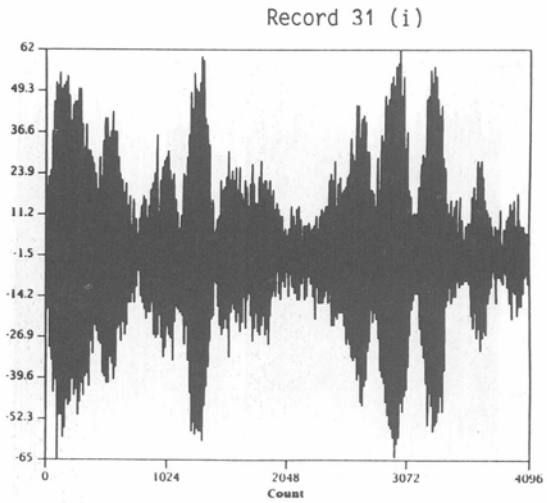
Record 31 (i)
62
49.3
36.6
23.9
11.2
-1.5
-14.2
-26.9
-39.6
-52.3
-65
0
1024
2048
3072
4096
Count

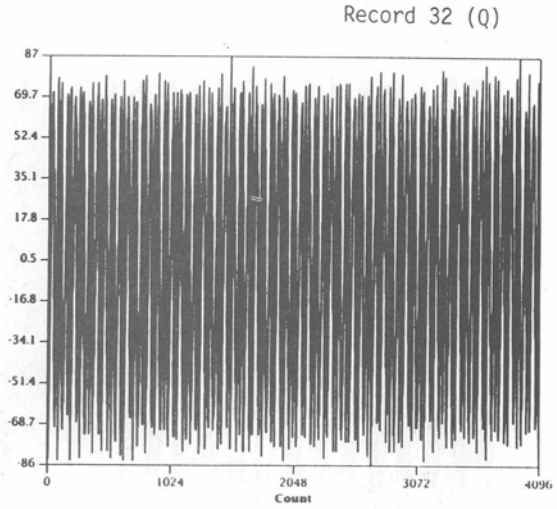
Record 32 (Q)
87
69.7
52.4
35.1
17.8
0.5
-16.8
-34.1
-51.4
-68.7
-86
0
1024
2048
3072
4096
Count

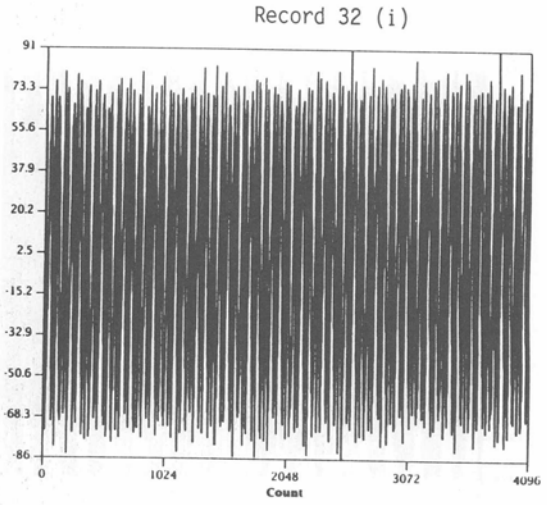
Record 32 (i)
91
73.3
55.6
37.9
20.2
2.5
-15.2
-32.9
-50.6
-68.3
-86
0
1024
2048
3072
4096
Count

Record 33 (Q)

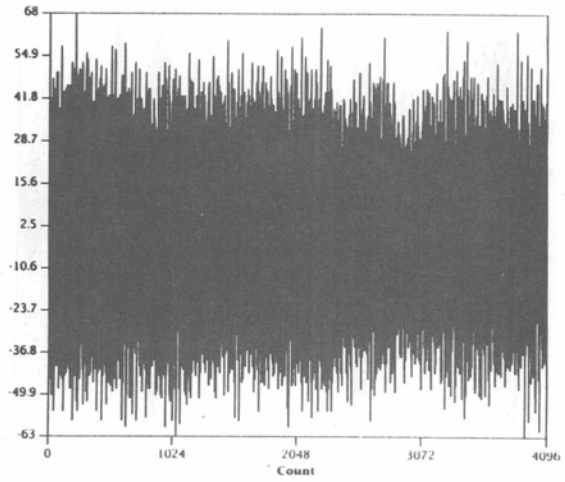

Record 33 (i)

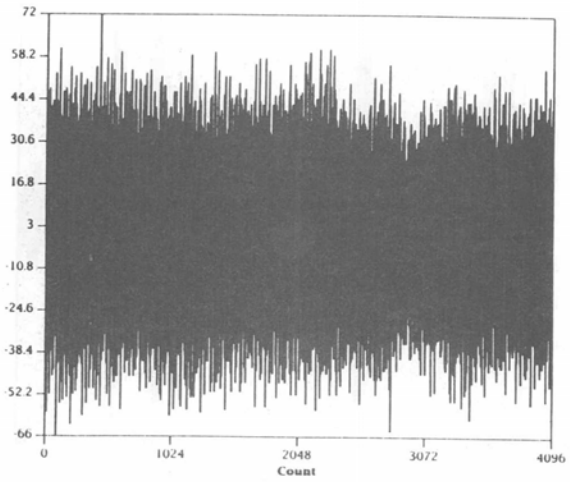

Record 34 (Q)

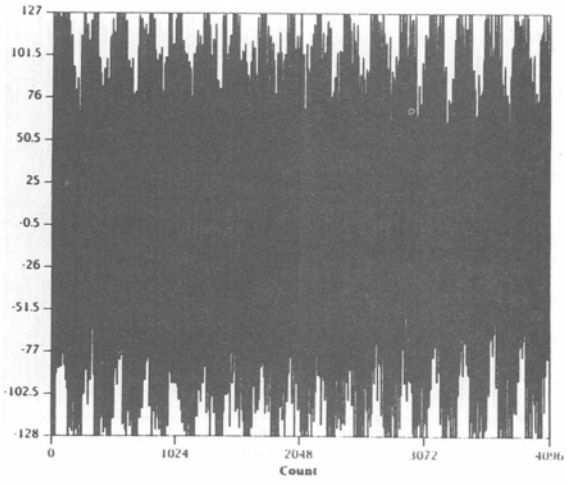

Record 34 (i)

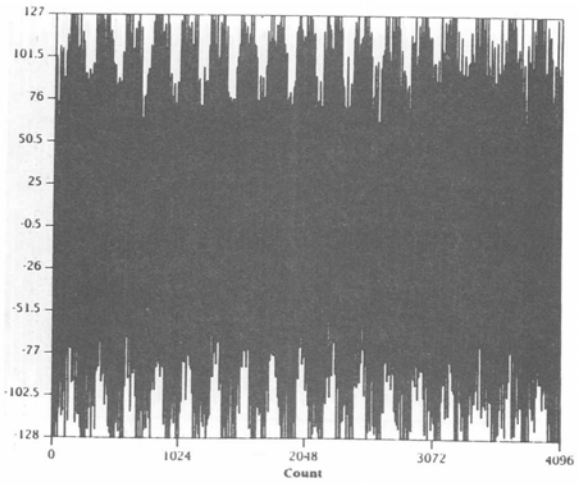

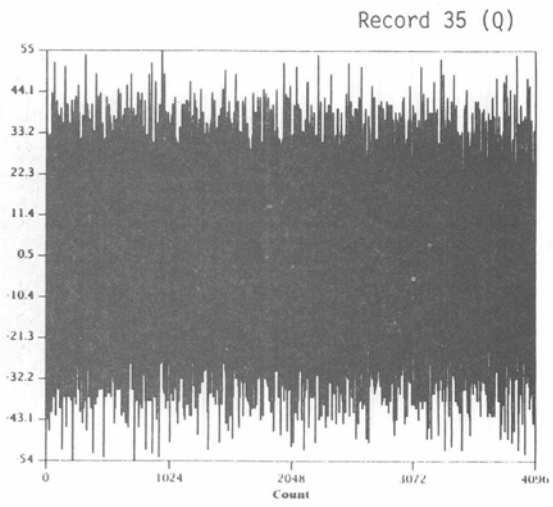
Record 35 (Q)
55
44.1
33.2
22.3
11.4
0.5
-10.4
-21.3
-32.2
-43.1
-54
0
1024
2048
3072
4096
Count

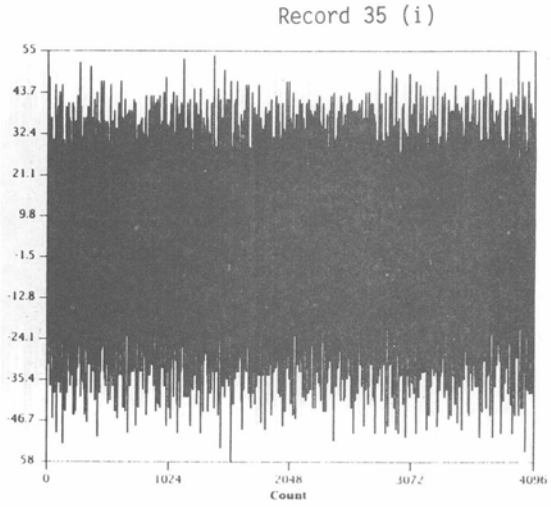
Record 35 (i)
55
43.7
32.4
21.1
9.8
-1.5
-12.8
-24.1
-35.4
-46.7
-58
0
1024
2048
3072
4096
Count

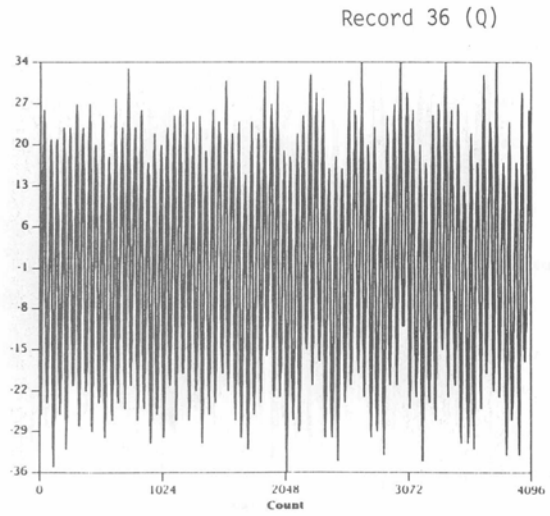
Record 36 (Q)
34
27
20
13
6
-1
-8
-15
-22
-29
-36
0
1024
2048
3072
4096
Count

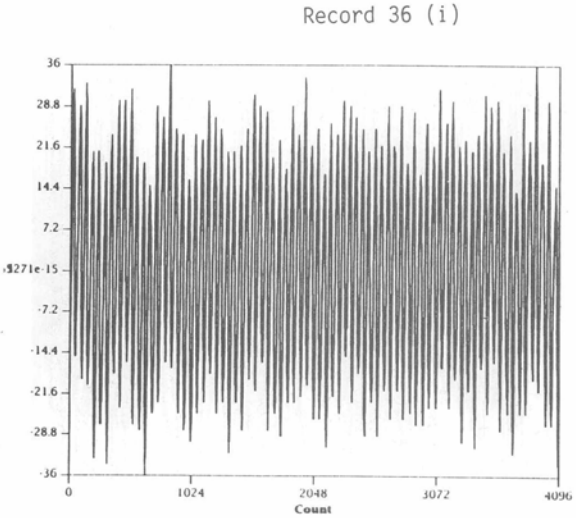
Record 36 (i)
36
28.8
21.6
14.4
7.2
3271e-15
-7.2
-14.4
-21.6
-28.8
-36
0
1024
2048
3072
4096
Count

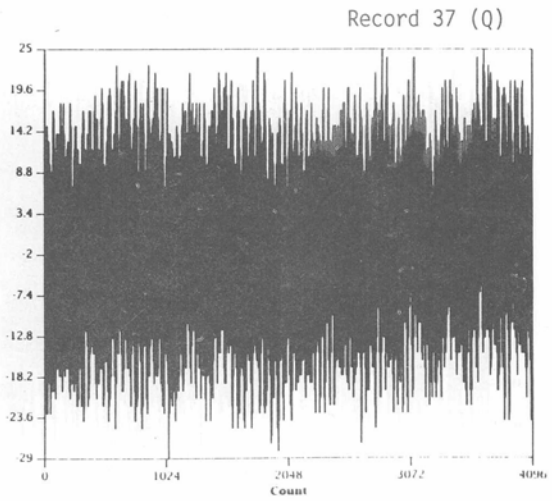
Record 37 (Q)
25
19.6
14.2
8.8
3.4
-2
-7.4
-12.8
-18.2
-23.6
-29
0
1024
2048
3072
4096
Count

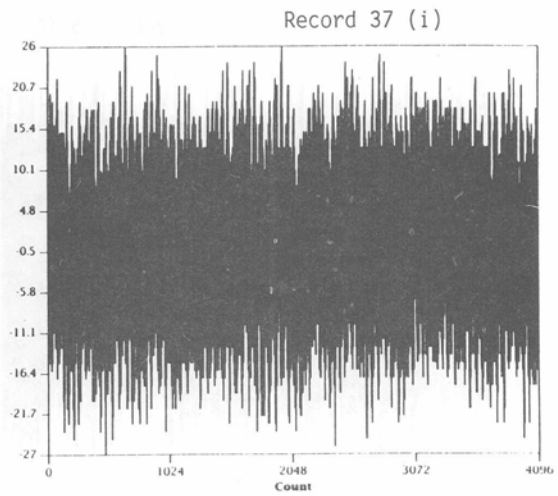
Record 37 (i)
26
20.7
15.4
10.1
4.8
-0.5
-5.8
-11.1
-16.4
-21.7
-27
0
1024
2048
3072
4096
Count

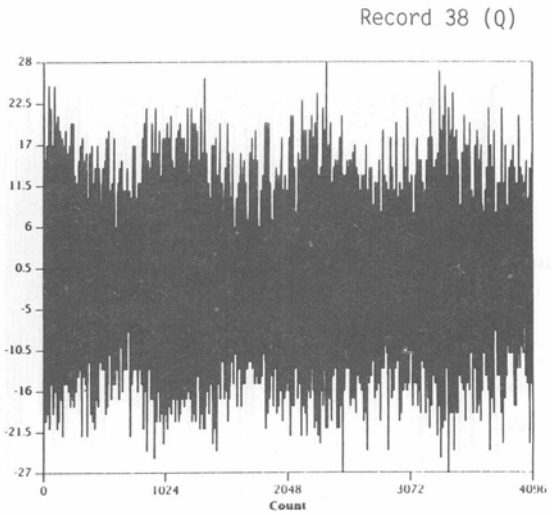
Record 38 (Q)
28
22.5
17
11.5
6
0.5
-5
-10.5
-16
-21.5
-27
0
1024
2048
3072
4096
Count

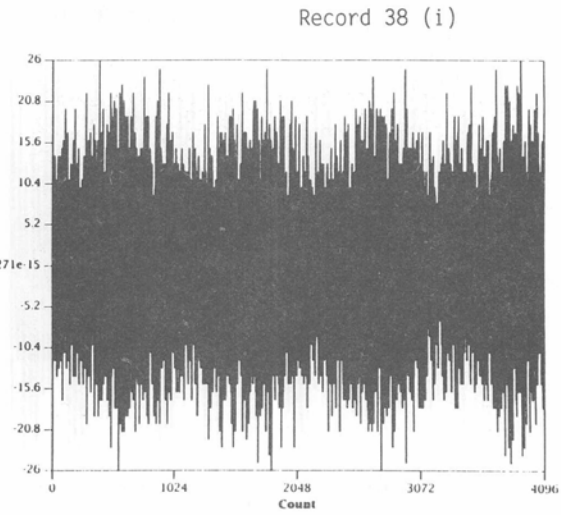
Record 38 (i)
26
20.8
15.6
10.4
5.2
1.271e-15
-5.2
-10.4
-15.6
-20.8
-26
0
1024
2048
3072
4096
Count

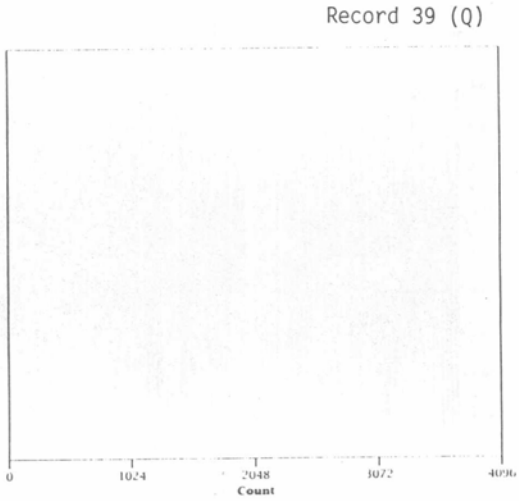
Record 39 (Q)
0
1024
2048
3072
4096
Count

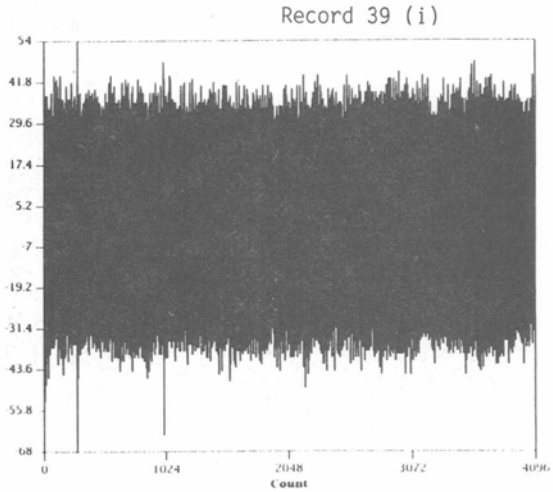
Record 39 (i)
54
41.8
29.6
17.4
5.2
-7
-19.2
-31.4
-43.6
-55.8
-68
0
1024
2048
3072
4096
Count

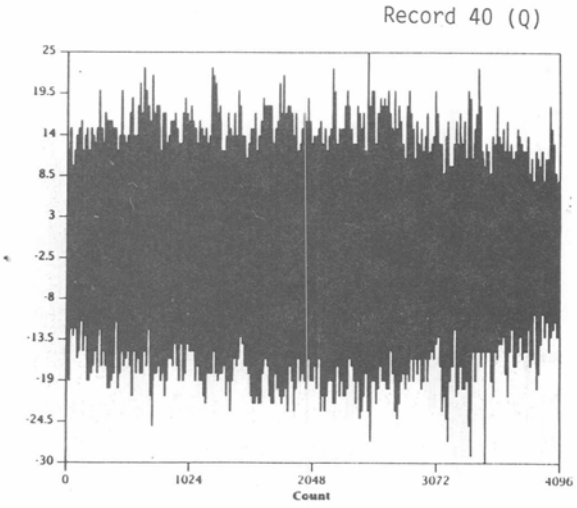
Record 40 (Q)
25
19.5
14
8.5
3
-2.5
-8
-13.5
-19
-24.5
-30
0
1024
2048
3072
4096
Count

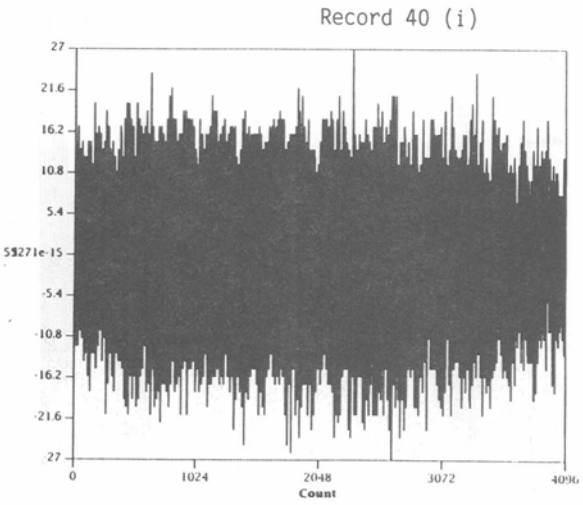
Record 40 (i)
27
21.6
16.2
10.8
5.4
5.271e-15
-5.4
-10.8
-16.2
-21.6
-27
0
1024
2048
3072
4096
Count

Record 41 (Q)

Record 41 (i)

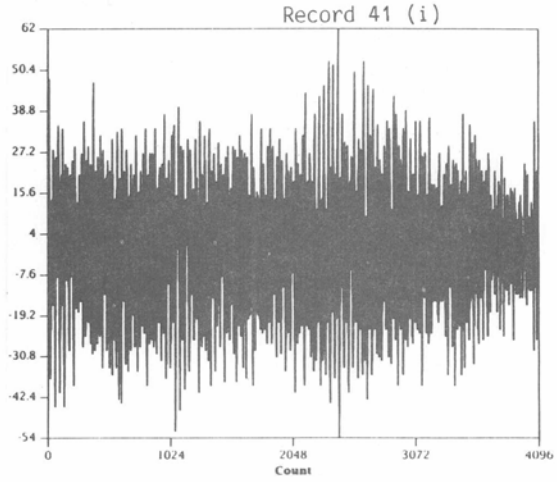

Record 42 (Q)

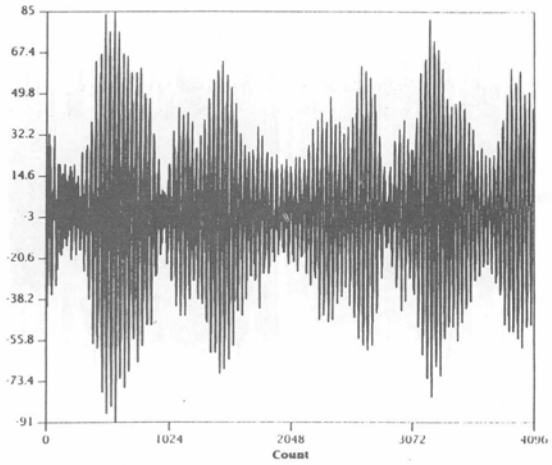

Record 42 (i)

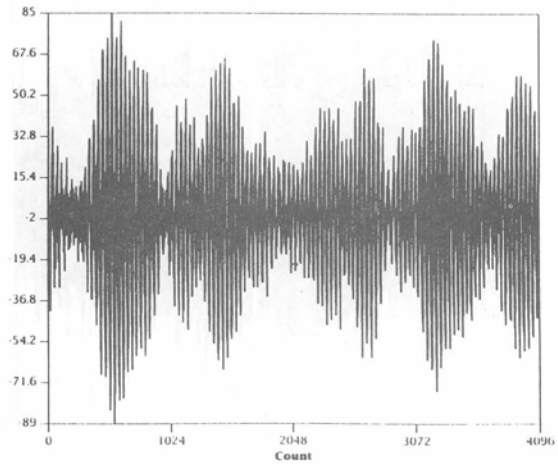

FORM **NTIA-29**
(4-80)

U.S. DEPARTMENT OF COMMERCE
NAT'L. TELECOMMUNICATIONS AND INFORMATION ADMINISTRATION

BIBLIOGRAPHIC DATA SHEET

	1. PUBLICATION NO.	2. Gov't Accession No.	3. Recipient's Accession No.

4. TITLE AND SUBTITLE

Wideband HF Noise/Interference Modeling
Part I: First-Order Statistics

5. Publication Date
April 1991

6. Performing Organization Code
NTIA/ITS.N2

7. AUTHOR(S)

John J. Lemmon and Christopher J. Behm

9. Project/Task/Work Unit No.

8. PERFORMING ORGANIZATION NAME AND ADDRESS

National Telecommunications and Information Admin.
Institute for Telecommunication Sciences
325 Broadway
Boulder, CO 80303

10. Contract/Grant No.

11. Sponsoring Organization Name and Address

Commander, HQ, CECOM, AMSEL-ED-ED-RF-2
Ft. Monmouth, NJ 07703

12. Type of Report and Period Covered

13.

14. SUPPLEMENTARY NOTES

15. ABSTRACT *(A 200-word or less factual summary of most significant information. If document includes a significant bibliography or literature survey, mention it here.)*

This report discusses the development of a wideband HF noise/interference model. The model is based on measured data and is suitable for implementation in a wideband HF channel simulator. The measured data are described and analyses performed on the data are discussed. Then the proposed noise/interference model is presented. Example results from the model are compared with measured data, and aspects of the model development which require further investigation are discussed.

16. Key Words *(Alphabetical order, separated by semicolons)*

Key Words: channel simulator; noise/interference; wideband HF

17. AVAILABILITY STATEMENT

☒ UNLIMITED.

☐ FOR OFFICIAL DISTRIBUTION.

18. Security Class. *(This report)*
Unclassified

20. Number of pages
110

19. Security Class. *(This page)*
Unclassified

21. Price:

☆U.S. GOVERNMENT PRINTING OFFICE: 1991 -573 -002/21060